PRELIMINARY STUDIES ON WING-BODY INTERFERENCE

BY
S. R. SIDDALINGAPPA

DEPARTMENT OF AERONAUTICAL ENGINEERING
INDIAN INSTITUTE OF TECHNOLOGY KANPUR

AUGUST 1971

PRELIMINARY STUDIES ON WING-BODY INTERFERENCE

A Thesis Submitted
In Partial Fulfilment of the Requirements
for the Degree of
MASTER OF TECHNOLOGY

BY
S. R. SIDDALINGAPPA

to the

DEPARTMENT OF AERONAUTICAL ENGINEERING
INDIAN INSTITUTE OF TECHNOLOGY KANPUR
AUGUST 1971

CERTIFICATE

Certified that this work titled "Preliminary Studies on Wing-Body Interference" has been carried out under my supervision and that this has not been submitted elsewhere for a degree.

S.M. Ramachandra

S.M. Ramachandra
Professor, Department of
Aeronautical Engineering
Indian Institute of Technology/Kanpur

ACKNOWLEDGEMENT

I wish to take this opportunity of expressing my sincere thanks and gratitude to Professor S.M. Ramachandra for suggesting the topic and giving me his valuable guidance throughout the course of this work.

I will be failing in my duty if I do not acknowledge the most constructive help and cooperation always extended to me by departmental workshop staff and particularly Mr. R. Krishna Murthy for suggesting valuable points in designing experiments. Thanks are due to Wg. Cdr. N.W. Tilak and Mr. V.V. Nanda for flying the airborne model experiments and Mr. M.P. Mathew and his staff of the Flight Laboratory for installation and instrumentation on the Rohini glider.

I extend my thanks to the Ministry of Defence for proposing the grant-in-aid project under which the present work was done, and the financial assistance given through the project. Thanks are also due to the Director, National Aeronautical Laboratory, Bangalore for assistance in the manufacture of Five component strain gauge balance at N.A.L., Bangalore

Thanks are also due to M/S. Hindustan Aeronautics, Kanpur for machining the Six component internal strain gauge balance and calibration fixtures. I sincerely

convey my thanks to Shri R.K. Bera my colleague for his valuable suggestions and help extended in programming.

Thanks are also due to Shri S.R. Gupta for his assistance in typing the manuscript.

CONTENTS

ABSTRACT

This is a preliminary investigation, both theoretical and experimental on the wing-body interference of a class of bodies, wings and their combination. The formulation of the problem holds good both in supersonic and subsonic flow regimes based on linearised equations. A case of a wing alone and body alone are studied both experimentally and theoretically in a subsonic flow regime. A different wing-body combination has been experimentally investigated for the combined aerodynamic characteristics. The results of wind tunnel tests are also compared with the results of some free-flight data for the same wing-body combination.

LIST OF SYMBOLS

$A.R.$ = aspect ratio

b = span

C = chord

d = distance Fig.(2.4)

$2D$ = fuselage diameter

$D(k)$ =

$E(k)$ = elliptic integrals

$K(k)$ =

K = Mach factor

ℓ = length over which each singularity is distributed

L = panel sweep

M = Mach number

m = line source strength per unit length

P_0 = free stream static pressure

P = local static pressure

q = source sink strength per unit length

q_{mB} = source sink strength per unit length required to satisfy tangential flow boundary condition in the presence of the body

Re = real part, Reynolds number

$S(x)$ = cross section area

U, V, W = perturbation velocities in X,Y,Z direction

ΔU_{mw} = pressure discontinuity required to satisfy tangential flow condition in the presence of the body

ΔU = pressure discontinuity across wing panel

V_{q_X} = horizontal component of perturbed velocity due to source-ring

V_{q_r} = radial component of perturbed velocity due to source-ring

U_{zc} = horizontal coponent of perturbed velocity due to source-ring

V_U = lateral component of perturbed velocity due to source-ring

W_Z = vertical component of velocity due to source-ring

U, V_∞ = free stream velocity

XYZ = Cartesian coordinates

r' = source-ring radius

r, θ = angular coordinates

x, r, ϕ = cylindrical coordinates

Λ, ϕ = leading edge sweep

ξ, η = integration variables

ϕ = velocity potential

ϕ^W = velocity potential for wing

ϕ^B = velocity potential for body

$\phi_{(W)}$ = velocity potential for wing-body combination

ϕ^2 = interference potential function due to wing-boy combination

ϕ^{Wi} = interference potential function due to presence of wing in the visinity of body

ϕ^{Bi} = interference potential functio. due to presence of body in the vicinity of wing

Φ^{MW} = velocity potential function for the wing in the presence of body

Φ^{MB} = velocity potential function for the body in the presence of wing

C_ℓ = section lift coefficient

C_L = total lift coefficient

C_m = pitching moment coefficient

C_D = drag coefficient

Z = normal force

X = chord force

Y = side force

ℓ = rolling moment

m = pitching moment

n = yawing moment

Γ = circulation

Subscripts

k = corner point

n = number

r = radial

θ = tangential

∞ = free-stream

W = wing

B = body

M, m = model (wing-body combination)

i = interference

LIST OF FIGURES

CHAPTER I

INTRODUCTION

I.1 General:

The problem of wing-body interference is important particularly in the case of low aspect ratio wing-body combinations. The lift and lift curve slopes of low aspect ratio wings are generally influenced by the presence of bodies. Even in the case of large aspect ratio wings two dimensionality of flow on the wing strictly exists only near the semi mid-span region. This influence of bodies on wings can be expressed in terms of interference coefficients. The term interference is used here in the sense of a change in fluid dynamic characteristics of a body due to the presence of another body. Theoretically the problem has defind a complete, and more so, a simple general solution useful in practical cases.

The aerodynamic characteristics of an indivisual component of an aircraft are generally known in more certain terms. However, the interference of one part on another is the most difficult to estimate as they are not easily amenable to mathematical analysis, and it cannot be ignored either.

Many theories and their variations exist for the wing alone, the body alone, and their combination

in all the flow regimes. Results of experimental investigations for the same theories are seldom available to compare. This is more so in the particular cases of wings, bodies and their combinations. Evaluation of the interference effects experimentally, is the best method available to get more concrete results and provide a test of the extent of validity of the various theories.

I.2. Subsonic and Supersonic Theories for Wings, Bodies and their Combination.

The simplest three-dimensional wing theory in subsonic flow is the lifting line theory which is applicable to unswept wings of high aspect ratio. ($AR \geq 6$). The solutions of the integro-differential equation are given by Glauert[1], Lotz[2], Multhopp[3], Gates[4], Hildebrand[5] and Sears[6]. The lifting line theory is not sufficiently accurate for wings of $AR < 6$ or swept wings, if the sweep angle $> 20°$. In such cases Weissinger's[7] theory is more appropriate. This is a first approximation to the lifting surface theory. On similar lines lifting surface theories due to Blenk[8], Falkner[9], H.Schlichting and H.H.M. Thomas[10], are also available. In these lifting surface theories the Blenk's theory is the most exact formulation. The next in order of approximations are the theories of Falkner, Schlichting and Thomas. The Weissinger theory comes in the end. De Young and Barling[11], have given empirical corrections which bring the seven-point Weissinger method

into better agreement with experiment and with the results of more accurate calculations based on the 15-point Weissinger method. Diederich and Zlotnick[12] have given sets of aerodynamic influence coefficients based on the 15-point Weissinger method for a wide class of wings, they have also given the actual spanwise loading distributions on the wings and for various power law, twist distribution along the span, both symmetric and antisymmetric. In Weissinger's theory it is assumed that the chordwise center-of-lift is at the $\frac{1}{4}$-chord point. This becomes less and less valid as the aspect ratio falls below 2.0 and approaches zero. (It is at 20% chord for a rectangular wing of aspect ratio 1.6).

Relatively simple closed form lifting surface solution for lift distributions can be obtained for a wide variety of wing planforms and angle of attack distributions in supersonic three-dimensional flows. This is possible l because of the integral equations of linearized lifting surface theory may be inverted by a number of special techniques[13]. Harmons[14] and Kainer, J.[15] deal with the cases of linearized potential fields and spanwise lift and moment distributions for tapered wings with supersonic edges linear, quadratic, and cubic twist distributions both symmetric and antisymmetric along the span. Evvard's[16,16'] method is useful in analysing subsonic edges adjacent to a supersonic edge such as occurs at the tip of a rectangular wing.

This method is not applicable to wings without supersonic leading edge as for example delta wings and other highly swept back wings. Another planform not amenable to Evvard's method is the swept wing with subsonic leading and trailing edges. Works of Cohen[17] gives solution for the lift of flat plate swept wings with subsonic leading and trailing edges taking into account tip effects. The results of this work are often useful in assessing the importance of various features of wing geometry on load distribution. Numerical methods are available due to Etkin and Woodward[18], and Neuringer[19]. These methods involve division of the wing surface (and sometimes certain regions of wing surface) into grids of parallelograms. The contributions of each cell to the potential at any point can be summed numerically for arbitrary angle of attack distributions over the surface.

The bodies in fluid flows can be simulated by singularities like line sources and line doublets. Whem these singularities are distributed along the body axis, they represent the effects of body volume, incidence and camber. The characteristics of these singularities are given in Woodward's[20] work. Bodies at an angle of attack can also be represented by circular source rings of varying strength[21]. An extensive compilation of theories existing for slender bodies are given in the book of J.N. Nielsen[22].

There are many subsonic, and supersonic flow theories which are available for wing body combinations. Subsonic flow theories:

The mutual interference of a fuselages and wings of high aspect ratio in subsonic, incompressible flows have been studied by Lennertz[23], Wieselsbergh[24], Pepper[25] and Multhopp[26].

A method for circular bodies involving the use of a number of horse-shoe vortices on the wing and their images in the body has been suggested by Zlotnick and Robinson[27], using conformal mapping to transform the cross-section in a Trefftz plane to that of a flat plate. Spreiter[28] and Ward[29] obtained a closed form solution for the case of slender wings mounted on cylindrical bodies. The same case with elliptical body section has been studied by Nonweiler[30] and Kahane[31] Mirels[32] has studied the problem of wing-body combinations with a gap at the wing-body juncture on similar lines. The results of his study are unrealistic as he neglects viscous and compressibility effects. Lawerence[33] gives a theory for low aspect ratio wings with straight trailing edges centrally mounted on an infinite circular cylinder. This theory holds good even for bodies which are not slender for which it was originally formulated.

The same theory has been extended to arbitrary body cross-sections by Lawrence and Flax[34]. (Lagerstrom, Graham[35]),Moskowitz[36] and (Adams, Sears)[37], have studied

the lift on after bodies in presence of wing trailing vortices. The case of an after-body of decreasing cross section area in the presence of wing wake is also studied by Adams and Sears. A first approximation for slender after-bodies behind non-slender wing-body combinations can also be obtained from Ref. 34,36.

Supersonic Flow Theories:

Problem of very high aspect ratio wings mounted on a conical body considering the interference effect as simply the increased lift on wings due to the increased angle of attack produced by the upper surface flow around the body has been considered by Kirkby and Robinson[38]. Ferrari[39,40] gave an iterative procedure which may be shown to converge starting with the body alone and the wing alone solution and proceeding to correct the solution in such a way that at each stage of the iteration process, the boundary condition on either the wing or the body is satisfied exactly while the boundary condition on the other is violated. Since the process is convergent, a sufficient number of terms will give the desired accuracy. Calculations have been done upto only the first two steps. His results for the first iteration for high aspect ratio rectangular wings mounted on a pointed body of revolution show fairly good agreement with experiment.

The problem of rectangular wing and infinite cylindrical body of circular cross section at zero angle

to the main stream on similar lines as those of Ferrai were obtained by Nielson[41]. The basis for his formulation of the problem was the work of Lagerstrom and Vandyke[42]. Here the basic wing passing through the body gives one part of the solution. The flow set up by this wing violates the boundary conditions of zero velocity normal to the body. A second part to the solution is then obtained which cancels the flow normal to the body without at the sametime producting any new velocities normal to the wing surface. Thus the iteration is terminated in two steps. Nielson solves the this boundary value problem by taking the Laplace transform of the governing equation. He was able to invert the transform of the solution only in terms of a new set of functions, one for each term of the fourier series. Only the first four of these functions were tabulated.

A unified theoretical approach in the field of wing-body combination has been tried by many people. Among them the work of Woodward's[20] is of considerable importance. He deals with the problem by considering the singularities simulating the wings, bodies and their geometrical characteristics. The potential functions for the singularities are made to satisfy the Prandtl-Glauert equation along with the boundary conditions. As the theory is linear, the indivisual potentials can be added and the solution can be obtained for the complete combined flow field. To get the pressure coefficients for the fields the linearised Bernoulli's equation for steady compressible flow is used along with Prandtl-Glauert equation.

I.3. Present Work:

In this thesis, the wing alone case is solved by Weissinger's method. Aerodynamic characteristics are calculated for a class of wings. A rectangular unswept, low aspect-ratio, three-dimensional wing with no twist and taper, at different angles of attack is studied both theoretically and experimentally. Results are compared and discussed. A slender body of revolution is studied for its aerodynamic characteristics both theoretically and experimentally. Aerodynamic characteristics have been measured experimentally for a particular cruciform wing-body model both in free-flight and in the wind tunnel. The results are discussed and compared.

The instrumentation required for this program of studies in wing-body interference has been developed. The instrumentation consists of a pair of strain gauge balances, a calibration rig for the strain gauge balances, models of wing and body of revolution with static pressure holes on them. This instrumentation was designed and tested out as a part of this work to enable a continuing program in this field.

CHAPTER II

II.1. Formulation of the Problem:

In the following discussion we shall assume the wing to be thin and the body to be slender, so that the perturbations caused by the presence of the wing and body combination are small compared to the free stream velocity. Flow field due to the wing and the body can be represented as equivalent to the surface distribution of vortices, over the wing and the surface distribution of sources over the body.

These singularities represent appropriate discontinuities in the u,v, or w velocity components across the wing or body panels and along the body axis. The linearized potential function must satisfy the Prandtl-Glauert equation.

$$\left(1 - M_{\infty}^{2}\right)\phi_{xx} + \phi_{yy} + \phi_{zz} = 0 \quad \text{---} (1)$$

The strengths of the singularities are found by satisfying the tangential flow boundary conditions at the selected control points to get the given configuration. The shrouded part of the wing by the body is assumed to be of zero camber, zero thickness and zero incidence. The theory applies to both subsonic and supersonic flows, since the linearized potential function and the above Prandtl-Glauert equation hold for these flows.

The linearized differential equations for the purturbation potential of the wing alone and body alone are

$$(1-M^2)\phi^{W}_{xx} + \phi^{W}_{yy} + \phi^{W}_{zz} = 0 \qquad \text{.....(2)}$$

$$(1-M^2)\phi^{B}_{xx} + \phi^{B}_{yy} + \phi^{B}_{zz} = 0 \qquad \text{....(3)}$$

For the combined flow field of a wing and a body the total velocity potential is not a simple sum of two individual potentials. But the combined potential should yield a flow which satisfies the boundary conditions on both the wing and body simultaneously. Writing down the combined velocity potential as

$$\phi_M = \phi^{B} + \phi^{W} + \phi^{i} \qquad \text{.....(4)}$$

Many approximate mathematical theories have been put forward for the explicit expression of the interference velocity potential function.[43,36,44,45,20] Interference potential is written as

$$\phi^{i} = \phi^{W_i} + \phi^{B_i} \qquad \text{.....(5)}$$

where

ϕ^{W_i} = interference potential due to wing on body

ϕ^{B_i} = interference potential due to body on wing

Therefore:

$$\phi_M = \phi^B + \phi^W + \phi^{W_i} + \phi^{B_i}$$

$$= (\phi^W + \phi^{B_i}) + (\phi^B + \phi^{W_i})$$

$$= \phi^{MW} + \phi^{MB} \qquad \ldots\ldots(6)$$

Where

ϕ^{MW} = the potential function of wing in presence of body

ϕ^{MB} = the potential function of body in presence of wing

These three potentials individually satisfy the equation (1).

$$(1-M^2)\,\phi^{MW}_{xx} + \phi^{MW}_{yy} + \phi^{MW}_{zz} = 0 \qquad \ldots\ldots(7)$$

$$(1-M^2)\,\phi^{MB}_{xx} + \phi^{MB}_{yy} + \phi^{MB}_{zz} = 0 \qquad \ldots\ldots(8)$$

$$(1-M^2)\,\phi^{M}_{xxe} + \phi^{MB}_{yy} + \phi^{M}_{zz} = 0 \qquad \text{.....(9)}$$

Equation 9 = Equation 7 + Equation 8.

Since V is a constant, the second derivative of it's potential is zero, and therefore these potential's may be regarded as the perturbation potential. These potential functions are evaluated by appealing to appropriate theories mentioned in Chapter I, for the cases of wing alone, body alone, and their combinations. The linearized pressure coefficients are obtained by linearizing Bernouli's equation for steady, compressible flow,

$$C_p = \frac{P - P_0}{\frac{1}{2}\rho_0 U_\infty^2} = -\frac{2u}{U_\infty} \qquad \text{.....(10)}$$

where $u = \varphi(x)$ is the x-perturbation velocity. As the whole theory is built on small perturbations; it is assumed that the same linear solutions also hold good even in the neighbourhood of the wing-body junction.

The pressure discontinuity across the upper and lower surfaces of the wing panel is given by

$$C_p = C_{p_{lower}} - C_{p_{upper}}$$

$$= 2\left(\frac{\Delta u}{U_\infty}\right) \qquad \text{.....(11)}$$

where Δu is the velocity difference on the two sides of the wing. The perturbation velocity components are given by

$$u = \frac{\partial \phi}{\partial x} \; , \; v = \frac{\partial \phi}{\partial y} \; ; \; w = \frac{\partial \phi}{\partial z} \qquad \ldots\ldots(12)$$

II.2: Wing Alone:

(i) Vortex Theory: Weissinger's theory can be considered as an extension of lifting line theory or a first approximation to the lifting surface theory. The induced angle measured at the $\frac{3}{4}$ chord point of the wing is considered to be that arising from the bound vortex at the $\frac{1}{4}$-chord line of the wing and the trailing vortex and equals the geometrical angle at the $\frac{3}{4}$-chord point. The significance of the $\frac{3}{4}$-chord point is that in two dimensional flow this is the centroid of the function $\sqrt{\frac{b-x}{b+x}}$ which appears in the Munk's integral for the lift. In fact for an airfoil section with angle of attack plus parabolic camber, the exact two-dimensional lift is obtained by considering the entire airfoil as a flat plate at an angle of attack equal to the local angle of attack of the $\frac{3}{4}$-chord point of the airfoil.

The integral equation of the Weissinger theory may be written for swept wings as[46],

$$w\vartheta(y) = -\frac{1}{2\pi}\int_{-S_0}^{S_0}\frac{\Gamma'(\eta)}{y-\eta}\,d\eta$$

$$-\frac{1}{2\pi}\int_{-S_0}^{S_0}\frac{L(y,\eta)}{c(y)}\,\Gamma'(\eta)\,d\eta \qquad \text{.....(13)}$$

for $y>0$:

$$L(y,\eta) = \frac{1}{2}\,\frac{c}{y-\eta}\left\{\frac{\sqrt{\{(\tfrac{1}{2}c+\epsilon y+\eta)\tan\varphi)^2+(y-\eta)^2\}}}{2y\tan\varphi+\tfrac{1}{2}c}-1\right\}$$

$$+2\tan\varphi\,\frac{\sqrt{\{(\tfrac{1}{2}c+y\tan\varphi)^2+y^2\}}}{2y\tan\varphi+\frac{1}{2}c}$$

$$;(\eta<0)$$

.....(14)

and

$$L(y,\eta) = \frac{1}{y-\eta}\left\{\sqrt{[(\tfrac{1}{2}c+(y-\eta)^2+(y-\eta)^2]}-\tfrac{1}{2}c\right\}$$

$$;(\eta>0)$$

.....(15)

The coordinate systems are given in Fig.2.1.

The boundary condition is satisfied at the $\frac{3}{4}$-chord point i.e.

$$x = |y| \tan\varphi + \frac{1}{2} c(y) \quad \ldots\ldots(16)$$

The complete procedure of getting the solution is explained in Ref.46.

(ii) Source-Vortex Theory:[20] The effects of wing thickness are given by planar source distributions. The wing camber, twist and incidence effects are given by a planar vortex system. These singularities can be evaluated in terms of the potential function which satisfies the Prandtl-Glauert eqn. (1) along with boundary conditions. The potential for the planar singularities can be written down as:

$$\phi_\eta = \frac{k}{\pi} \iint \frac{f_\eta(\xi,\eta)\, d\xi\, d\eta}{\sqrt{(x-\xi)^2 + (1-M^2)[(y-\eta)^2 + z^2]}}$$

$$+ \frac{1-k}{\pi} \iint \frac{z\, d\xi\, d\eta}{(y-\eta)^2 + z^2} \quad \ldots\ldots(17)$$

where

$k = 0.5$ for $M \leq 1$

$k = 1.0$ for $M > 1$

$f_3 = -1$ represents a constant source distribution

$f_4 = L\eta - \xi$ represents a linearly varying source distribution

$$x = x_p - x_k$$

$$y = y_p - y_k$$

$$z = z_p$$

The wing thickness is represented by constant source panels, and linear source panels. The wing lift and interference is represented by constant pressure vortex panel.

The integration limits are defined by the panel boundaries. For one corner element the potential function is given by, (Fig. 2.3 gives the coordinate systems).

$$\phi_k^W = \frac{k}{2}\frac{\Delta u}{A}\Big[(x - Ly)(F_3 + F_4) + z\Big[(L^2 + 1 - M^2)F_2 - L(F_1 - F_5) - yF_6\Big]\Big] \quad \text{.....(18)}$$

where

$2\Delta u$ = pressure discontinuity across the panel

$$F_1 = \mathrm{Re}\left(\log \frac{x+d}{\sqrt{|1-M^2|}\,r}\right)$$

$$F_2 = \frac{1}{\sqrt{L^2+1-M^2}}\,\mathrm{Re}\left(\log \frac{x'+d'}{\sqrt{|1-M^2|}\,r'}\right)$$

$$F_3 = \mathrm{Re}\left(\tan^{-1}\frac{zd}{Lr-xy}\right)$$

$$F_4 = \tan^{-1}\frac{y}{z} \quad \text{for } M<1$$

$$= 0 \quad \text{for } M\geq 1$$

$$F_5 = \log \frac{L\sqrt{y^2+z^2}}{\sqrt{(x-Ly)^2+(L^2+1-M^2)z^2}} \qquad 18(A)$$

$$= \log \frac{Lr}{r'} \quad \text{for } M\leq 1$$

$$= 0 \quad \text{for } M>1$$

$$F_6 = \frac{x+d}{r^2} \quad \text{for } M\leq 1$$

$$= \frac{d}{r^2} \quad \text{for } M>1$$

$$r = \sqrt{y^2 + z^2}$$

$$d = \sqrt{x^2 + (1-M^2) r^2}$$

$$y' = x - Ly$$

$$x' = Lx + (1-M^2) y$$

$$r' = \sqrt{(x-Ly)^2 + (L^2+1-M^2) z^2}$$

$$d' = \sqrt{x'^2 + (1-M^2) r'^2} \qquad \text{.....(18a)}$$

The potential at a point $P(x_p, Y_p, Z_p)$ is given by

$$\phi^W(P) = \phi_1^W - \phi_2^W - \phi_3^W + \phi_4^W$$

where $K = 1,2,3,4$ is the potential due to one corner point element of the constant pressure discontinuity. The partial derivatives of eqn.(18) gives the perturbation velocity component due to each corner element of the constant pressure panel.

$$u_K = \frac{K\Delta u}{2\pi}\,(F_3 + F_4)$$

$$v_K = \frac{K\Delta u}{2\pi}\left[L\,(F_3 + F_4) - 2F_6\right]$$

$$w_K = \frac{K\Delta u}{2\pi}\left[(L^2 + 1 - M^2)F_2 - L(F_1 - F_5) - y\,F_6\right] \qquad \ldots\ldots(19)$$

The perturbation velocity components induced at a point P by a finite panel may be obtained by super position.

$$u_P = u_1 - u_2 - u_3 + u_4$$

$$v(P) = v_1 - v_2 - v_3 + v_4$$

$$w(P) = w_1 - w_2 - w_3 + w_4 \qquad \ldots\ldots\ldots(20)$$

The pressure coefficient C_P is obtained from eqn.(10) and (11).

II.3 Body Alone:

(iii) Source distributions of varying strength on a circle: When the axis of a body of revolution is inclined to the main stream, the solution can be obtained by using on the surface of the body singularities composed of source rings, the strength of which varies round the circumference according to, (Fig.2.2).

$$q_{(\varphi')} = q \sin\varphi'$$

where φ is the azimuthal angle θ

The velocity induced by an element of such a ring at any point (x, r, φ) is given by

$$d\vec{V} = \frac{q \sin\varphi'}{4\pi} \frac{ds}{R^2} \frac{\vec{R}}{R} \qquad \ldots\ldots(21)$$

The velocity components are obtained by integration round the circumference. These are given by,

$$u = \frac{q}{2\pi r'} \frac{2x\left[2K(k) - 2D(k) - E(k)\right]}{\sqrt{x^2 + (r+1)^2}} \times$$

$$\frac{\sin\varphi}{\left[x^2 + (r-1)^2\right]} \qquad \ldots\ldots(22)$$

$$v = \frac{q}{2\pi r'} \frac{1}{\sqrt{x^2 + (r+1)^2}\left[x^2 + (r-1)^2\right]} \times$$

$$\left\{\left[2r\sin^2\varphi + \frac{8}{k^2}(1 - 2\sin^2\varphi)\right]\right.$$
$$\left[2K(k) - 2D(k) - E(k)\right] -$$
$$8(1 - 2\sin^2\varphi)\left[K(k) - D(k)\right.$$
$$\left.\left. - 2\sin^2\varphi\ E(k)\right\}\right.$$

$$\ldots\ldots(23)$$

$$w = \frac{q}{2\pi\gamma'} \frac{\sin 2\varphi}{\sqrt{x^2+(\gamma+1)^2}\left[x^2+(\gamma-1)^2\right]} \times$$

$$\left\{\left(\gamma - \frac{8}{k^2}\left[2K(k) - 2D(k) - E(k)\right]\right.\right.$$

$$\left.\left. + 8\left[K(k) - D(k)\right] - E(k)\right\}\right.$$

.....(24)

$$u = v_x(x, \gamma, \varphi)$$

$$v = v_y(x, \gamma, \varphi)$$

$$w = v_z(x, \gamma, \varphi)$$

The down-wash velocity is given by

$$\frac{w}{U} = B\,q$$

where

$$B = \frac{q}{2\pi\gamma'} \frac{1}{\sqrt{\{x^2+(\gamma+1)^2}\left[x^2+(\gamma-1)^2\right]} \times$$

$$\left\{\left[2\gamma \sin^2\varphi + \frac{8}{k^2}(1-2\sin^2\varphi)\right] \times \right.$$

$$\left[2K(k) - 2D(k) - E(k)\right] - 8(1-2\sin^2\varphi) \qquad \text{.....(25)}$$

$$\left.\left[K(k) - D(k)\right] - 2\sin^2\varphi\, E(k)\right\}$$

where the value of K(k) E(k) and D(k) are given by

$$K(k) = \int_0^{\pi/2} \frac{1}{\sqrt{1 - k^2 \sin^2\alpha}}\, d\alpha$$

$$E(k) = \int_0^{\pi/2} \sqrt{1 - k^2 \sin^2\alpha}\, d\alpha$$

$$D(k) = \int_0^{\pi/2} \frac{\sin^2\alpha}{\sqrt{1 - k^2 \sin\alpha}}\, d\alpha \qquad \ldots\ldots(26)$$

and these are elliptic integrals. The value of k is given by $k = \sqrt{\frac{4r}{x^2 + (r+1)^2}}$

where x and r non-dimensionalized with respect to the source ring radius r'.(Fig.2.2)

The body is ~~distributed~~ represented by a number of source ring along the axis and their induced velocity fields are calculated from above equation. The distribution of pressure coefficient over the body can be obtained by,

$$C_p = - \frac{2u + v^2}{U} \qquad \text{---} \quad 26(A)$$

(iv). The effect of body volume, incidence and camber are simulated by line sources and doublets distributed along the body axis. The strengths of these singularities are determined such that the resulting flow is tangential to the surface at each control point.[20]

The potential which satisfies the eqn. (1) for the line singularities can be written down as

$$\phi_\eta = \int \frac{f_\eta(\xi)\, d\xi}{\sqrt{(x-\xi)^2 + (1-M^2)\, y^2}} \qquad \ldots\ldots(27)$$

$f_1 = -\xi$ for line sources. (Fig.2.4)

$f_2 = \frac{\sin\theta}{r}\,\xi(x-\xi)$ for line doublets

Line source: The potential due to a finite line source of unit strength located along the X axis between X = 0 and X = 1 is obtained by integrating eqn.(27) for n = 1 between ξ = 0 and ξ = . In subsonic flow the integral can be integrated directly, but in supersonic flow the integral should be evaluated separately in each of the three regions bounded by the Mach cone from the origin and the Mach cone from the tail. (Fig.2.4).

In either case the result is given by

$$\phi_1 = Re\left(d_1 - d_2 - x_1 \log \frac{x_1 + d_1}{x_2 + d_2}\right) \qquad \ldots.(27a)$$

where

$$d_1 = \sqrt{x_1^2 + (1-M^2)\gamma^2} \qquad x_1 = x - x_k$$

$$d_2 = \sqrt{x_2^2 + (1-M^2)\gamma^2} \qquad x_2 = x - \ell$$

The velocity components are given by

$$u = Re\left(\log \frac{x_2 + d_2}{x_1 + d_1} + \frac{\ell}{d_2}\right) \qquad \text{.....(27b)}$$

$$V_r = \frac{1}{r} Re\left(d_1 - \frac{d_1^2 - x_1\ell}{d_2}\right) \qquad \text{.....(27c)}$$

Line doublet: For line doublet of unit strength located along with X axis is obtained by integrating eqn.(27) for n = 2 between limits $\xi = 0$ and $\xi = \ell$. The potential function valid for both subsonic and supersonic flow is given by

$$\phi_2 = \frac{\sin\theta}{r} Re\left\{x_1(d_2 - d_1 + \ell d_2 - (1-M^2)\gamma^2 \log \frac{x_1 + d_1}{x_2 + d_2}\right\} \qquad \text{.....(27d)}$$

d_1, d_2 are same as before and θ is measured from the

X - Y (horizontal plane), axis. The corresponding velocity components are

$$U_2 = \frac{\sin\theta}{r} Re\left[d_1 - d_2 \frac{x_2 \ell}{d_2}\right] \qquad \ldots\ldots(27e)$$

$$V_{r_2} = \frac{\sin\theta}{2r^2} Re\left[x_1 (d_2 - d_1 + \ell d_2 - (1-M^2) r^2 \left[\frac{2\ell}{d_2} - \log \frac{x_1 + d_1}{x_2 + d_2}\right]\right] \qquad \ldots\ldots(27f)$$

$$V_{\theta_2} = \frac{\cos\theta}{2r^2} Re\left[x_1 (d_2 - d_1) + \ell d_2 - (1-M^2) r^2 \log \frac{x_1 + d_1}{x_2 + d_2}\right] \qquad \ldots\ldots(27g)$$

These values of perturbation velocities can be used to calculate the interference fields on the wing due to body.

II.3. Wing-body Combination:

The potential function for the combined flow field of a wing body combination is obtained by using eqn. (27) and (17). A typical wing body combination is given in (Fig.2.7). The wing and the surface of the body are subdivided into a large number of quadrilateral panels. These panels define the boundaries of planar singularities used to simulate effects of wing lift, thickness, and wing body interference. Additional line singularities located along the body axis are used to simulate the lift and volume effects of the body.

The velocity potential function in the present work is given by replacing the wing by pressure discontinuities across the horizontal panel and the body by a distribution of source ring singularities. (Fig.2.8).

The potential function for constant pressure singularity is given by eqn.(17) and the corresponding vertical components of perturbation velocity by eqn.(19). Velocity potential for the wing and the corresponding induced velocity may be written in the form

$$\phi^{MW}(P) = \phi_1^{MW} - \phi_2^{MW} - \phi_3^{MW} + \phi_4^{MW}$$

AND

$$W_K = \frac{K\Delta U_{mW}}{2\pi}\left[(L^2+1-M^2)F_2 - L(F_1-F_5) - yF_6\right] \qquad \ldots\ldots(28)$$

The down-wash velocity at any point $P(X_P, Y_P, Z_P)$ is given by

$$W(P) = W_1 - W_2 - W_3 + W_4$$
$$= C_W U_{MW} \qquad \ldots\ldots(29)$$

where

$$C_W = \frac{k}{2\pi} \Big[\Big\{ (L^2+1-M^2) F_2 - L(F_1 - F_5) - yF_6 \Big\}_{K=1} - \Big\{ (L^2+1-M^2) F_2 - L(F_1-F_5) - yF_6 \Big\}_{k=2} - \Big\{ (L^2+1-M^2) F_2 - L(F_1-F_5) - yF_6 \Big\}_{k=3} + \Big\{ (L^2+1-M^2) F_2 - L(F_1-F_5) - yF_6 \Big\}_{k=4} \Big]$$

$\ldots\ldots(30)$

The graphical or numerical integration of the velocity field for the body the numerical value of the potential function is obtained. When the axis of the body is inclined to the free stream a varying circular source and distribution is taken as the singularity. This simulates the effect of wing interference on the body. The expressions

for the velocity components of a source distribution of varying strength on a circle are given by eqn. 22,23,24. The resultant vertical component of velocity due to source ring and vortex distribution is given by algebraic sum of two components.

Taking n pressure panel singularities on the wing and m source ring singularities on the body we have n control points on the wing and m control points on the body.

The total down-wash at any control point on the wing is given by algebraic sum of the velocity due to wing pressure singularities of eqn.(30) and those due to source ring singularities of eqn.(24).

$$W_W = \sum_{i=1}^{n} C_{WW,i} \Delta U_{mW,i} + \sum_{j=1}^{m} D_{BW,j} q_{mB,j} \qquad \ldots\ldots(31)$$

The down-wash at any of the body control points is given by

$$W_B = \sum_{i=1}^{n} C_{WB,i} \Delta U_{mW,i} + \sum_{j=1}^{m} D_{BB,j} q_{mB,j} \qquad \ldots\ldots(32)$$

The down-wash at (m+n) control points is given by

$$W_{mn} = \sum_{i=1}^{n} C_{W\cdot i}\, \Delta u_{mn,i} + \sum_{j=1}^{n} D_{B,j}\, q_{mB,j} \qquad \text{.....(33)}$$

$\frac{W_{mn}}{U}$ = surface slope at the (m+n) control points

The system of simultaneous linear equations are solved[47] by Gauss-Jordon method to satisfy the tangential flow condition.

The new potential function for the wing in the presence of the body is given by equation (34)

$$\phi_K^{MW} = \frac{k\,\Delta u_m W}{2\pi}\left[(x - Ly)(F_3 + F_4) + Z\left\{(L^2+1-M^2)F_2 - L(F_1 - F_5) - yF_6\right\}\right] \qquad \text{.....(34)}$$

$(2\Delta U_{mw})$ = pressure discontinuity across the panel

The value of the potential function at any point $P(X_P, Y_P, Z_P)$ is given by

$$\phi^{MW}(P) = \phi_1^{MW} - \phi_2^{MW} - \phi_3^{MW} + \phi_4^{MW} \qquad \text{.....(35)}$$

The value of the interference potential due to body on wing is given by eqn. (6).

$$\phi^{Bi}(P) = \phi^{MW}(P) - \phi^{W}(P) \qquad \text{.....(36)}$$

Body potential due to source ring is

$$\phi^{B} = \int_0^{r} V_{q_r}\, dr + \int_0^{x} V_{q_x}\, dx \qquad \text{.....(37)}$$

For a varying source distribution.

$$\phi^{MB} = \int_0^{x} u\, dx + \int_0^{y} v\, dy + \int_0^{z} w\, dz$$

$$\phi^{Wi} = \phi^{MB} - \phi^{B}$$

$$= \int_0^{x} u\, dx - \int_0^{y} v\, dy + \int_0^{z} w\, dz - \int_0^{r} V_{q_r}\, dr - \int_0^{x} V_{q_x}\, dx \qquad \text{.....(38)}$$

The values for u,v,w, $\vartheta_{qx}, \vartheta_{qr}$ are given by 22,23,39.

$$V_{qx}(x,r) = \frac{q}{2\pi r'} \frac{2x \quad E(k)}{\sqrt{x^2+(r+1)^2}\left[x^2+(r-1)^2\right]}$$

$$V_{qr}(x,r) = \frac{q}{2\pi r'} \frac{1}{r\sqrt{x^2+(r+1)^2}} \times$$

$$\left\{K(k) - \left[1 - \frac{2r(r-1)}{x^2+(r-1)^2}\right] E(k)\right\} \ldots\ldots (39)$$

A case of rectangular wing with variable sweep angles over a body is investigated, for the effect of body over spanwise lift distributions on the wing.

CHAPTER III

EXPERIMENTAL METHODS USED

III.1 Introduction:

The schematic block diagram shown in Fig.3.1, reveals the procedure generally adopted to evaluate the coefficients of force, moments, interference, etc. related to an aerodynamic model. The various aerodynamic shapes of bodies on which the present studies have been made are shown in Fig.3.2. Design of experiments has been done keeping in view the possibility of testing a class of wings, a class of bodies, and their combinations by using same set of facilities. Most of the facilities have been developed specially for these experiments. The table 3A shows the details of the facilities and their versatility.

III.2. Design of Experiments:

(i) Wind Tunnel: A rectangular low aspect ratio wing with no twist and taper was manufactured. The section characteristics are as per NACA 66,012 airfoil[50]. The same mould can be used to fabricate wingsof different sweep and aspect ratio shown in Fig. 3.2(b),(c). A slender body shown in Fig.3.2 (c,d) was fabricated. The body has 4 sections A,B,C and D) as shown in Fig.3.2(j) and photo no.18 By suitably changing the parts A,B, C and D

a class of bodies can be obtained with differnet nose shapes cone angles and slenderness ratios. By suitably changing parts of Fig.3.2(j) and wing sections Fig.3.2(b) and(c) we get wing-body combinations as shown in Fig.3.2 (f),(g) and (h). By manufacturing different wings and sections A,B,C,D of Fig.3.2(j) we can generate a large number of wing-body combinations of practical interest The size and strengths of the models depends on the speed range and working sections size available in the wind tunnels. A strain gauge balance which can measure 5 components was designed out of S97 steel (B.S.S.) for 1 fairly heavy models. Another 6 (components strain gauge balance was designed for light models out of L83 light alloy,(B.S.S.) keeping in view the requirements of free flight testing and the existing low speed tunnel work. A model mounting system was designed to take up loads on the model by using 5 component balance mounted external to the tunnel. Fig.3.2 (k)(s) and (t) shows various arrangements. A calibration rig was designed to calibrate both the 5 component strain gauge balance. The capacity of the rig was kept fairly high to cater to the needs for calibrating high load range strain gauge balances.(for example balances suitable for transonic, shock loads, supersonic and high subsonic flows.).

The coordinate systems,[49] for which this calibration rig is suitable for calibration of strain gauge balances are shown in Fig.3.3.

With these facilities it is clear that a class of wings , bodies, and their combinations can be studied at low speeds.

(ii) Free-Flight: The model shown in Fig.3.2(e) was mounted externally on a five component balance. The whole assembly was mounted on the "nose boom" of a glider also termed the" aerodynamic platform. Fig.3.4 shows the sketch of the arrangement. The Rohini glider was towed by an powered aircraft 'Piper'. The level of flight for glider was kept well above compared to the airplane during tow. When sufficient height was reached the glider was released and was made to sink at a desired constant speed. Then the force measurements were done on the model for various angleSof attacks. (adjusted from the cockpit). The read-out system was a simple portable budd strain indicator. The results are discussed in Chapter V.

CHAPTER IV

PROCEDURE

IV.1. Introduction:

The whole set of experiments was carried out in the (2'x3'x5') 3-D test section (Photo 1) of the lowspeed wind tunnel of the Department of Aeronautical Engineering. As part of the test requirement, information regarding the flow characteristics in the test section was obtained through a detailed calibration of the tunnel. The strain gauge balances designed to measure the force systems on the models, were calibrated. Experiments on a rectangular wing (Photo 3,7), a body (Fig.3.2(d),(t), Phono Nos.2,17) and a cruciform wing body combinations (Fig.3.2(e), Photo No.1),were carried out. The cruciform wing body combination was tested both in the wind tunnel and in free-flight. Qualitative studies are made of the trailing vortex system for the rectangular wing model.(Phono No.8,8).

IV.2 Tunnel Calibration:[51]

Calibration of the flow in the tunnel test section is carried out for the following objectives:

a). Velocity distribution in the jet at various cross sections.(Fig.4.1).

b). Flow inclination of the jet.

c). Turbulence level. (FIG 4.2 (a))

d). Longitudinal static pressure gradient.

A). Dynamic head survey at various cross section were carried out by using a pitot-static tube (Fig.4.2). The dynamic pressure distributions in the rectangular test section are shown in Fig.(4.3 A,B,C,D). The region near the walls was avoided as the probe was subjected to strong boundary layer effects. The laminar boundary layer growth along the test section wall was calculated by using the expression[52] for a flat plate.

$$\delta_1 = 1.7208 \left(\frac{\nu x}{U_1}\right)^{1/2} \qquad \text{.....40}$$

$$\frac{\delta_1}{x} = 1.7208 \left(\frac{\nu}{U_1 x}\right)^{\frac{1}{2}} = \frac{1.7208}{\sqrt{Re_x}} \qquad \text{.....41}$$

Value of δ_1 was equal to 0.01213 inch. For a distance of 66" length. It was qualitatively observed that it was less than 0.2". (by using a thin total head tube and a stethoscope)

B). Flow inclination in the jet was measured by using three types of yaw probes(Photo No.10). All of them gave very nearly the same result. The flow inclination in the tunnel is 0.3 degrees, towards bottom wall of the test section.

C). The turbulence level in the wind tunnel section was calculated by using a sphere[53]. The turbulence factor in the tunnel is 1.35.

D). The observed static pressure gradient along the test section is plotted in Fig.4.4.

IV.3. Strain Gauge Balance Designs:

It is generally necessary to have a number of balances for different load ranges, and of different sizes for the same load range, for testing various type of models in a wind tunnel. There are many types of wind tunnel balances available in concept for design and fabrication. Each of them has it's own advantages and special characteristics. Survey of the litrature for concept revealed the characteristics which are tabulated in Table IV.A. The resistance type of strain-gauge balances are in common use as they are easy to design, fabricate, and simple to operate. The two strain gauge balances are designed in conformity with the following salient concepts[54,55,56,57,58,59].

1). The material chosen has the following characteristics:

a). good elastic properties

b). easy machinebility

c). minimum warping under heat treatment

d). compatibility with the strain gauges in respect of expansion coefficient and adhesion qualities

e). good strength and fatique properties

f). low thermo-elastic coefficients

2). Deflections under load to be minimum to give

a). low interactions

b). small clearance required between model & balance

c). elimination or reduction of model attitude control

d). high natural frequency

3). The measured strains were kept within 0.003 to 0.001 inch/inch to keep the temperature effects to a minimum.

4). Low stressed areas under gauge grid and low stress area under lead-wires.

5). Gauging area accessible for ease of locating, mounting, and servicing of gauges, but gauges should be protected to prevent damage from fouling under load or handling.

6). Precautions in choosing machining tolerences to make sure the interaction due to dimensional differences or angular misalignments be kept to a minimum.

7). Strain gauges of the same bridge are exposed to equal temperature.

8). Strain gauges locations to be placed where unwanted asymmetric high stresses do not exist.

9). The spring constants are the same for both positive and negative loads to eliminate two sets of calibration data.

The drawings of the balances giving physical dimensions are shown in Fig.4.5 and 4.6. The specification and load ranges for the balances are as follows:

A). Five-Component Balance:(Photo No.11)

Material	Steel S.97 (B.S.S.)
Physical dimensions	2"x2" square section of 9" length
Weight	1.2 kgs.
Component full load ranges	
Normal force	100 lbs.
Pitching moment	100" lbs.
Side force	100 lbs.
Yawing moment	100" lbs.
Chord force	15 lbs.

C_p travel with the model allowed from the centre of the balance is $\pm$ 1".

B). Six-component Balance: (Photo No.12,13)

Material	Light aircraft aluminium alloy L.83 (B.S.S.)
Physical dimensions	0.75" diameter cross section Length: 7.5"
Weight	0.75 lbs.
Component full load ranges	
Normal force	50 lbs.
Pitching moment	50" lbs.
Side force	50 lbs.
Yawing moment	50" lbs.
Chord force	5 lbs.
Rolling moment	50" lbs.

C_P travel with the model allowed from the centre of the balance is $\pm$ 0.75".

IV..4 Calibration Rig:

This equipment helps in loading the strain gauge balances and calibrate them, (Photo Nos.14,15,16,19) shows details of the equipment. The balance along with it's calibration fixtures, (Fig.4.7,Photo Nos.18,15,16) are fixed on the rig and taken through the axis system shown in Fig.4.8. At each position of the coordinate system shown we will be loading normal force pitching moment,sideforce, yawing moment, rolling moment and drag respectively.

The loading weights were purchased commercially and calibrated to an accuracy of ± 0.01%. The loading is done through cables. The sting end of the balances are to be of one standard dimensions, so that they can be quickly assembled on the Rig. (Fig.4.7). Otherwise adapters have to be manufactured before starting of work. The loading range capability of the rig is given below:

Normal force	1000 lbs.
Pitching moment	1000" lbs.
Side force	1000 lbs.
Yawing moment	1000" lbs.
Rolling moment	500 " lbs.
Drag	100 lbs.

Though the present balances do not use the full capabilities of the rig, it is built keeping in view future possible needs as already explained in Chapter III.

A static load deflection survey of a balance can be conducted by using the rig. This information will be useful in making corrections for angle of incidence with models in the airflow.

IV.5. Calibration of Wind tunnel Balance:

This phase of the work is very important in making the effort of many man days of design, fabrication worthwhile in terms of dependable aerodynamic measurements. Calibration

of the balance has the following objectives?[54]

a). to proof load the balance

b). to determine calibration slopes for each component

c). to determine component sensitivity

d). to determine balance interactions

e). to determine deflections under load

f). to check repeatability of load data

Although in the balance design the greatest possible emphasis is placed on eliminating sources of non-repeatable or indeterminate errors, large interactions may appear, due to dimensional limitations and manufacturing inaccuracies on balance design. However, these interactions are repeatable and can be accurately determined, so that the balance output data can be corrected with acceptable accuracy.

To load the balance accurately a fixture which simulates the model to be tested is fabricated.(Photo No.15,16,18 Fig. No.4.7). This will transmit loads to the balance in the same manner as the model during a wind tunnel test. This fixture should be attached precisely as the model is attached to the balance, and should have reference surfaces which will remain fixed with respect to the balance reference, as the balance being loaded.

The output from an indivisual bridge is due to it's own component loading plus that due to loading of other components. The first one is called as "component output", and the second, as "interaction output". Thus for example the normal force output can be expressed as $\theta_1 = f(z, x, y, l, m, n)$ is the normal force output. This can be written as

$$\theta_1 = f(z, x, y, l, m, n)$$
$$= N_1(z) + I_1(x, y, l, m, n)$$

where

$N_1(z)$ = normal force component output

$I_1(z)$ = normal force interaction output

We assume here only linear interactions. Writing down in general terms the output of each indivisual bridge as below will simplify the procedure for evaluating calibration constants for a balance.

$$\theta_1 = a_{11}z + a_{12}x + a_{13}y + a_{14}l + a_{15}m + a_{16}n$$
$$\theta_2 = a_{21}z + a_{22}x + a_{23}y + a_{24}l + a_{25}m + a_{26}n$$
$$\theta_3 = a_{31}z + a_{32}x + a_{33}y + a_{34}l + a_{35}m + a_{36}n$$
$$\theta_4 = a_{41}z + a_{42}x + a_{43}y + a_{44}l + a_{45}m + a_{46}n$$
$$\theta_5 = a_{51}z + a_{52}x + a_{53}y + a_{54}l + a_{55}m + a_{56}n$$
$$\theta_6 = a_{61}z + a_{62}x + a_{63}y + a_{64}l + a_{65}m + a_{66}n$$

.....42

This can be written down further as

$$[\Theta] = [A][F]$$

$$[\Theta] = \begin{bmatrix} \Theta_1 \\ \Theta_2 \\ \Theta_3 \\ \Theta_4 \\ \Theta_5 \\ \Theta_6 \end{bmatrix} \qquad [A] = \begin{bmatrix} a_{11} & a_{12} & a_{13} & a_{14} & a_{15} & a_{16} \\ a_{21} & a_{22} & a_{23} & a_{24} & a_{25} & a_{26} \\ a_{31} & a_{32} & a_{33} & a_{34} & a_{35} & a_{36} \\ a_{41} & a_{42} & a_{43} & a_{44} & a_{45} & a_{46} \\ a_{51} & a_{52} & a_{53} & a_{54} & a_{55} & a_{56} \\ a_{61} & a_{62} & a_{63} & a_{64} & a_{65} & a_{66} \end{bmatrix}$$

$[\Theta]$ = output Matrix $\quad$ $[A]$ = coefficient Matrix

$[F]$ = Force Matrix

Each diagonal term of the Matrix $[A]$ is the component output slope. The other coefficients of the Matrix $[A]$ are the slopes due to interactions.

The aim of a good balance design is to get (i) the coefficients other than the principal diagonal coefficients equal to zero in the Matrix $[A]$ and (ii) to get as high a value as possible for the principal diagonal coefficients.

This means , a sensitive, interaction free balance. The criteria is then of diogonalizing the Matrix [A]
The terms a_{ij} , $i \neq j$ should be expressed in terms of the geometry and tolerances of manufacture of the balance indimensionless form. An approach in this direction may contribute to the design of balances.

The force Matrix in terms of inverse of coefficient Matrix and the output Matrix is

$$[F] = [A]^{-1} [\theta] \qquad \ldots\ldots 44$$

The Matrix $[A]^{-1}$ is a fixed property of the balance, so that for any measured strain Matrix the corresponding force Matrix is obtainable. The results of calibration of the five component balance is plotted in Fig.4.9. The six component balance is fabricated and strain gauged. As the wiring is not yet ready the calibration data is not available. All the experiments were carried out by using five component balance.

IV.6. Wing Model:

A rectangular symmetrical wing of aspect ratio 2.5 with no twist and taper was fabricated. (Photo No.3,7). The airfoil section is of NACA 66_1-012 data[49]. As the wing has a symmetrical cross section the top half surface to

the left and bottom half surface to the right is tapped for pressures. A total of 12 chord positions pressures can be tapped one at a time. Each chord contains 13 pressure taps. At various angles of attack in the flow the pressures were measured and simultaniously, the balance output were taken and the results are shown in Fig. 4. 10, The model was exited by a step function without wind and with wind. The time for decay to half amplitude in both cases are calculated and compared. This gives an idea of the aerodynamic damping on the wing. (Appendix A).

IV.7. Body Model:

A slender body is fabricated in four separable parts. (Photo No.17). The reasons for doing so has already been explained in Chapter III. The distribution of pressure coefficients along the model is measured at various angles of attack in the flow. The same is plotted in Fig.4.11. Simultaneously balance outputs were recorded and plotted. (Fig.4.11).

Dynamic measurements are done on the body, just on the same lines as for the wing. The results are in Appendix A, The body mounted in the tunnel test section is shown in Photograph No.2.

IV.8. Cruciform Wing-Body Combination:

A slender body with cruciform wings is shown in Photograph No.1. This model was tested for force measurements using the five component strain gauge balance. First it was airborne on an "Aerodynamic Platform" as explained in Chapter III. Then the same model was tested in a wind tunnel. The results are shown in Fig. 4.13.

Dynamic measurements are carried out on this model, as in the case of wing and body mentioned above. The results are shown in Appendix A.

IV.9. Vortex Studies:

The trailing vortex system for the rectangular wing at negative stalling angle of attack is visualized by using a tuft grid. (Photo No.8,9). The grid is moved, behind the wing and observed trailing vortices. The results are shown in Fig.4. 14 The following points were observed in these studies:

a). The two trailing tip vortices are symmetrically placed.

b). The starting of tip vortex takes place just about of the inboard.

c). The tip vortex is circular in shape.

d). The size of the vortex increases with the distance

e). The vortex system moves more and more inboard with distance.

f). Appears to have an overlapping shedding frequency over and above the vortex system

CHAPTER V

DISCUSSION AND CONCLUSIONS

V.1. Introduction:

In Chapter I, the various theories for wings, bodies, and their combination in 3-dimensional flows were reviewed. In Chapter II, the formulation of the problem was done. In Chapter III, the experimental technique used in the present investigation is explained. In Chapter IV, the procedures followed to obtain the experimental results are discussed. The results obtained from such procedures are discussed in the following articles.

V.2. General:

The flow characteristics in the tunnel test section are very suitable for experiments of pressure plots, and force measurements. The corrections regarding static pressure gradient, flow inclination are negligible. The high value obtained for the turbulence factor is on higher side as the turbulence sphere used for measurement was not either spherical or smooth precisely. It can be expected to be much less than 1.35. It is necessary to make a more accurate measurement of the turbulence factor using a better sphere than was available for the present experiments. As for the present investigations it is hoped this will not effect the results seriously.

The strain gauge balance calibration was conducted only on the five component balance. The six component

balance is now ready for wiring. After wiring the balance can be calibrated and used for further investigations. From the calibration results of the five component strain gauge balance it is seen that the balance measurement are well within 0.1% of the full load for all the arms of the balance.

V.3. Wing Model:

It may be seen from Fig.4.9 that the chordwise pressure distribution agrees well with the theoretical values. The descripency in the experimental points on chord stations 5,6 are due to the influence field of the support system. (Photo No. 3,7). The spanwise lift distribution calculated by Weissinger's method and Woodward's method agree very well with the experimental results of pressure plotting. The force coefficients obtained by pressure plots agree well with the force measurements done by the five component strain gauge balance. The only discropency occures in the drag coefficient plot. The drag coefficients obtained by pressure plots do not agree with the measured drag force, one of the reasons being that the pressure plots do not included the induced drag. The trailing vortex system was studied qualitatively. The location and field of the trailing vortices are plotted from a survey of the tufts grid behind the wing. A closer measurement of the down-wash field of the wing and wing-body combination will be necessary to estimate the influence field due to the interference.

The dynamic measurements conducted on the wing showed that it is a highly damped system in the air-flow for pitching disturbances. From a comparison of the measurements of the damping in pitch of the wing alone with and without wind (Appendix A). The time for decay to half the reference amplitude for the wind-on case was 1/3, that of the wind off case. The inertia system of the balance and support are treated as constant in this case.

V.4. Body Model:

A body model for pressure plots was tested in the wind tunnel. The results show a good agreement with the theoretically calculated values for a varying source ring distribution. At zero degree incidence the flow is axisymmetric over the body. This checks indirectly the flow characteristics of the test section also. The discrepancy in the hiegher angles of attack can be attributed to

a). the viscous effects

b). the interference field due to support system

c). influence of base pressure upstream

The more predominant of them is the interference of model support system. The other contributions can be assessed only after further investigations.

The flow over the cone is smooth at lower angle of attack. At hiegher angles the flow may have separated and possibly reattached to the body. The conclusions anyway are open for further investigations. From an integration of the

pressures over the body it is seen that most of the lift of the body arises from the conical portion.

The values of the force coefficients obtained for this model from strain gauge balance are also plotted. The damping coefficient in pitch is small for this body but is found to be $\frac{1}{2}$ that of the wind off case.

V.5. Cruciform Wing-body Model:

With a view to develop a technique of testing aerodynamic models airborne, particularly for V/STOL models an attempt was made to test this wing-body model both in "free-flight" and in the wind tunnel. The same five component strain gauge balance was used in both experiments. A plot of the results reveal that a good future exists there for testing airborne models. The scatter in free-flight data can be minimised by designing a low interference model support system. This technique eliminates the strong wall interference effects present in conventional wind tunnels on V/STOL models.

V.6. The wing-body Combination:

Theoretical calculations using the method of Woodward's[20] were made for the present wing-body combination*. The interference field of the body on the spanwise lift distribution of the wing for sweep angles 0°,45°,60° were calculated. Measurements for comparing these values with experimental values are to be continued further.

* Fig 3.2(f) and 5.1.

V.7. Conclusions:

The present work has formed a basis for further work in the field. It is possible to investigate many bodies, wings and their combinations and generate valuable aerodynamic data for wing-body combination at low speed.

REFERENCES

1. Glauert,H., Airfoil and Airscrew Theory, Cambridge Univ. Press, 1937

2. Lotz,I., Berechnung der Auftriebsverteilurg beliebig geformter Flügel.Z.Flugtech. U.Motorluftschiffahrt 22,189-95,1931

3. Multhopp,H., DIe Berechnung der Auftn-ebsverteilung von tragflugetov. Luftfhrtforschung 15,153-69,1938 (RTP translation 2392)

4. Gates, S.B., An Analysis of a Rectangular Monoplane with Winged Tips, British Research Council Report and Memorandum, 1175, 1928

5. Hildebrand,F., A Least Square Procedure for Solution of the Lifting Line Integral Equation, NACA Tech.Note 925,1944

6. Sears,W.R., A New Treatment of Lifting Line Theory, with Applications to Rigid and Elastic Wings, Qurt.Appl.Math.6,3,239-255,1948

7. Weissinger, J., The Lift Distribution of Swept Back Wings, NACA Tech. Memo. 1120, 1947.

8. Blenk, H., Der Eindecker als tragende Wirbelflache,Z, angew, Math, Mech. Vol.5, pp.36-47, 1925

9. Falkner, V.N., The Calculation of Aerodynamic Loading On Surfaces of Any Shape, Memor.Aero.Res.Comm.Lond. No.1910, 1943

10. Schlichting, H. and H.H.B.M. Thomas, Note on the Calculations of Lift Distribution of Swept Wings, Royal Aircraft Establishment Rep. No.Aero2236, 1947

11. De Young, J. and Barling, W.H., Corrections of Additional Span Loadings Computed by the Weissinger Seven-Point Method for Moderately Tapered Wings of High Aspect Ratio, NACA Tech. Note 3500, 1955

12. Diedrich and Zlotnick, Calculated Spanwise Lift Distributions and Aerodynamic Influence Coefficients for Swept Wings in Subsonic Flow, NACA Tech.Note 3476,1955

13. Sears, W.R., Editor - General Theory of High Speed Aerodynamics, Vol.VI, Sec 12,13,14 (Princeton series)

14. Harmon, S.M., Correspondence Flows for Wings in Linearized Potential Fields at Subsonic and Supersonic Speeds, N.A.C.A. Tech. Note. 2303, 1951

15. Kainer, J., Equations for the Loading on Triangular Wings having Supersonic Leading and Trailing Edges Due to Various Basic Twist Distributions, J. Aeronaut. Sci.,20,469-476,1953

16. Reference 13, Vol.VI,D. Eqn.(12-29).

16'. Evvaard, J.C., Use of Source Distributions for Evaluating Theoretical Aerodynamics of Their Finite Wings at Supersonic Speeds, NACA Rept. 951, 1950

17. Cohen, D., The Theoretical Lift of Flat Sweep Back Wings at Supersonic Speeds, NACA Tech. Note 1555,1948

18. Etkin, B. and Woodward, F.A., Lift Distribution on Supersonic Wings with Subsonic Leading Edges and Arbitrary Angle of Attack Distribution, Art. in Second Can.Sym. on Aerodynamics Proc. 25-26, Univ. Toronto Int, Aerophys, 1954.

19. Neuringer, J., A Grid Procedure for Calculating Aerodynamic Loads on Symmetric Elastic Delta Wings with Supersonic Leading Edges., Rep. Aviation, Rept. ETL-6,1952

20. Woodward, F.A., A Unified Approach to the Analysis and Design of Wing-body Combinations at Subsonic and Supersonic Spees, AIAA Paper No.68-65, AIAA Aerospace Sciences Meeting Newyork, 1968

21. Kuchemann and Weber, Aerodynamics of Propulsion, McGraw Hill Publishing Co., 1953

22. Jack, N, Nielsen, Missile Aerodynamics, McGraw Hill Book Co.,1960 (Chapter 4)

23. Lennertz, J., NACA TN 400, 1927

24. Wieselsberger, C. and Lennertz, J., Aerodynamic Theory Vol.IV, div.K, Chap.III, W.F. Durand ed. Julius Springer (Berlin)1935

25. Pepper Perry, A., NACA TN 812, 1941

26. Multhop, H., NACA TN 1036, 1942

27. Zlotnick,M and Robinson, S.W.Jr.,
NACA RM L52J279, Jan.1953

28. Spreiter, J.R., NACA, Rept. 962, 1950

29. Ward, G.N.,Jour. Mech. & Math. Applied Math.
Vol.2, pp.75-97, 1949

30. Nanweiler, P., British ARC Corpn.,No.58(13,696),1951

31. Kahane, A., Republic Aviation Corpn., Rept. No.KDR-57-
152, Nov.,1952

32. Mireles, H., NACA TN 3105, 1954

33. Lawrence, H.R., J. Aero.Sci.,Vol.18,No.10,
pp 683-695, Oct.,1951

34. Flax, A.H. and Larrence, H.R., Proceedings of 3rd
Anglo-American Aeronautical Conference,pp 363-398,1951

35. Lagerstrom, P.A. and Graham, M.E., Douglas Aircraft Co.
Rept. No.SM-13743, 1950

36. Moskowitz,B., NACA TN 2669, April 1952.

37. Adams and Sears, Jour. of Aero. Sci. Vol.20, No.2,
pp 85-98, 1953

38. Kirley and Robinson of A., College of Aeronautics
Cranfield, Rep. No.7, Apr.1947

39. Ferrari, C., J. Aero. Sci., Vol.15, No.6,pp 317-
336, June 1948.

40. Ferrari, C., J. Aero. Sci., Vol.16, No.19,
pp. 542-546, Sept.,1949

41. Nielson, J.N., Supersonic Wing-body Interference
Thesis, Cal.Tech.Instt. 1951

42. Lagerstorm, P.A. and Van Dyke, M.D.,
Douglas Aircraft Co. Rept., S.M.13432, June 1949

43. Lawrence, H.R. and Flax, A.H.,
J. Aero. Sci, Vol.21, No.5, May 1954.

44. Nielsen,J.N. and Pitts, W.C.,
NACA TN2677, April 1952

45. Laitone, E.V., J. Aero. Sci. Readers Forum,
Vol.16, No.8, pp.510, Aug.,1949

46. Robinson and Lauremann, Wing Theory,
Cambridge Unvi. Press, 1956

47. Gupta, S.C., M.Tech. Thesis, Dept. of Aero. Engg., IIT Kanpur, June 1971

48. Bera, R.K., M.Tech. Thesis, Dept. of Aero. Engg., IIT Kanpur, Aug.,1969

49. Abbot, Doenhoff, Theory of Wing Section, Dover Publications, 1949

50. Perkins, Hage, Airplane Performance Stability and Control, Weiley Pub.,

51. Pope, Harper, Low Speed Wind tunnel Testing, John Wiley and Sons Inc., Newyork, 1966

52. Howarth, Modern Levelopments in Fluid Mechanics.

53. Pankrust & Holder, Wind Tunnel Technique

54. Pope, Goin, High Speed Wind Tunnel Testing

55. Donovan and Lowrence, High speed Problems of Aircraft and Experimental Methods, Princeton Series, Vol.VIII

56. Anderson, J.R., AGARDOGRAPH, Memorandum No.AG10/176,1953

57. Wood, J. and Tiffany, A, ARC, Bedford, 1958

58. Anderson, J.R., RAE Tech. Note. 2434

59. Hansen, AGARDOGRAPH 9,1953

60. Aerodynamics at NLR, Tech. Rept. of National Aerodynamic Aerospace Laboratory, Amsterdon, Netherlands, Jan.1969

APPENDIX A*

The equation of motion for a single degree of freedom pitching system with no air loading or air damping but with a mechanical spring that tends to return the model to an equilibrium position is as follows:

$$I\ddot{\theta}_f + C_1\dot{\theta}_f + K_1\theta_f = 0 \qquad \text{.....(1)A}$$

with air:

$$I\ddot{\theta} + (C_1 + C_2)\dot{\theta} + (K_1 + K_2)\theta = 0 \qquad \text{.....(2)A}$$

Solutions of eqns. (1)A and (2)A are

$$\omega_f = \frac{1}{2\pi}\sqrt{\frac{K_1}{I} - \left(\frac{C_1}{2I}\right)^2} \qquad \text{.....(3)A}$$

$$P_f = \frac{1}{\omega_f} \qquad \text{.....(4)A}$$

$$C_1 = \frac{1.5863\,I}{(T_{1/2})_f} \qquad \text{.....(5)A}$$

$$K_1 = I\left[\frac{4\pi^2}{P_f^2} + \left(\frac{0.69315}{(T_{1/2})_f}\right)^2\right] \qquad \text{.....(6)A}$$

$$\omega = \frac{1}{2\pi}\left[\frac{K_1 + K_2}{I} - \left(\frac{C_1 + C_2}{2I}\right)^2\right]^{1/2} \qquad \text{.....(7)A}$$

$$P = \frac{1}{\omega} \qquad \text{.....(8)A}$$

$$C_2 = 1.3863 I \left[\frac{1}{T_{1/2}} - \frac{1}{(T_{1/2})_f} \right] \qquad \ldots.(9)A$$

$$K_2 = I \left\{ 4\pi^2 \left(\frac{1}{P^2} - \frac{1}{P_f^2} \right) + (0.69315)^2 \left[\frac{1}{(T_{1/2})^2} - \frac{1}{(T_{1/2})_f^2} \right] \right\}$$

$\ldots..(10)A$

where subscript f is for case of without air

I = inertia of the model about the axis of rotation slugs/ft^2

θ = angle of attack of the model to the equillibrium position (usually zero, radians)

C_1 = a system damping constant ft lbs/(radians/sec)

K_1 = a system spring constant (ft lbs/radians)

C_2 = aerodynamic "damping moment" per unit value of ft lbs/(radians/sec)

K_2 = aerodynamic "restoring ~~meemtn~~" per unit value of ft lbs/radians

ω = model pitching frequency cycles/sec.

P = period of one cycle of oscillation sec

$T_{1/2}$ = time required for the amplitude of model oscillation to decay from reference value to a value equal to half the reference value sec.

REF. FIG A 1

TABLE A(1)

Sl. No.	Case	From Measurements (Graphs) P_f SEC/CYC	ω_f CYL/SEC	$(T_{1/2})_f$ SEC	P SEC/CYC	ω cycles/SEC	$T_{1/2}$ SEC
1.	*Wing-body combination (Centure Rocket Model) $\alpha = 0^\circ$	0.3	3.34	1.8	0.2	5.0	2.1
2.	*Rectangular wing alone $\alpha = 0^\circ$	0.16	6.67	2.24	0.140	7.15	0.16
3.	*Body alone (Pressure Model) $\alpha = 0^\circ$	0.3	3.34	1.16	0.35	2.58	2.25
4.	" $\alpha = +11^\circ$				.300	3.334	2.00

* All the models were exited by a step forcing function while they were mounted on the strain gauge balance. Ref. fig A-1

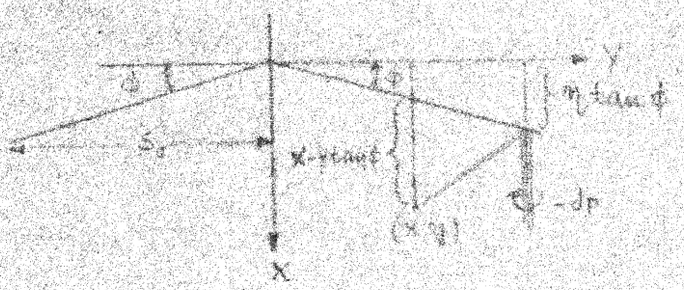

FIG 2.1. COORDINATES FOR WEISSINGER THEORY

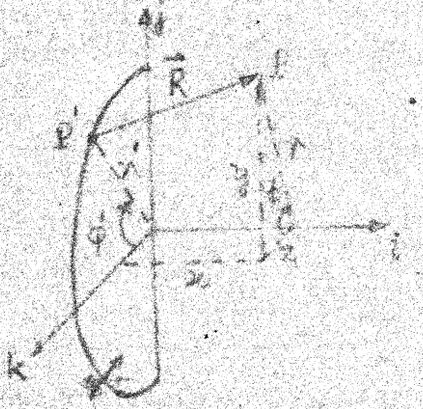

FIG 2.2. CIRCULAR SOURCE RING

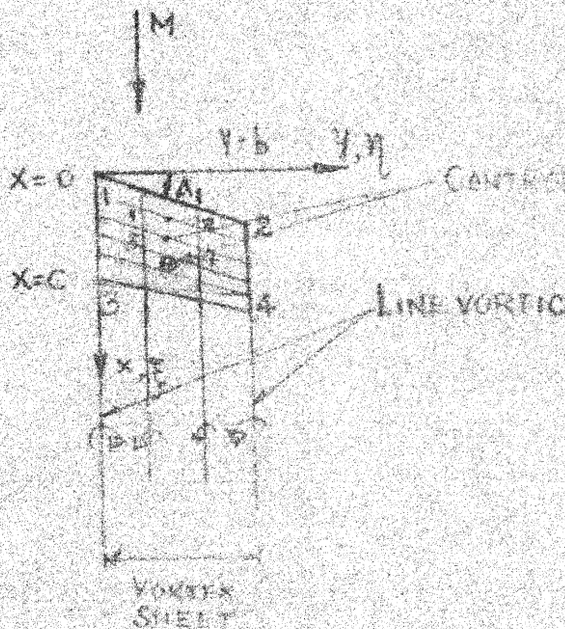

FIG 2.3. CONSTANT PRESSURE PANEL WITH TRAILING VORTEX SHEET

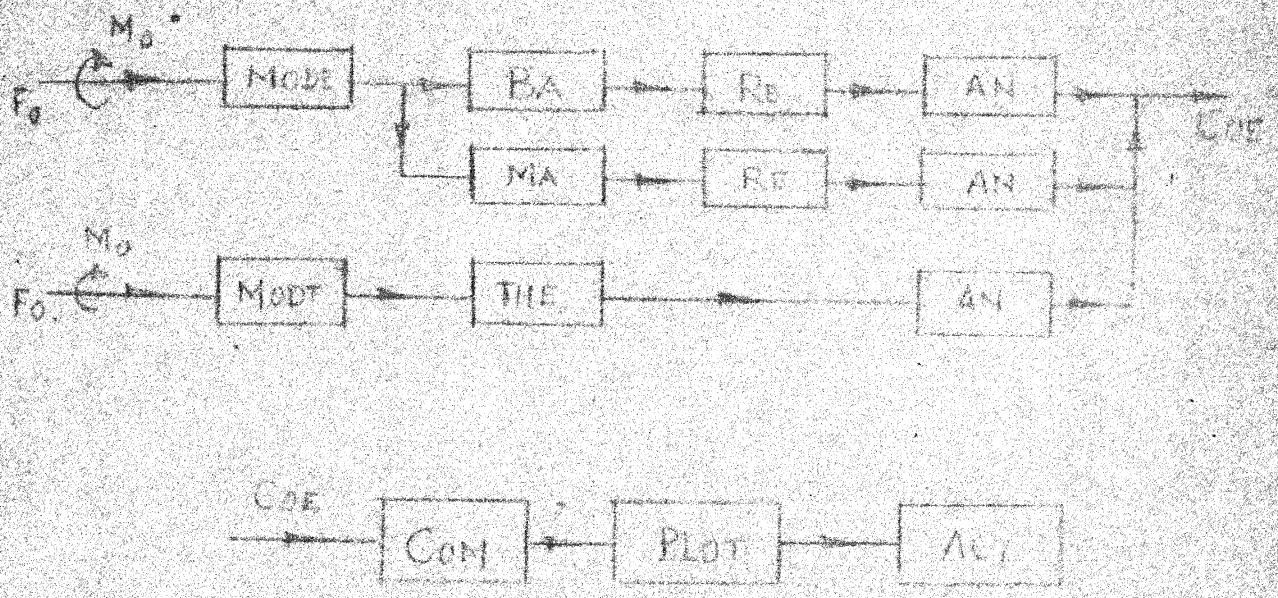

MODE. EXPERIMENTAL MODEL; BA. BALANCE OR ANY TRANSDUSER; RE. READOUT OR RECORDER (CAMERA MANUAL, AUTOMATIC OR SEMI AUTOMATIC)
AN. ANALYSIS; COE. COEFFICIENTS; MODT. MODEL THEORETICAL; THE. THEORY; AN. ANALYSIS; COM. COMPARISON; PLOT. PLOTS; F_0. FORCE; ACY. ACCURACY OF THE METHODS; M_0. MOMENT; MA. MANOMETER.

FIG. 3.1. SCHEMATIC BLOCK DIAGRAM

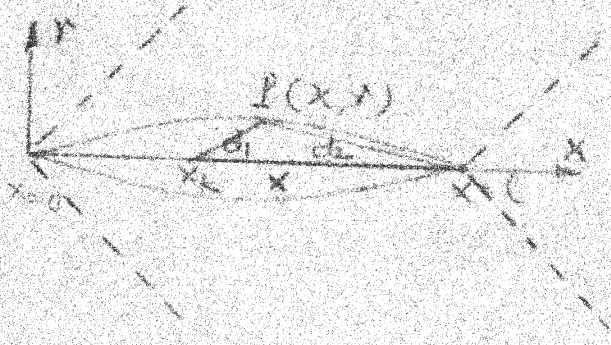

FIG. 2.4. LINE SOURCE.

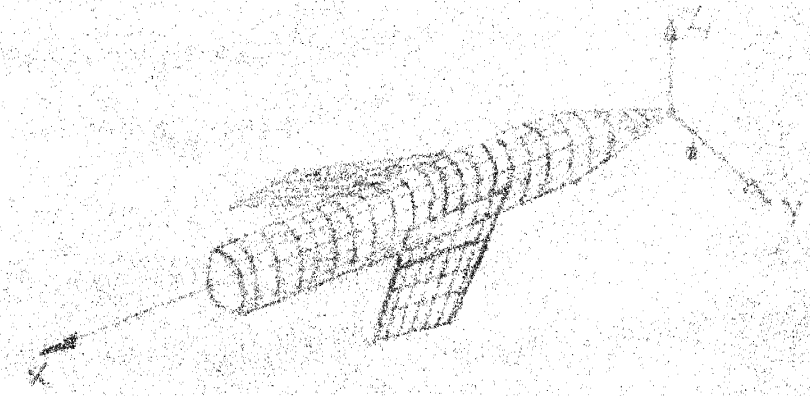

Fig. 2.7. Typical wing-body combination

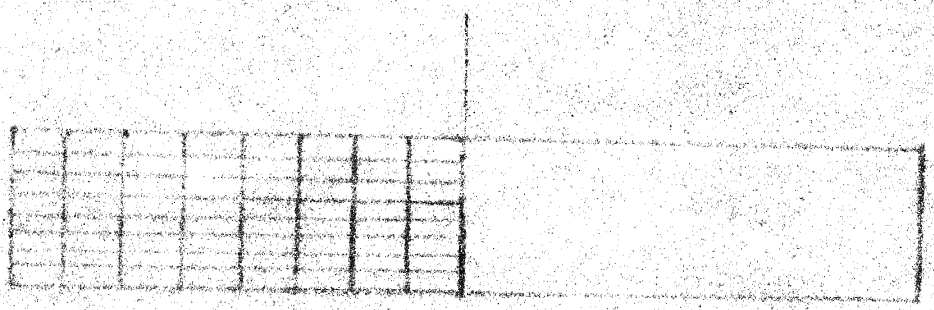

Fig 2.8(a) Wing

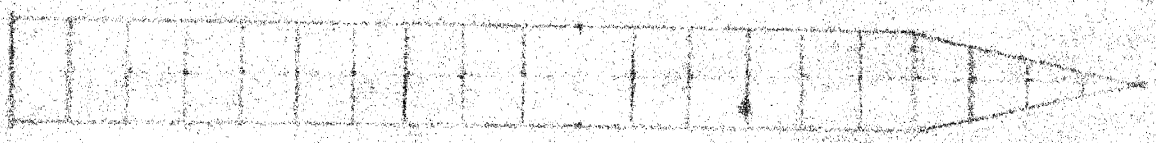

Fig 2.8 (b) Body.

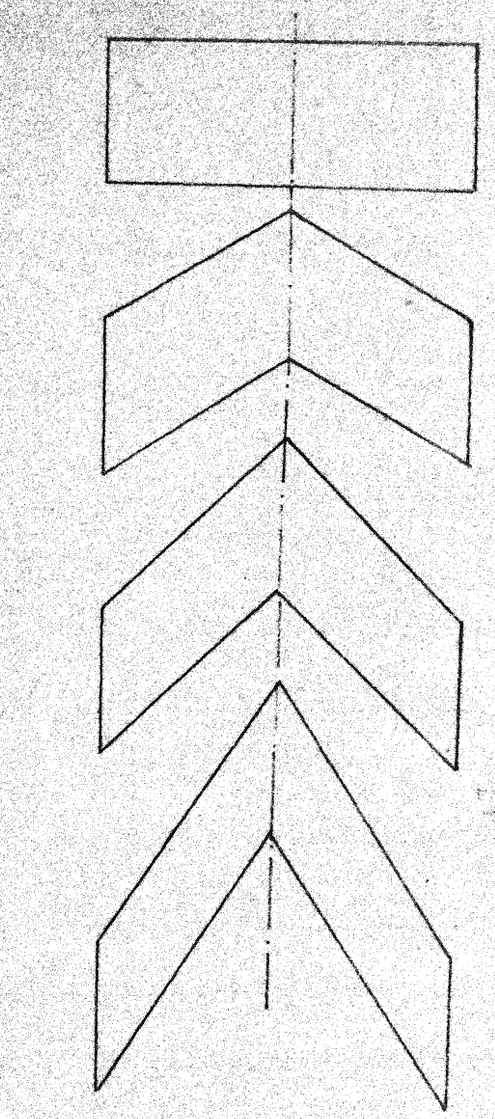

RECTANGULAR WING
SECTION NACA 66_012
AR=2.5 λ = 1.000

FIG. 3.2 (a) SEE PHOTO. NO 3, 7.

$\Lambda = 30°$

FIG. 3.2 (b)

$\Lambda = 45°$

FIG. 3.2 (b)

$\Lambda = 60°$

FIG 3.2 (c)

BODY

FIG. 3.2 (d)
SEE PHOTO NO 2,

$\Lambda = 0$

WING BODY

FIG 3.2
(f)

FIG 3.2, WINGS AND BODIES

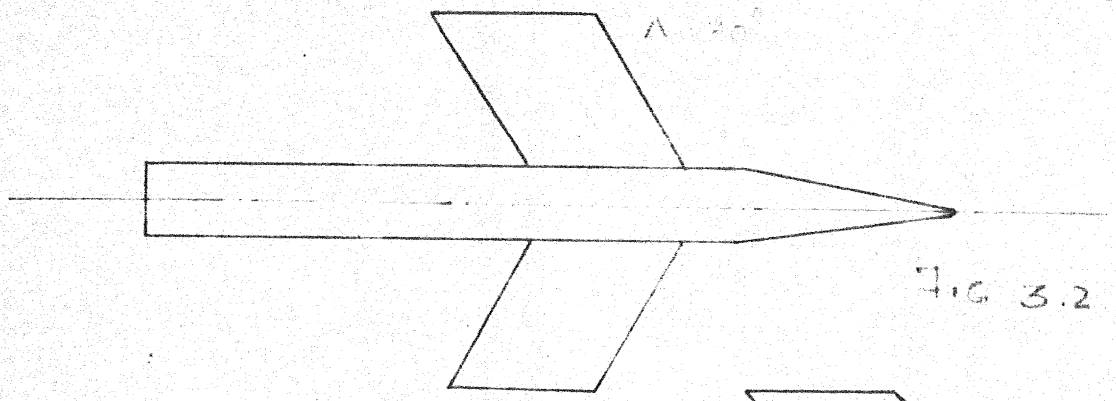

FIG 3.2 (f)

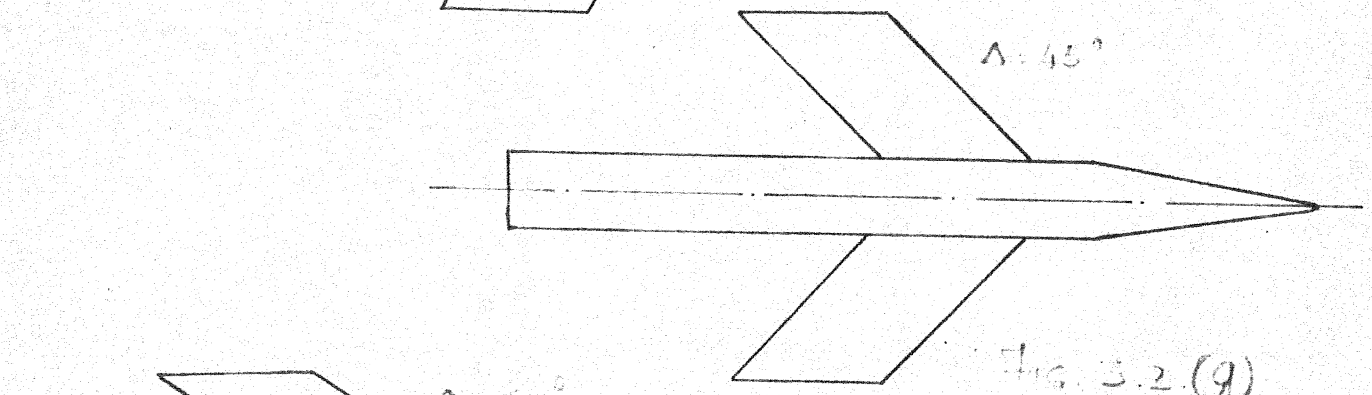

FIG 3.2 (g)

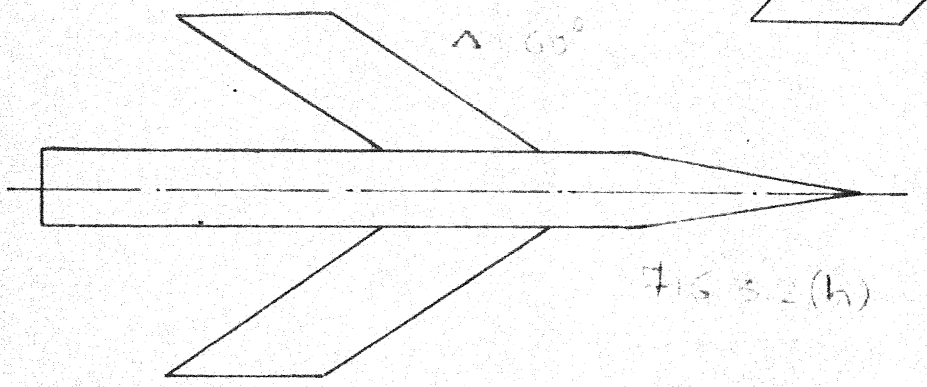

FIG 3.2 (h)

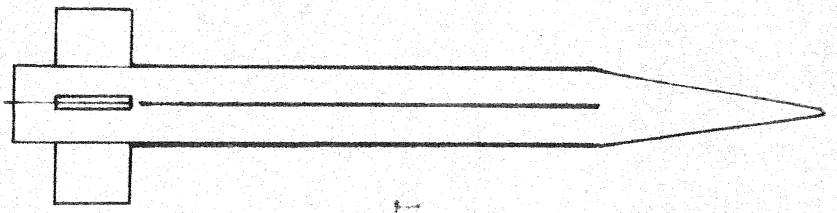

FIG 3.2 (e)

CENTURE ROCKET MODEL

SEE PHOTO NO. 1.

FIG 3.2 WINGS AND BODIES

FIG. 3.2. WINGS AND BODIES.

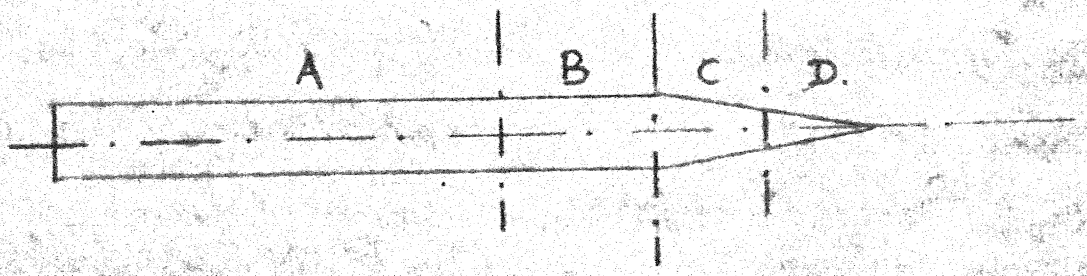

FIG. 3.2.(j)
SEE PHOTO. 17.

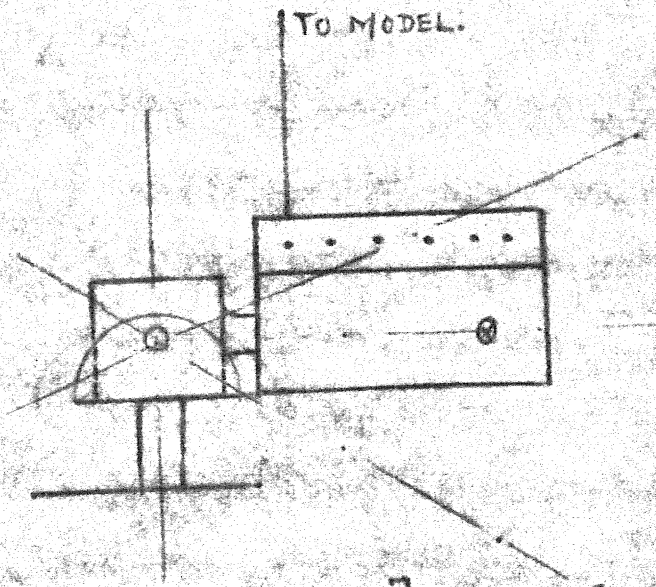

FIG. 3.2.(k) MODEL SUPPORT.
SEE PHOTO. 6.

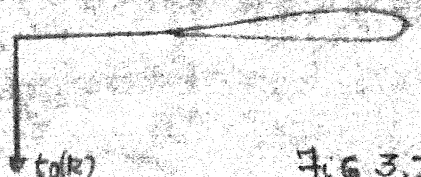

FIG 3.2 (l). SEE PHOTO 3.
WING MODEL.

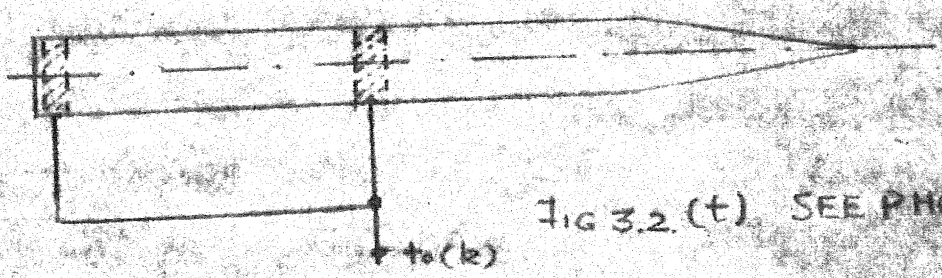

FIG 3.2. (t). SEE PHOTO 2.

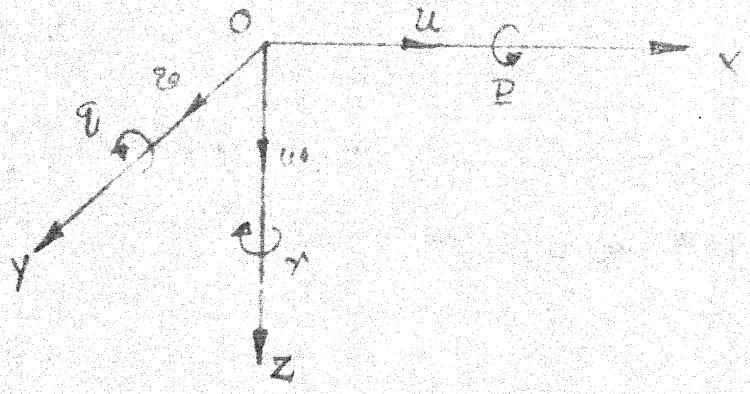

FIG 3.3 MODEL AXIS SYSTEM

AXIS	FORCE ALONG	MOMENT ABOUT	LINEAR VELOCITY	Angular displacement	Angular velocity	Inertia
x	F_x	L	u	ϕ	p	I_x
y	F_y	M	v	θ	q	I_y
z	F_z	N	w	ψ	r	I_z

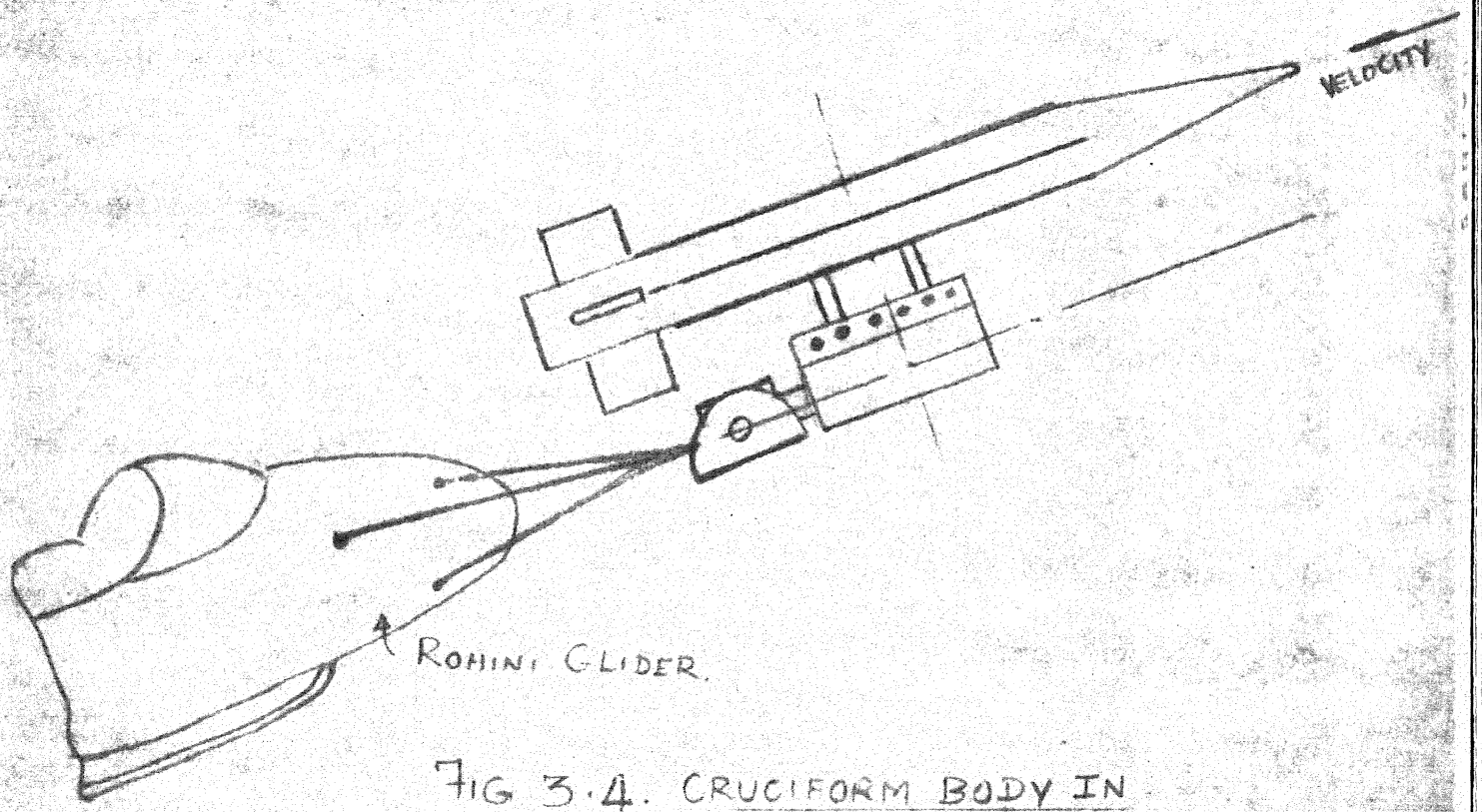

FIG 3.4. CRUCIFORM BODY IN FREE FLIGHT.

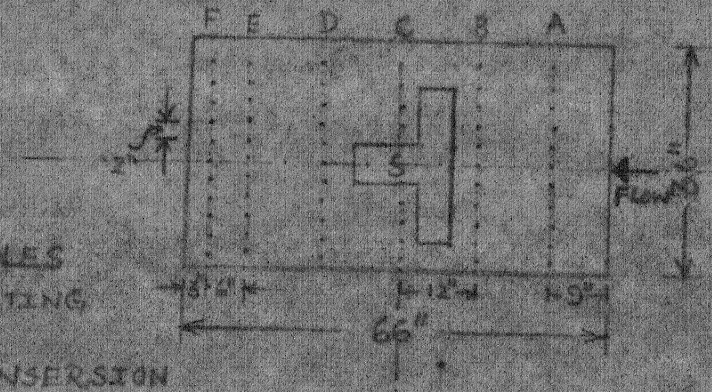

· = 3/4" dia HOLES FOR INSERTING PROBES.
S = MODEL INSERSION CUT OUT.

FIG. 4.1 PLAN OF TEST SECTION.

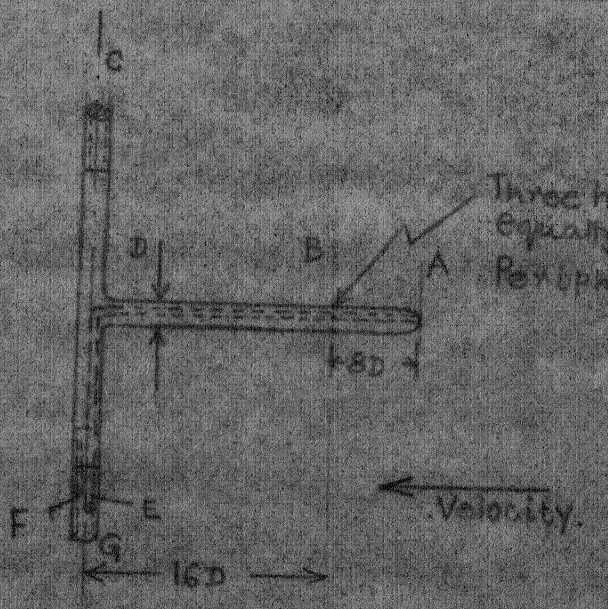

A: E: Total-head
B: F: static head
D: Diameter = 3/4"
C: to top WALL OF TEST SECTION.
G: to Bottom WALL OF TEST SECTION.

FIG 4.2 PITOT STATIC TUBE.

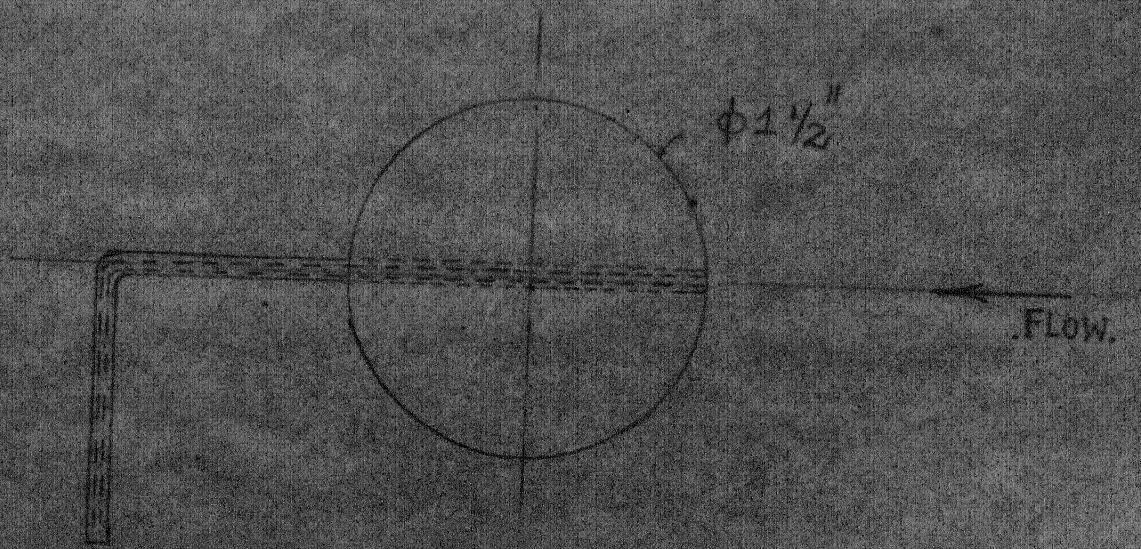

FIG. 4.2(a) TURBULANCE SPHERE

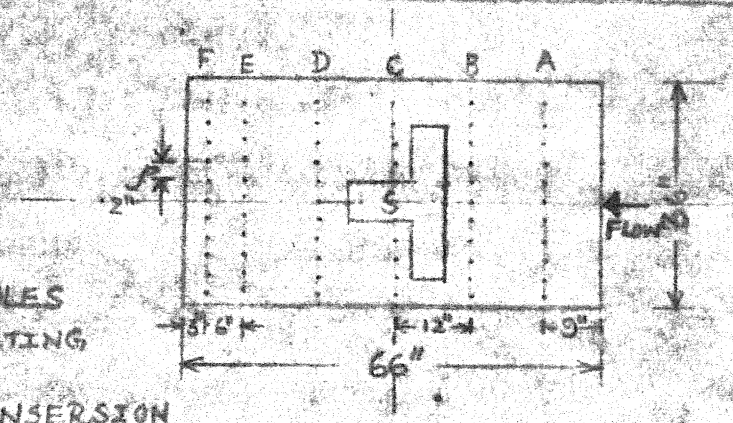

• = 3/4" dia HOLES FOR INSERTING PROBES.
S = MODEL INSERSION CUT OUT.

FIG 4.1 PLAN OF TEST SECTION.

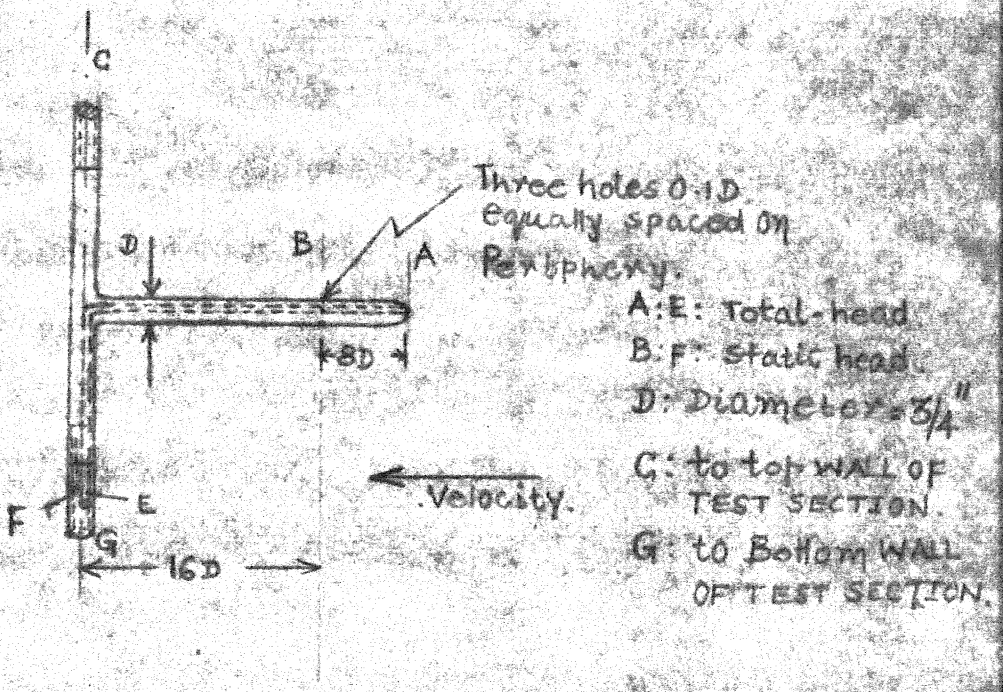

FIG 4.2 PITOT STATIC TUBE.

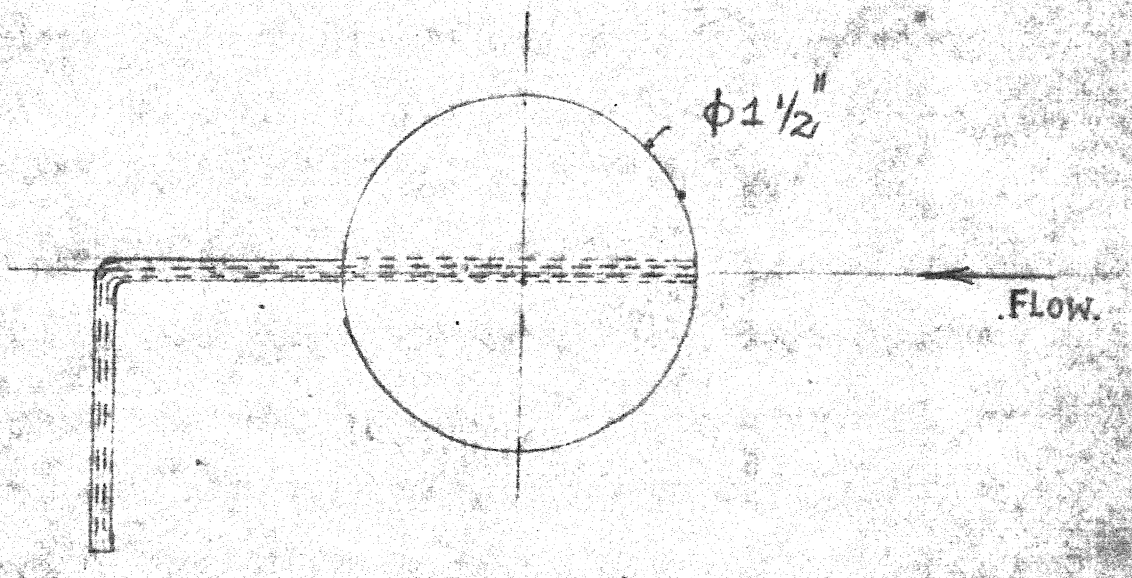

FIG. 4.2(a) TURBULANCE SPHERE.

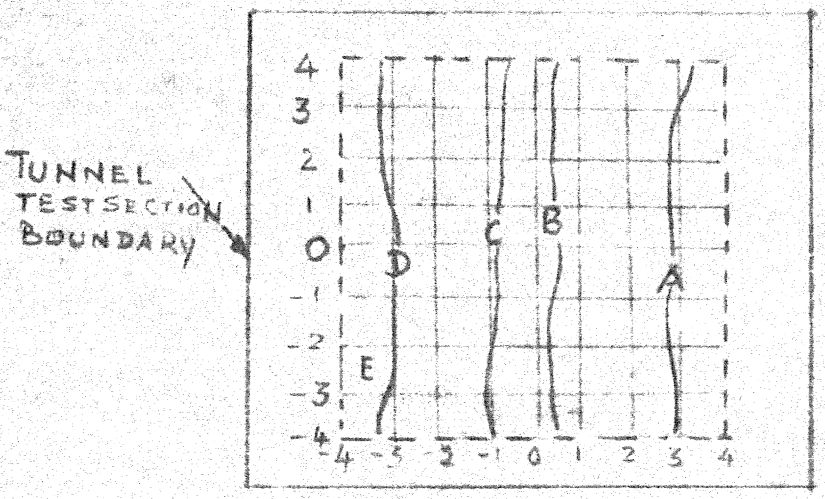

	ψ^*
A	1·000
B	0·996
C	1·010
D	0·995
E	1 019

4·3 (a) SECTION (A) of fig 4·1.

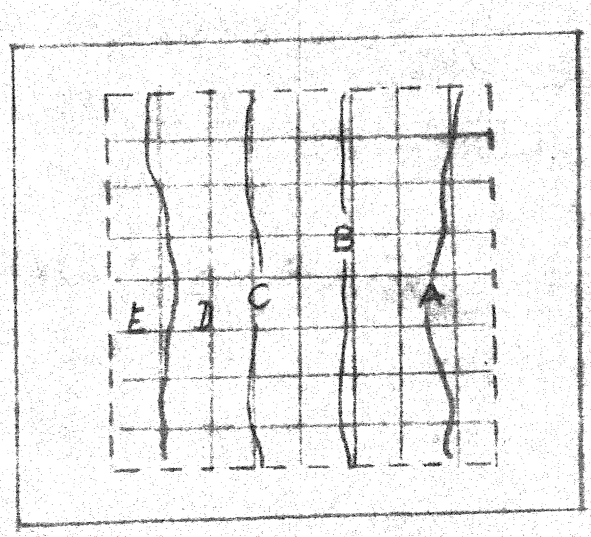

	ψ^*
A	1·010
B	1·000
C	1·020
D	1·000
E	1·020

4·3 (b) SECTION (C) of Fig 4·1.

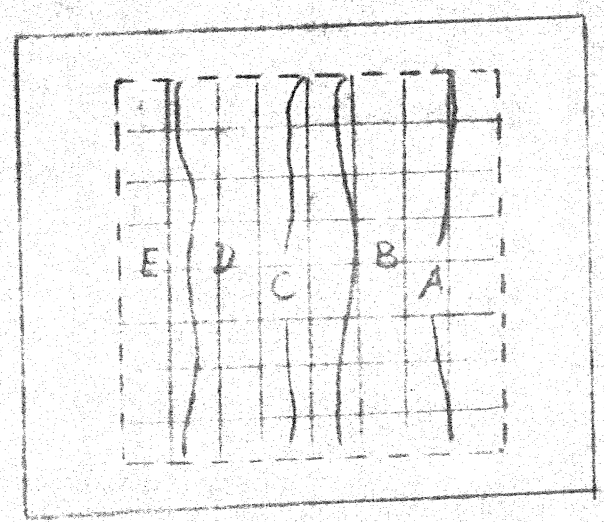

	ψ^*
A	1·020
B	1·000
C	1·025
D	1·000
E	1·020

4·3 (c) SECTION (D) of Fig. 4·1.

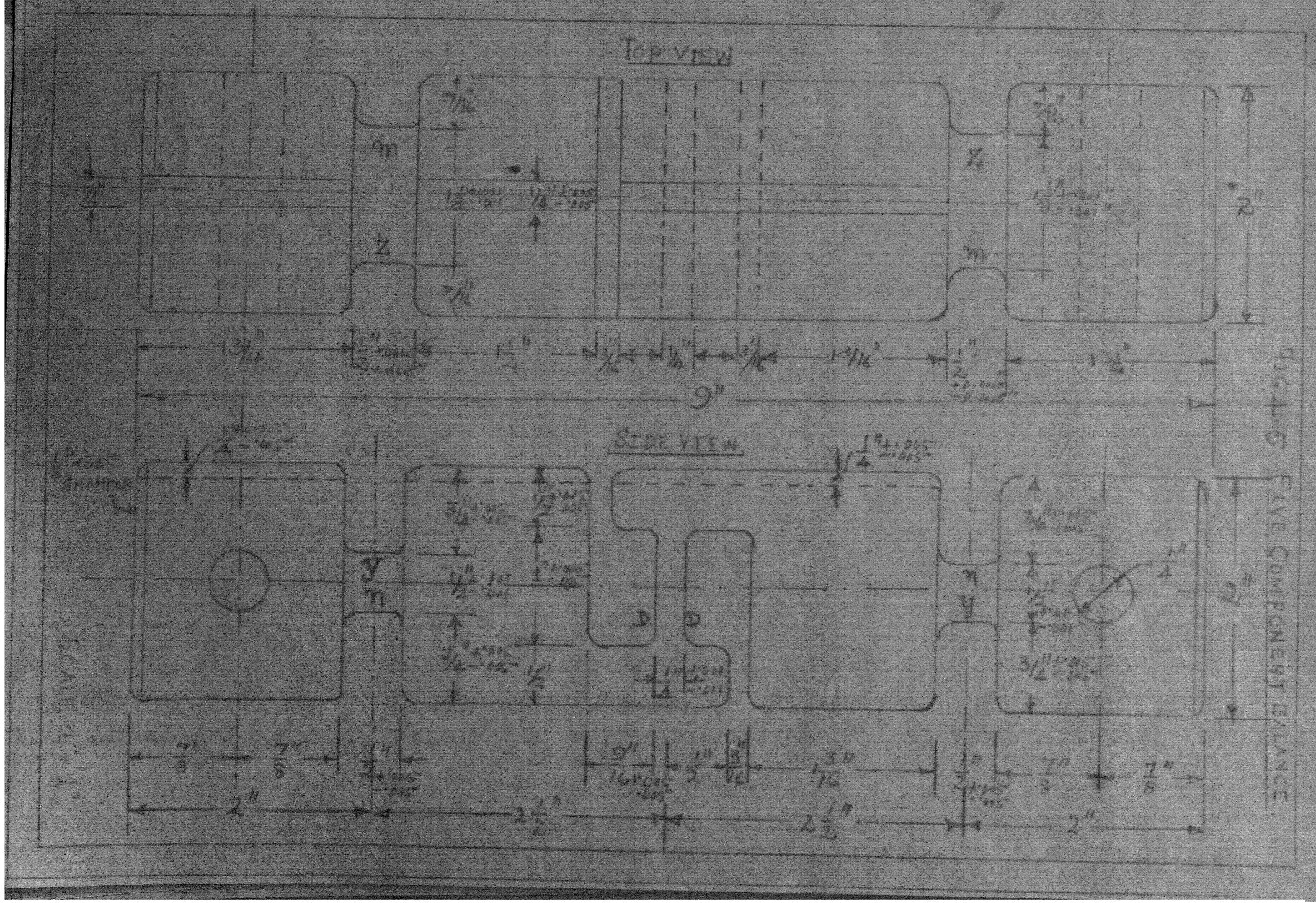
TOP VIEW
SIDE VIEW
9"
2"
FIVE COMPONENT BALANCE.

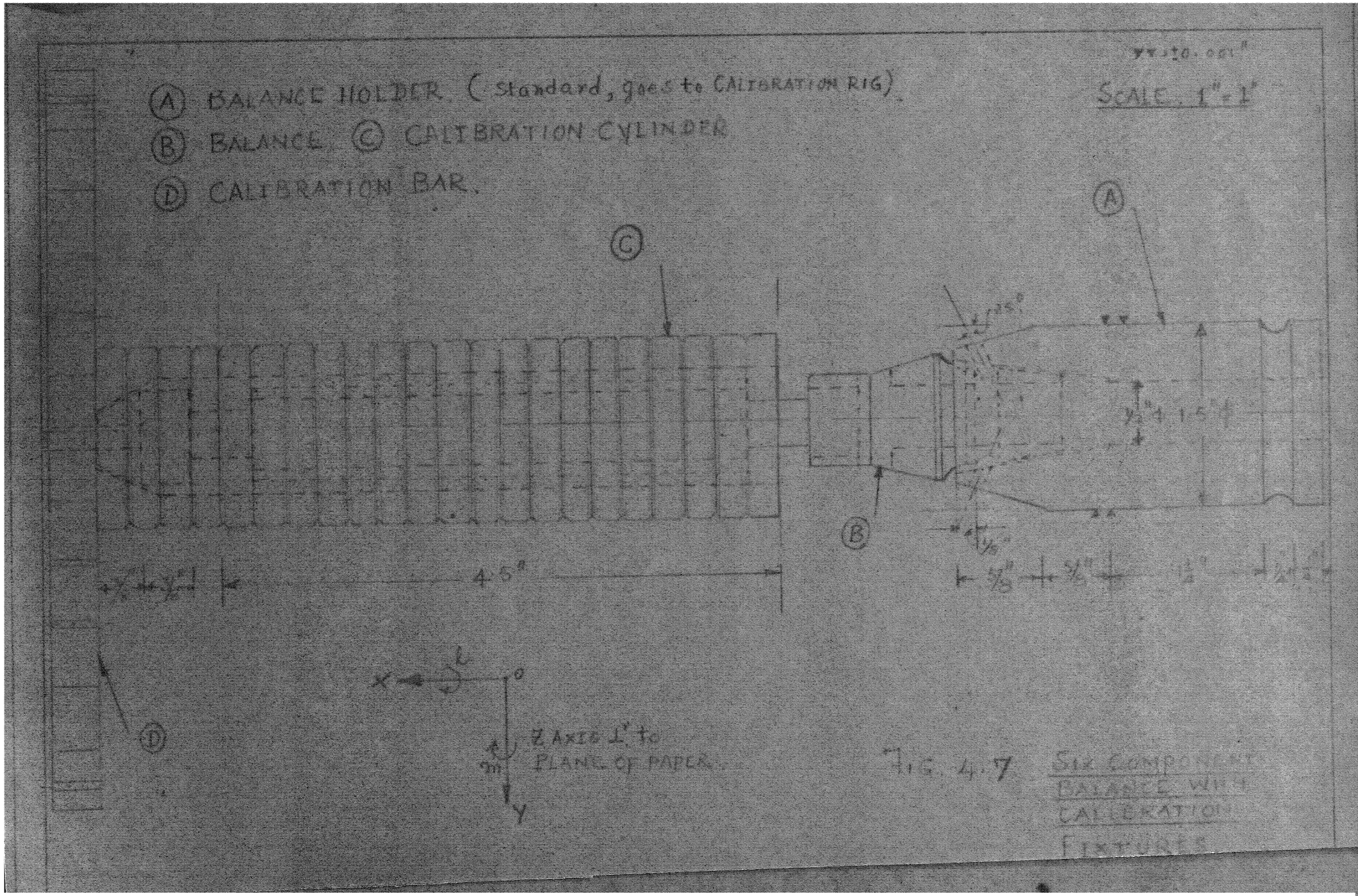

FIG. 4.7 SIX COMPONENT BALANCE WITH CALIBRATION FIXTURES

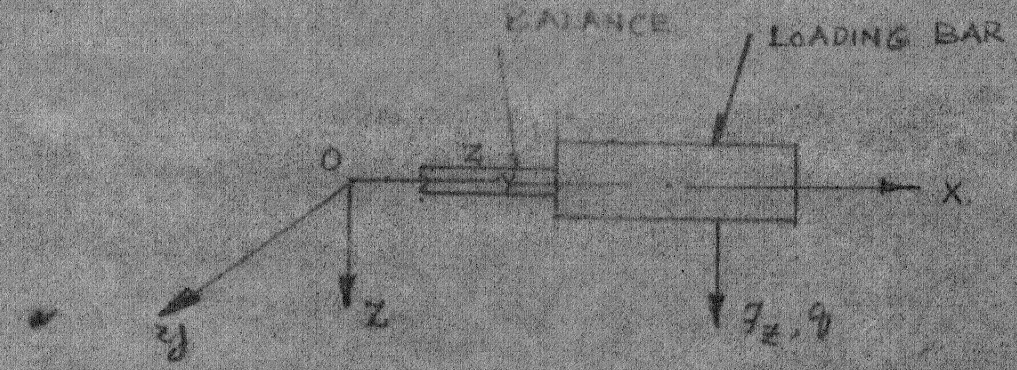

(a) NORMAL FORCE, PITCHING MOMENT.

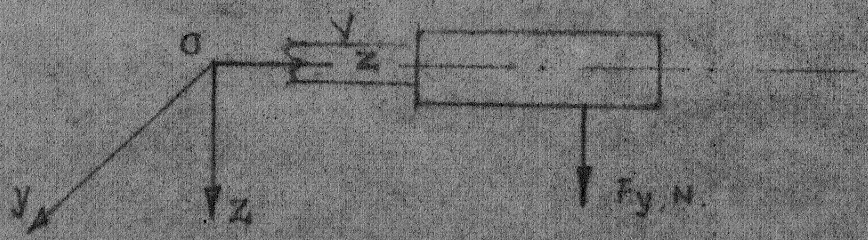

(b) SIDE FORCE YAWING MOMENT.

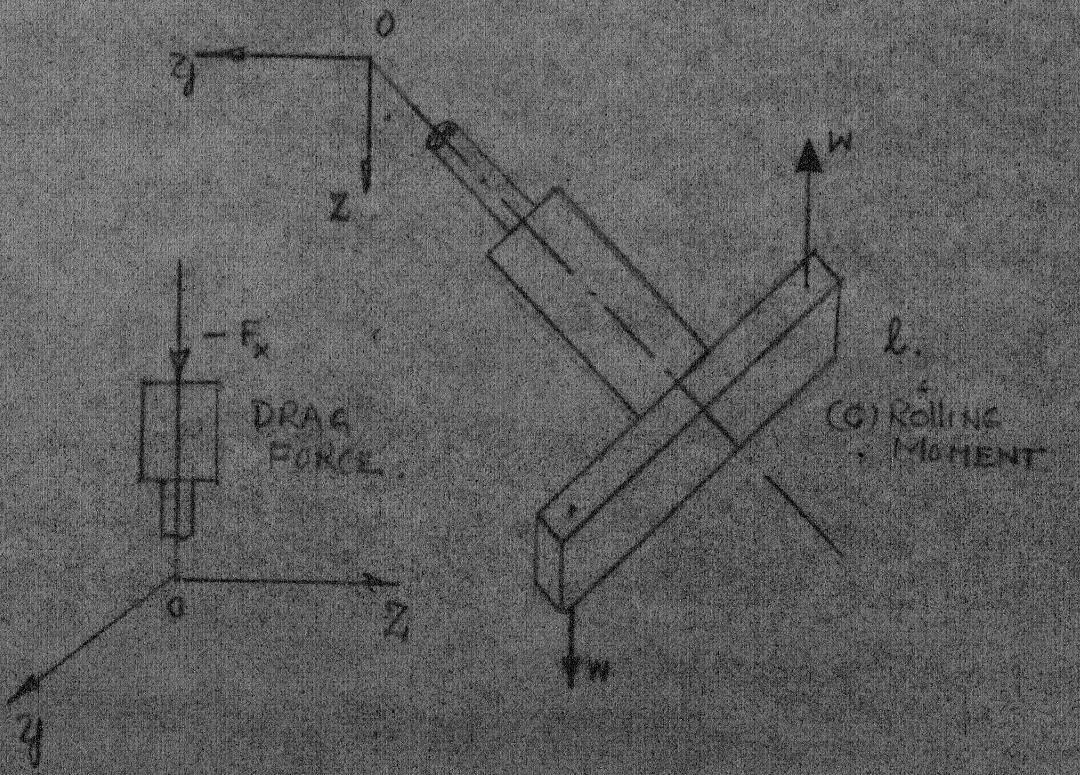

FIG. 4.8. LOADING CO-ORDINATES OF CALIBRATION RIG

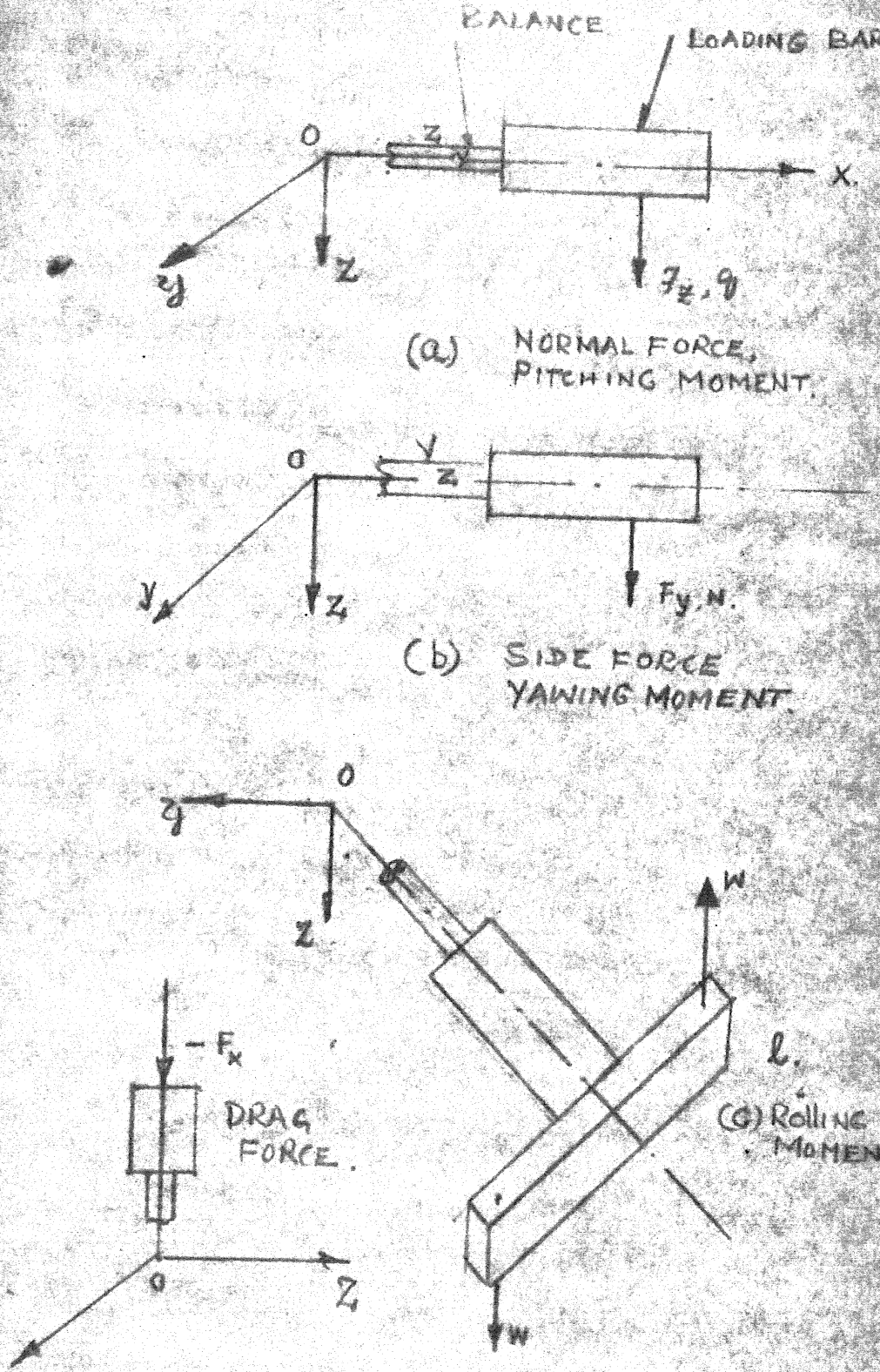

FIG. 4.8. LOADING CO-ORDINATES OF CALIBRATION RIG.

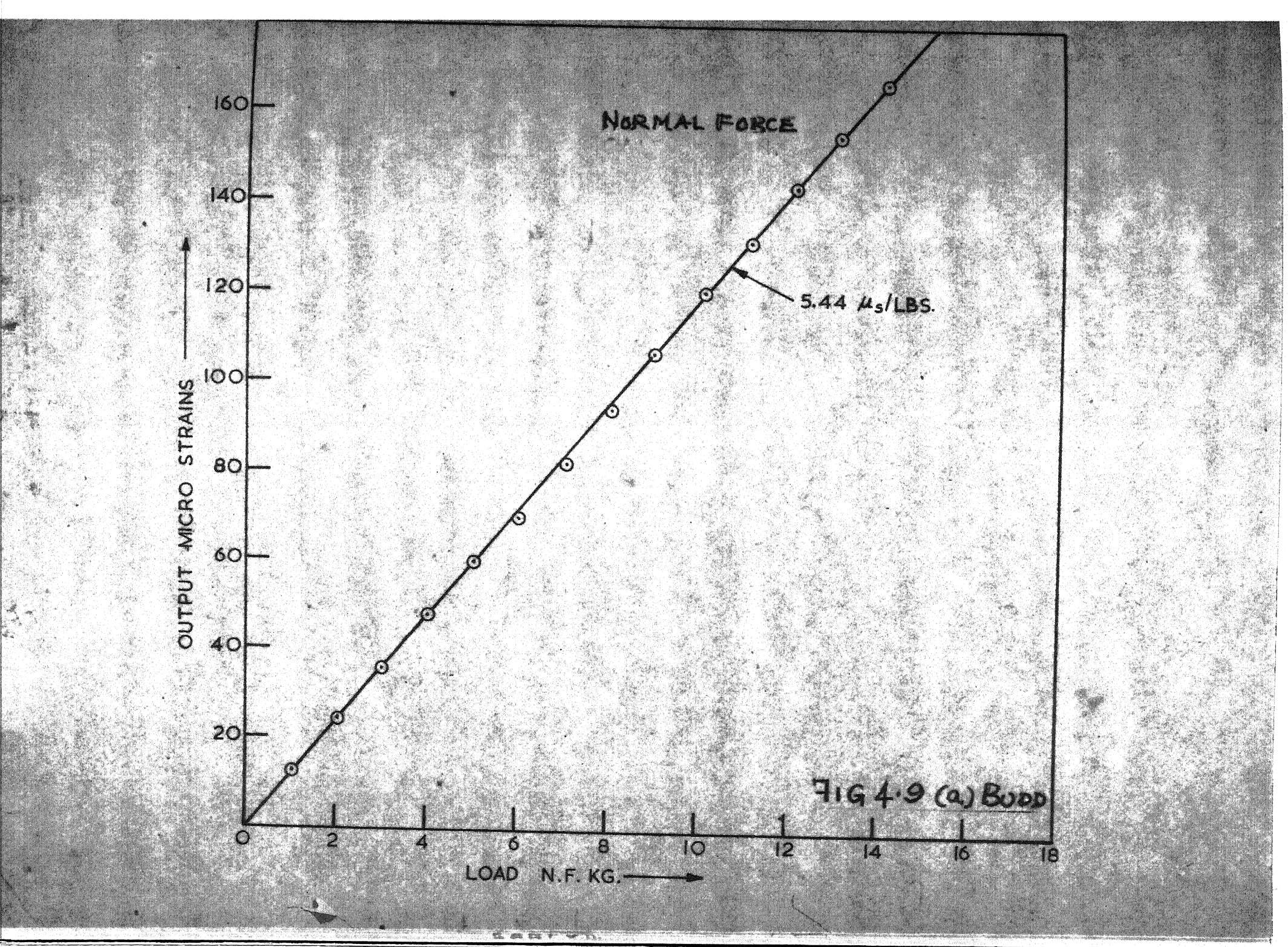
NORMAL FORCE
5.44 μs/LBS.
OUTPUT MICRO STRAINS
160
140
120
100
80
60
40
20
0
2
4
6
8
10
12
14
16
18
LOAD N.F. KG.

FIG 4·9 (a) BUDD

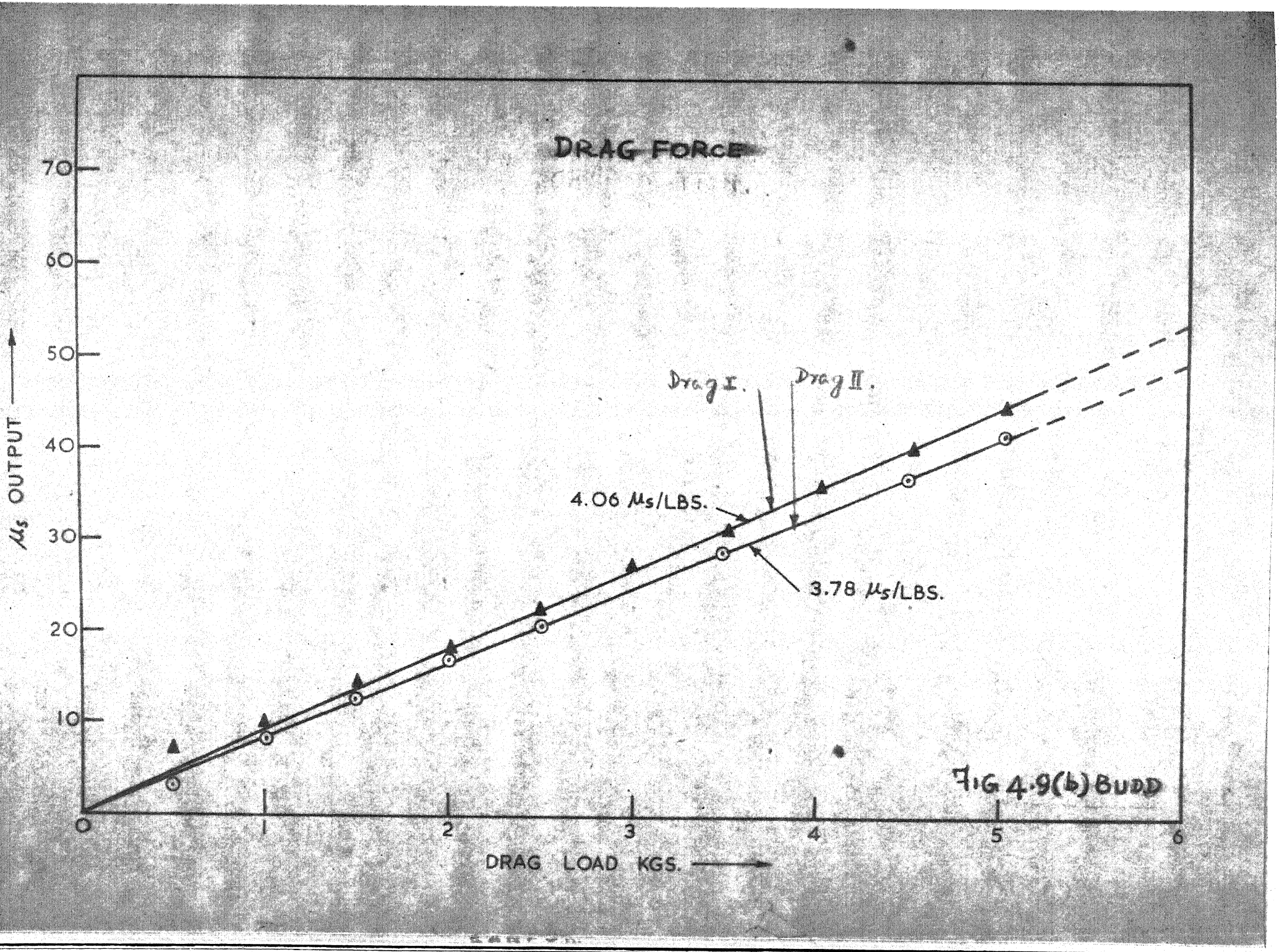
DRAG FORCE
70
60
50
40
30
20
10
0
1
2
3
4
5
6
μs OUTPUT
DRAG LOAD KGS.
Drag I.
Drag II.
4.06 μs/LBS.
3.78 μs/LBS.

FIG 4.9(b) BUDD

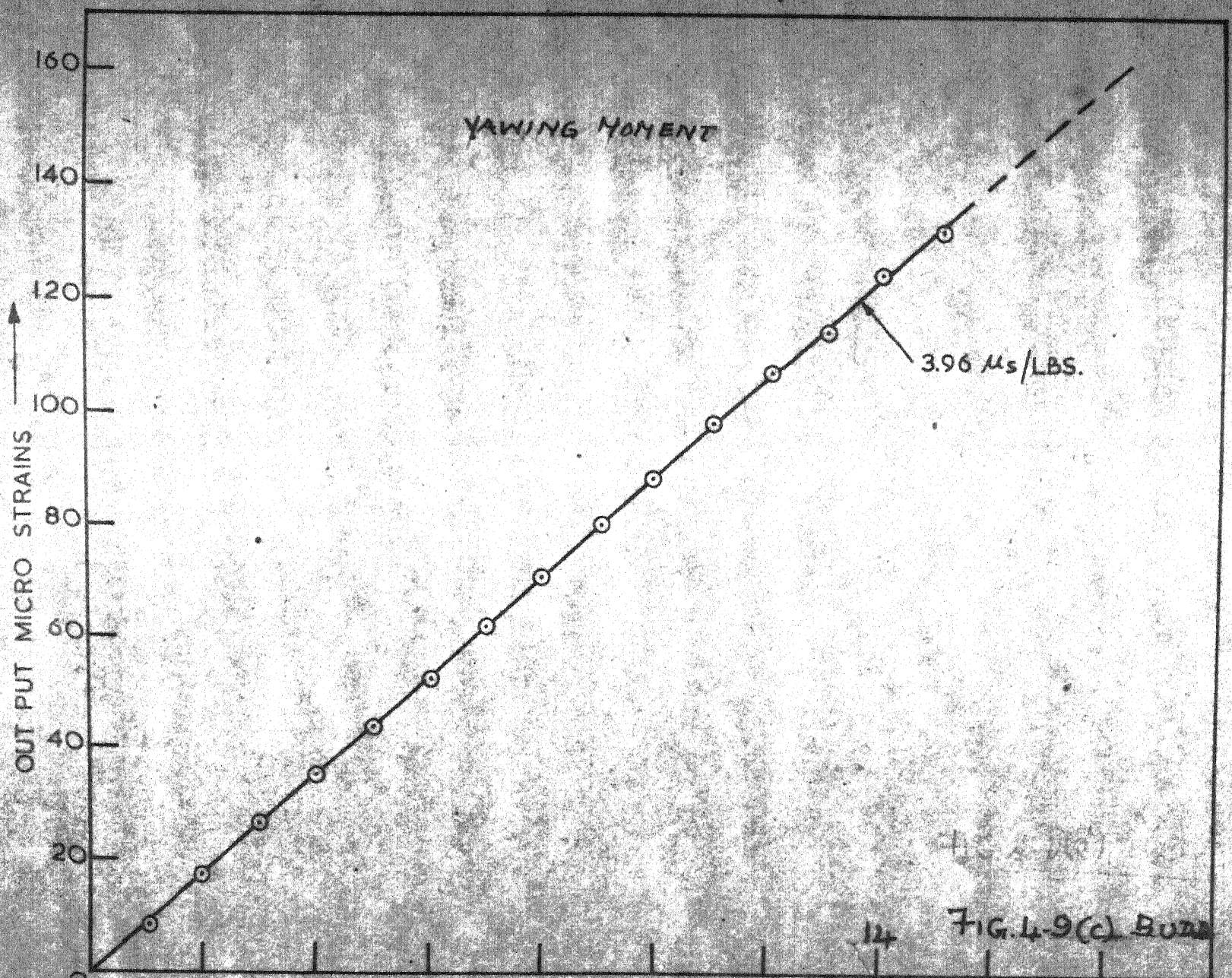
YAWING MOMENT
3.96 μs/LBS.
OUT PUT MICRO STRAINS
LOAD S.F.KG.
0
20
40
60
80
100
120
140
160
2
4
6
8
10
12
14
16
18

FIG. 4-9(c) BUM

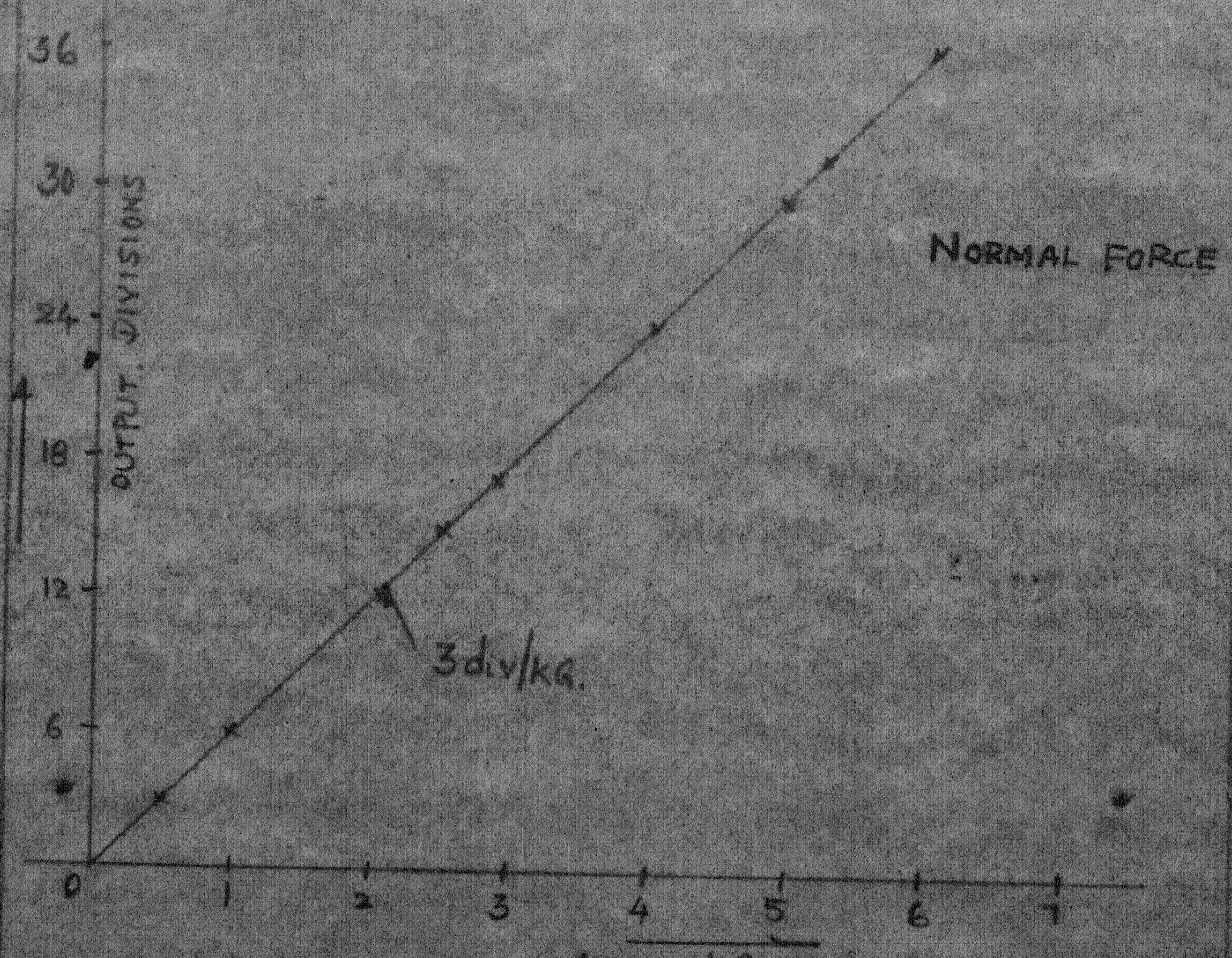

FIG. 4·9 (e) SANBORN

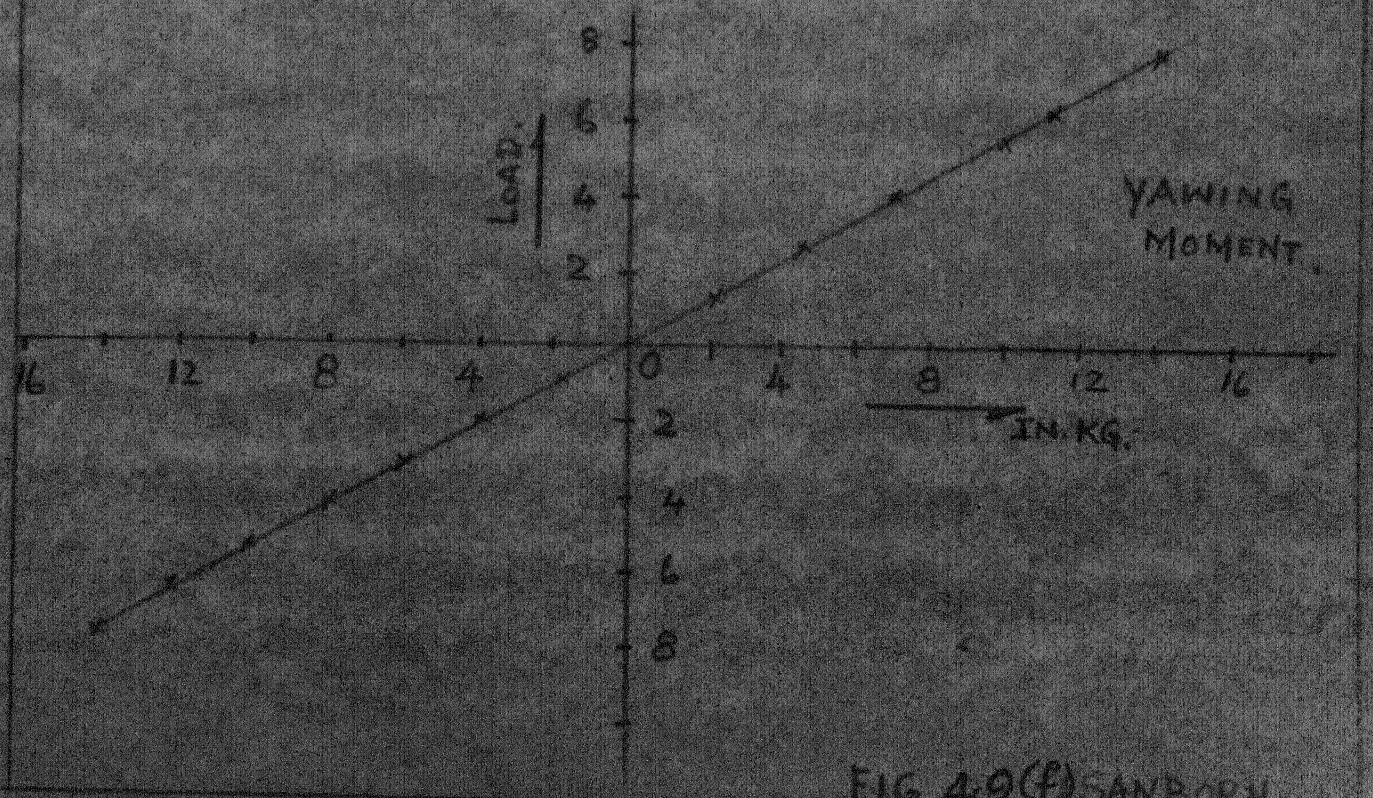

FIG 4·9(f) SANBORN.

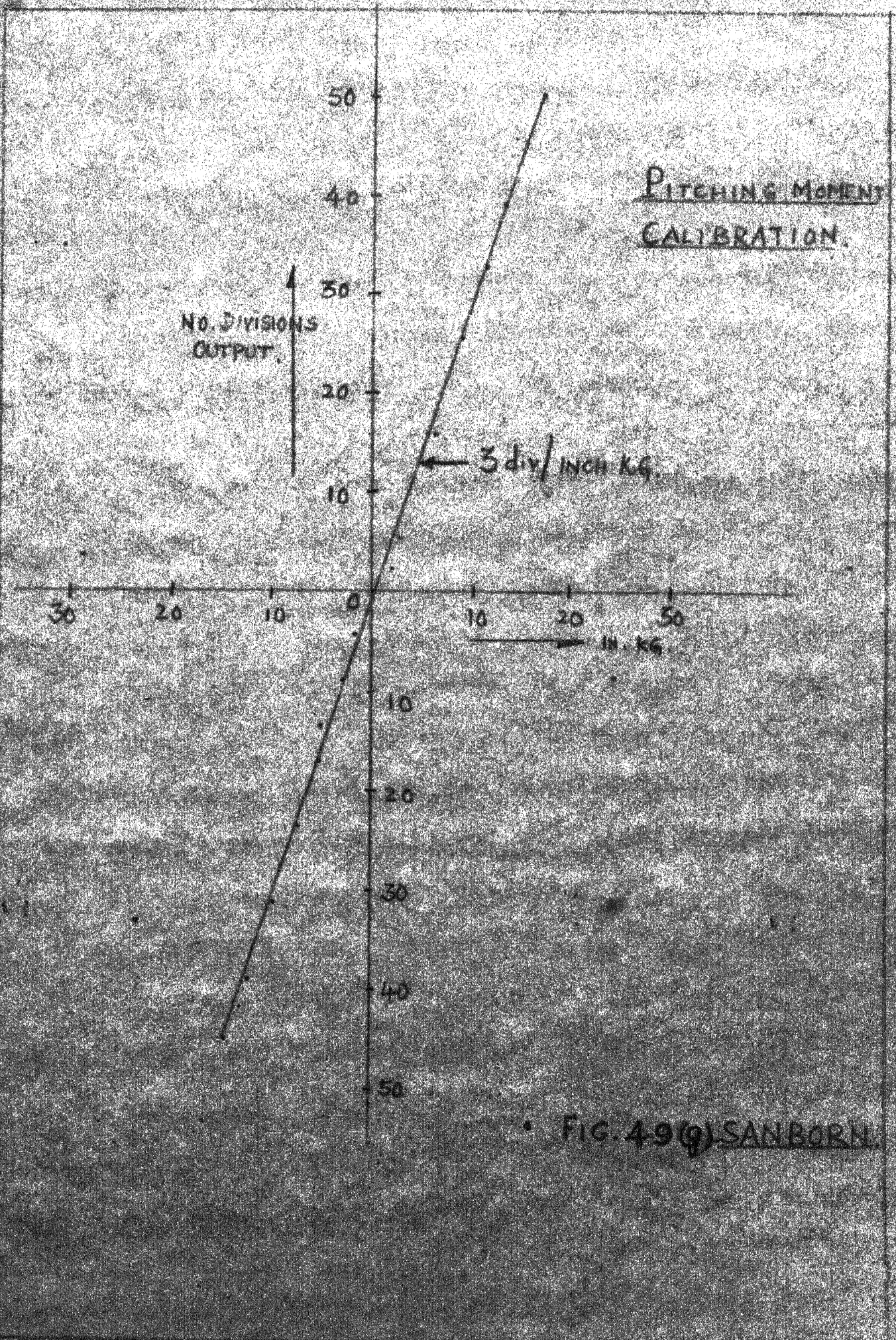

FIG. 49(9) SANBORN.

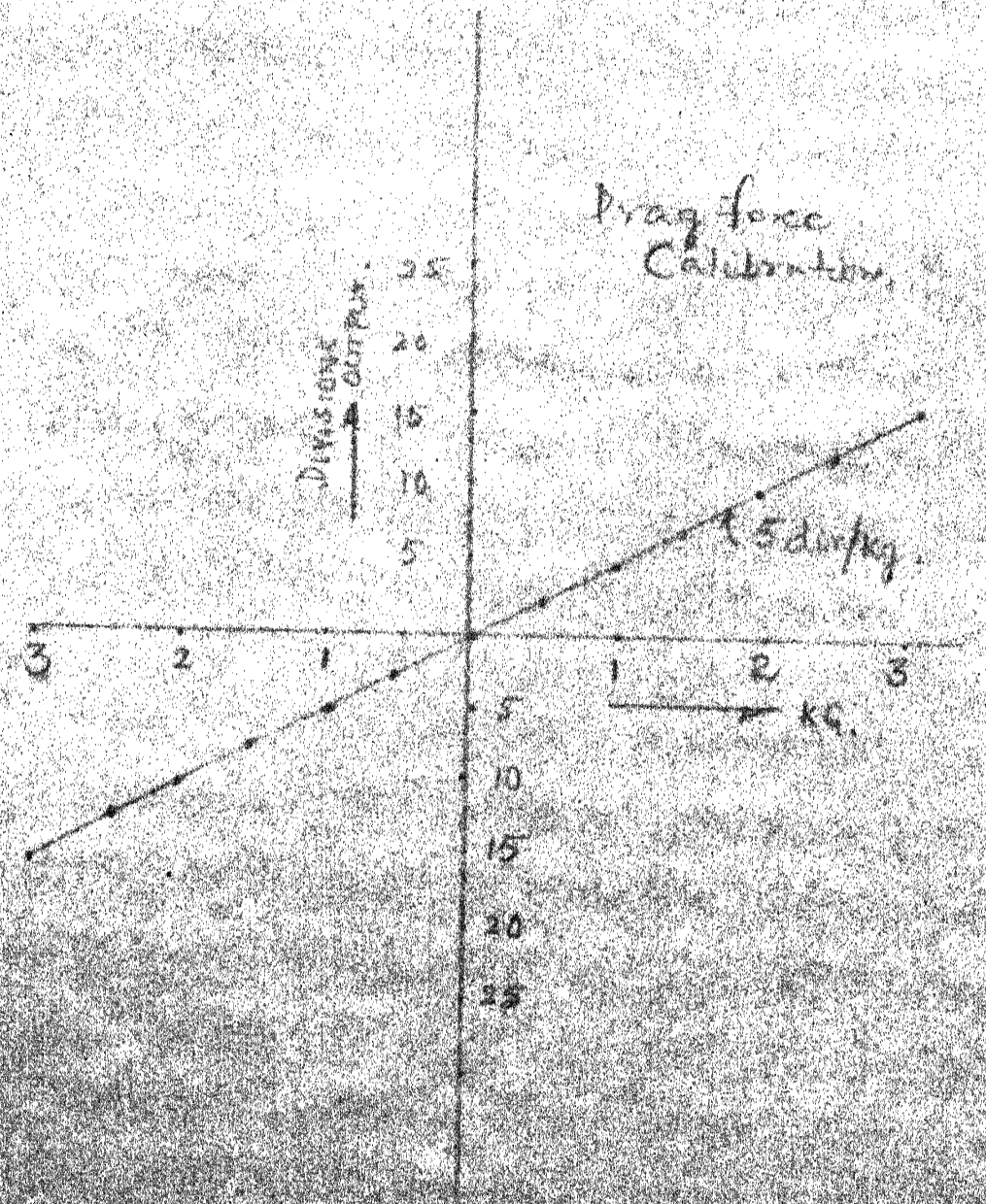

Fig. 4.9(b). SANBORN.

FIG 4.9 5-COMPONENT BALANCE CALIBRATION CURVES. USING "BUDD" AND "SANBORN" INSTRUMENTS.

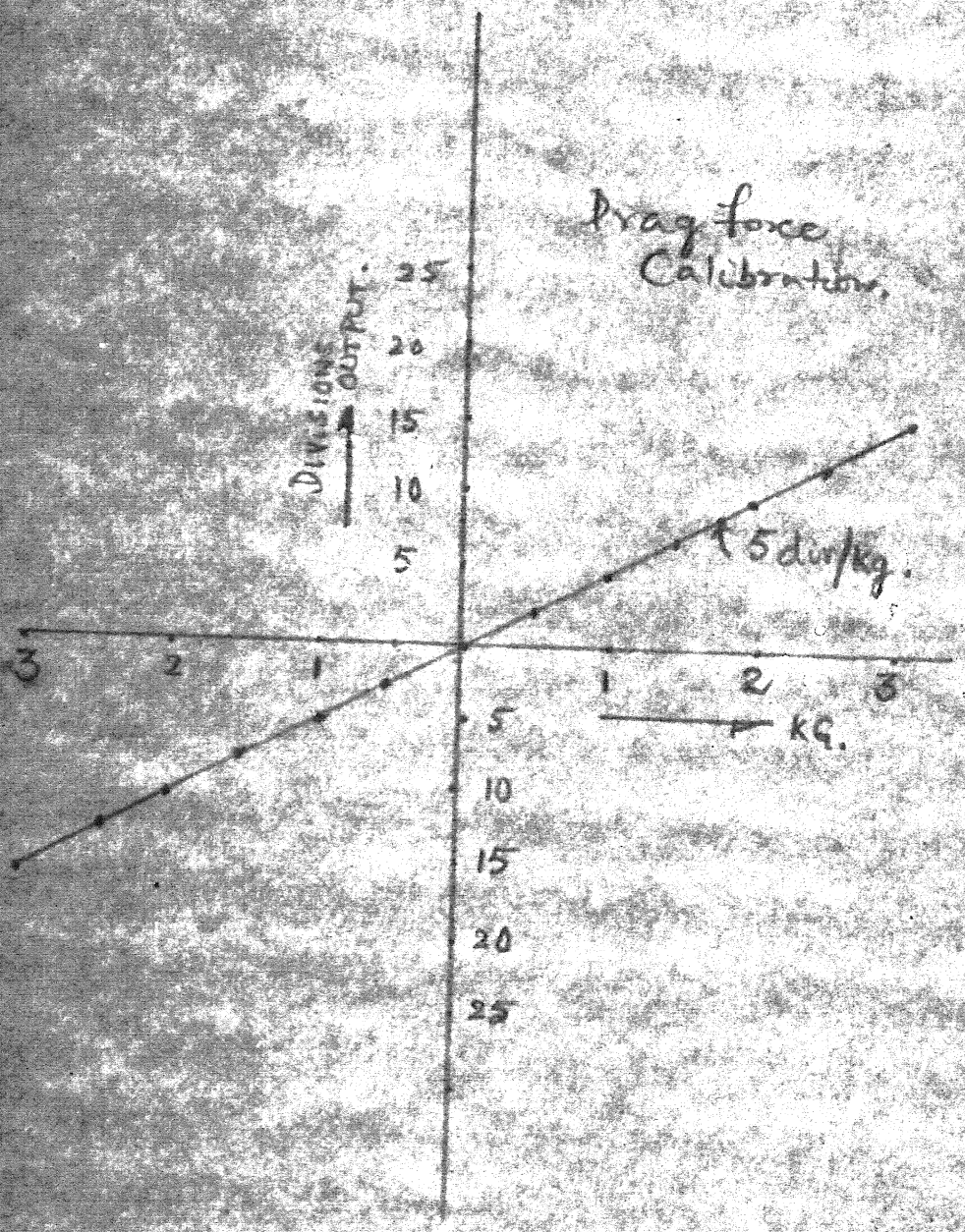

Fig: 4.9(h). SANBORN.

FIG 4.9. 5-COMPONENT BALANCE CALIBRATION CURVES. USING "BUDD" AND "SANBORN" INSTRUMENTS.

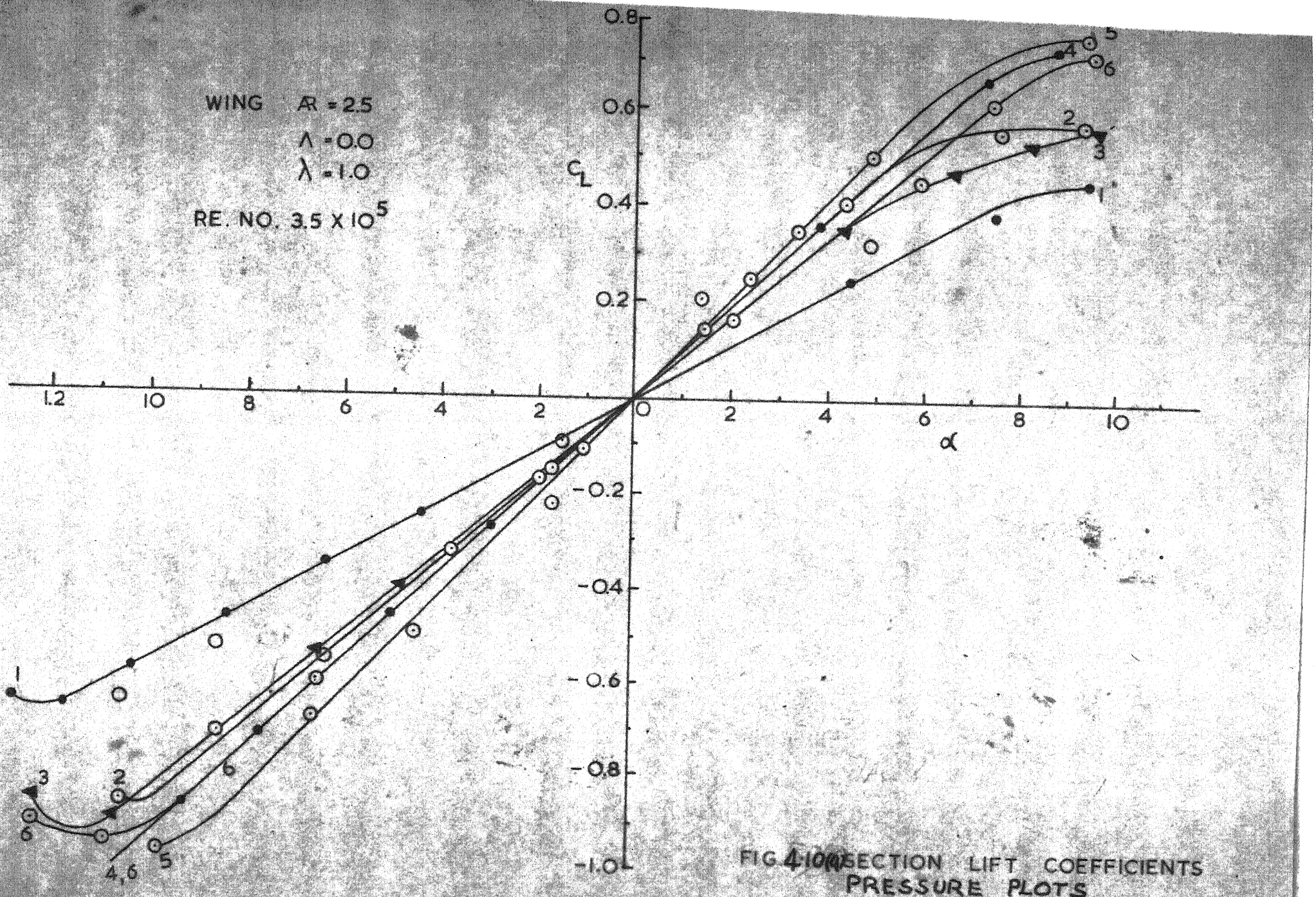

FIG 4.10(a) SECTION LIFT COEFFICIENTS PRESSURE PLOTS

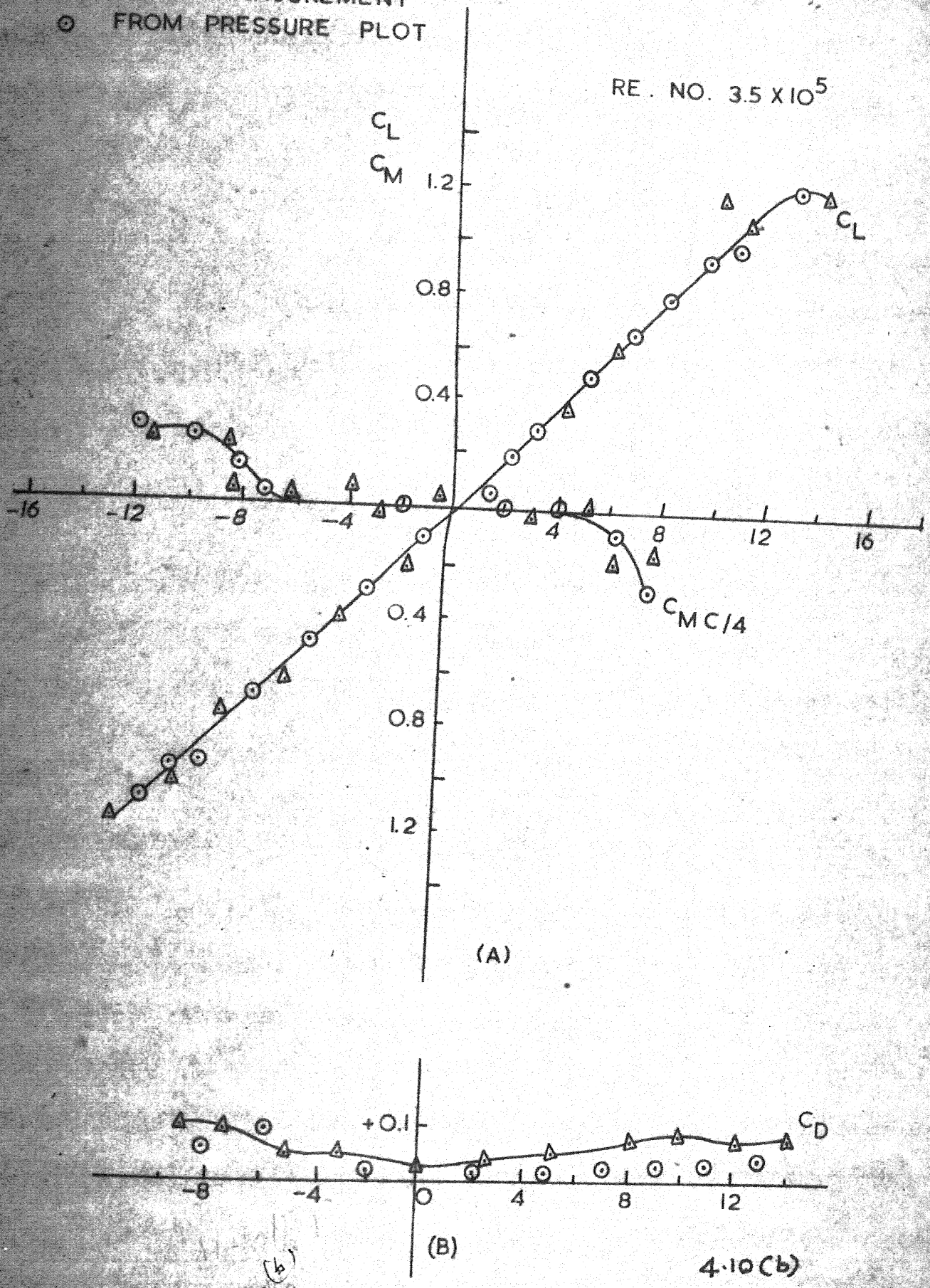

4·10(b)

FIG 4·10 WING ALONE CHARACTERSTIC

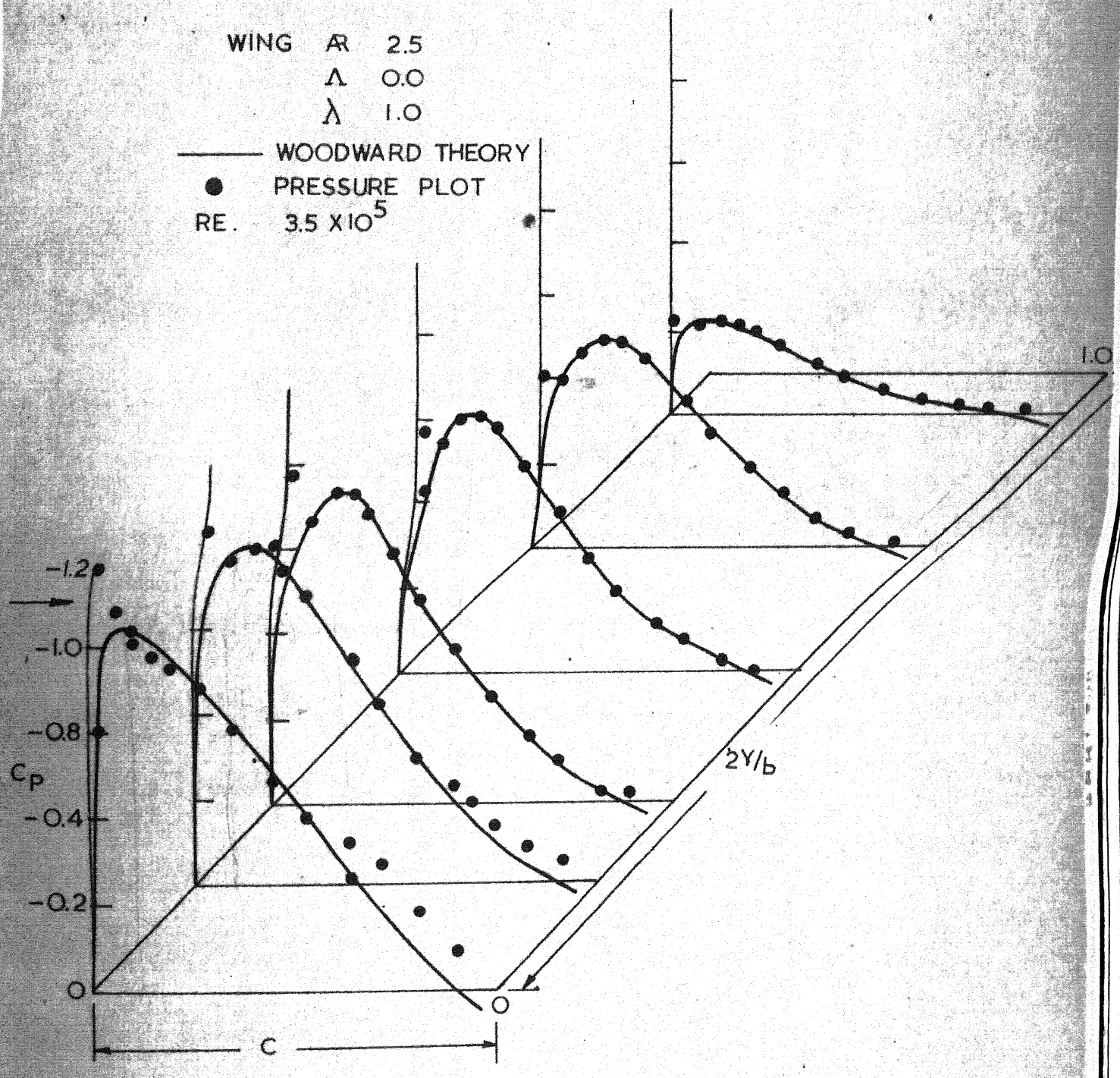

FIG. 4.10 (C) CHORD WISE PRESSURE DISTRIBUTION ON THE WING.

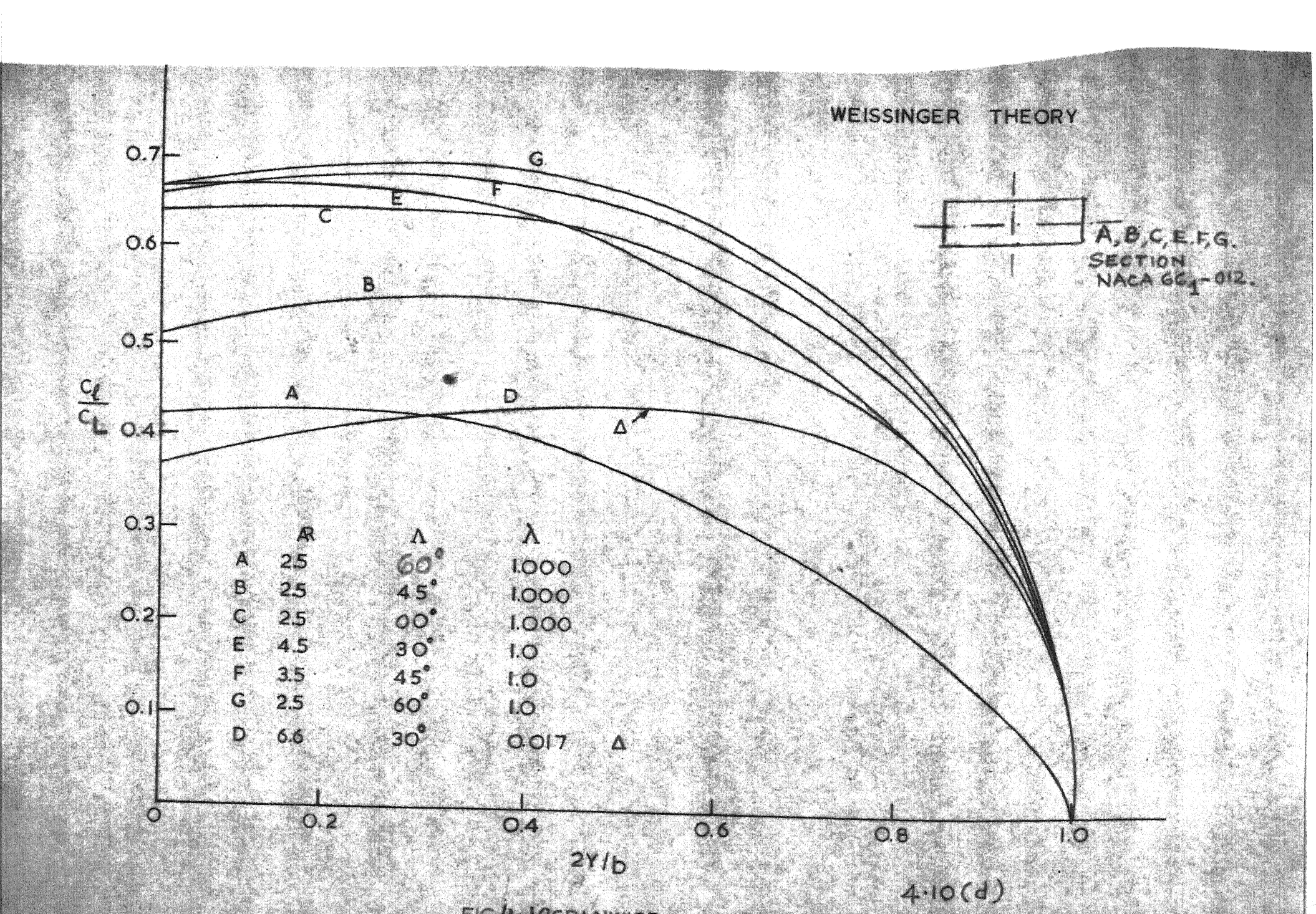

4·10(d)

FIG 4·10 SPANWISE LOADINGS

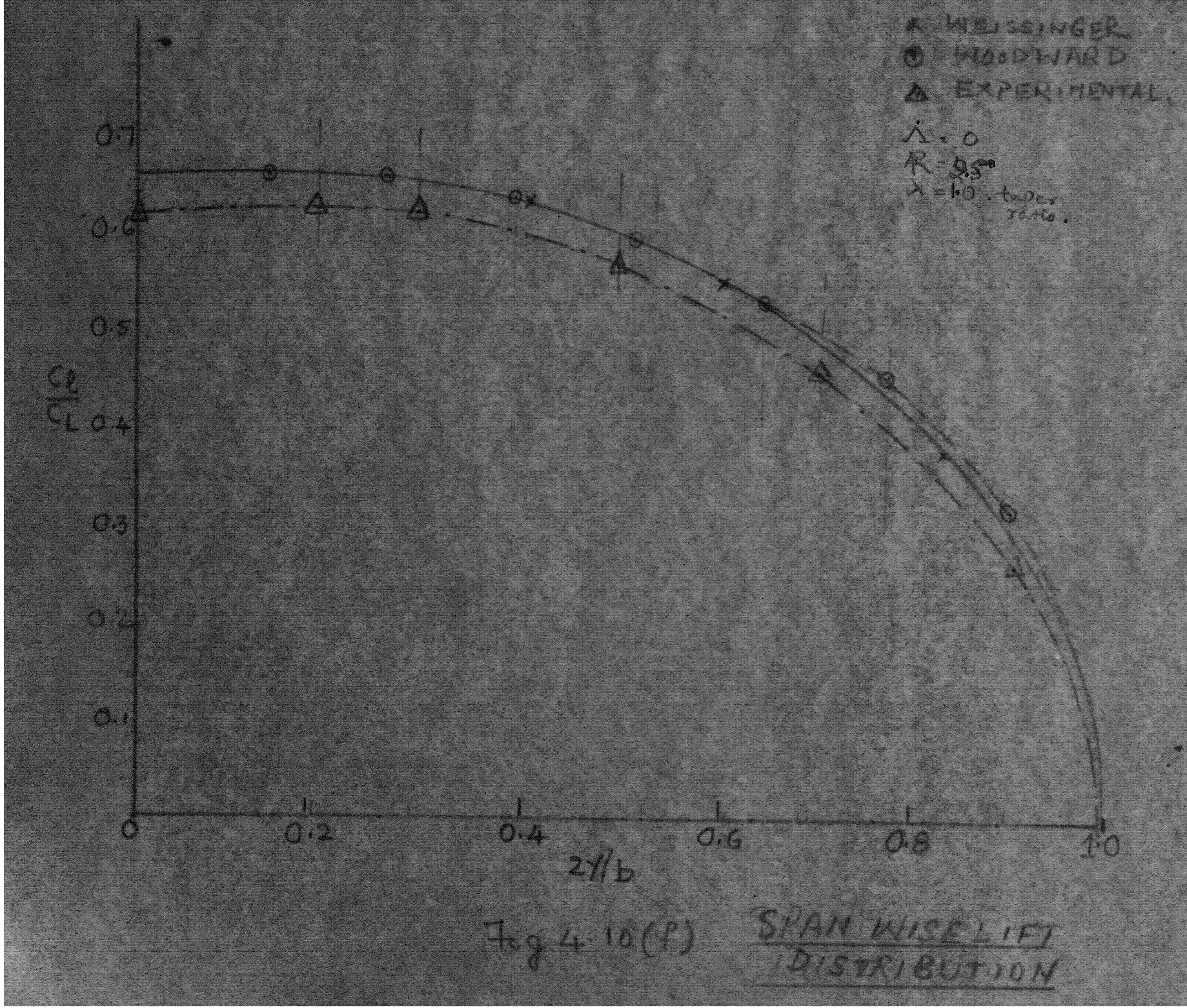

Fig 4.10(P) SPAN WISE LIFT DISTRIBUTION

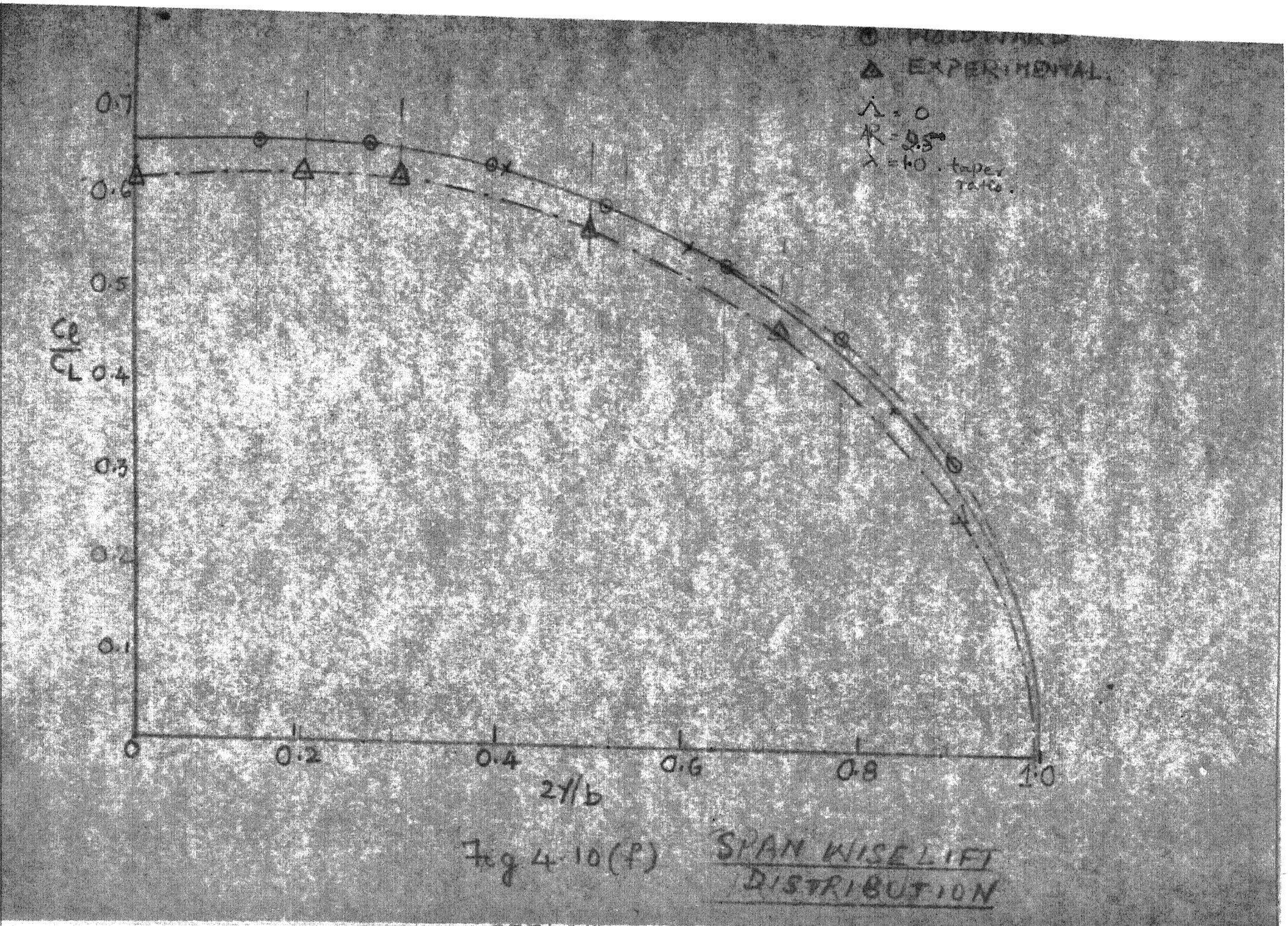

Fig 4.10(f) SPAN WISE LIFT DISTRIBUTION

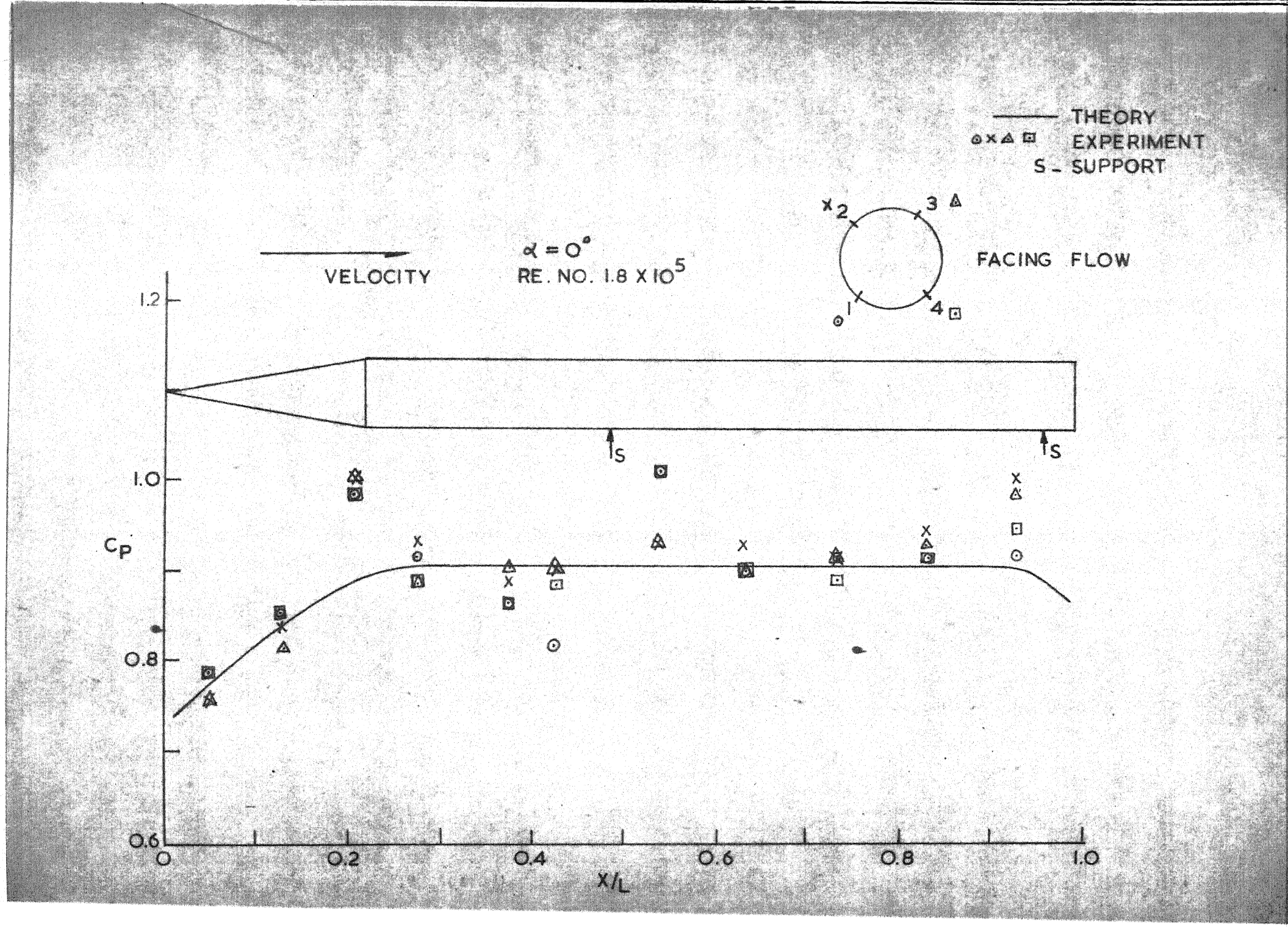
THEORY
EXPERIMENT
S - SUPPORT
VELOCITY
α = 0°
RE. NO. 1.8 X 10^5
FACING FLOW
1
2
3
4
S
S
1.2
1.0
0.8
0.6
C_P
0
0.2
0.4
0.6
0.8
1.0
X/L

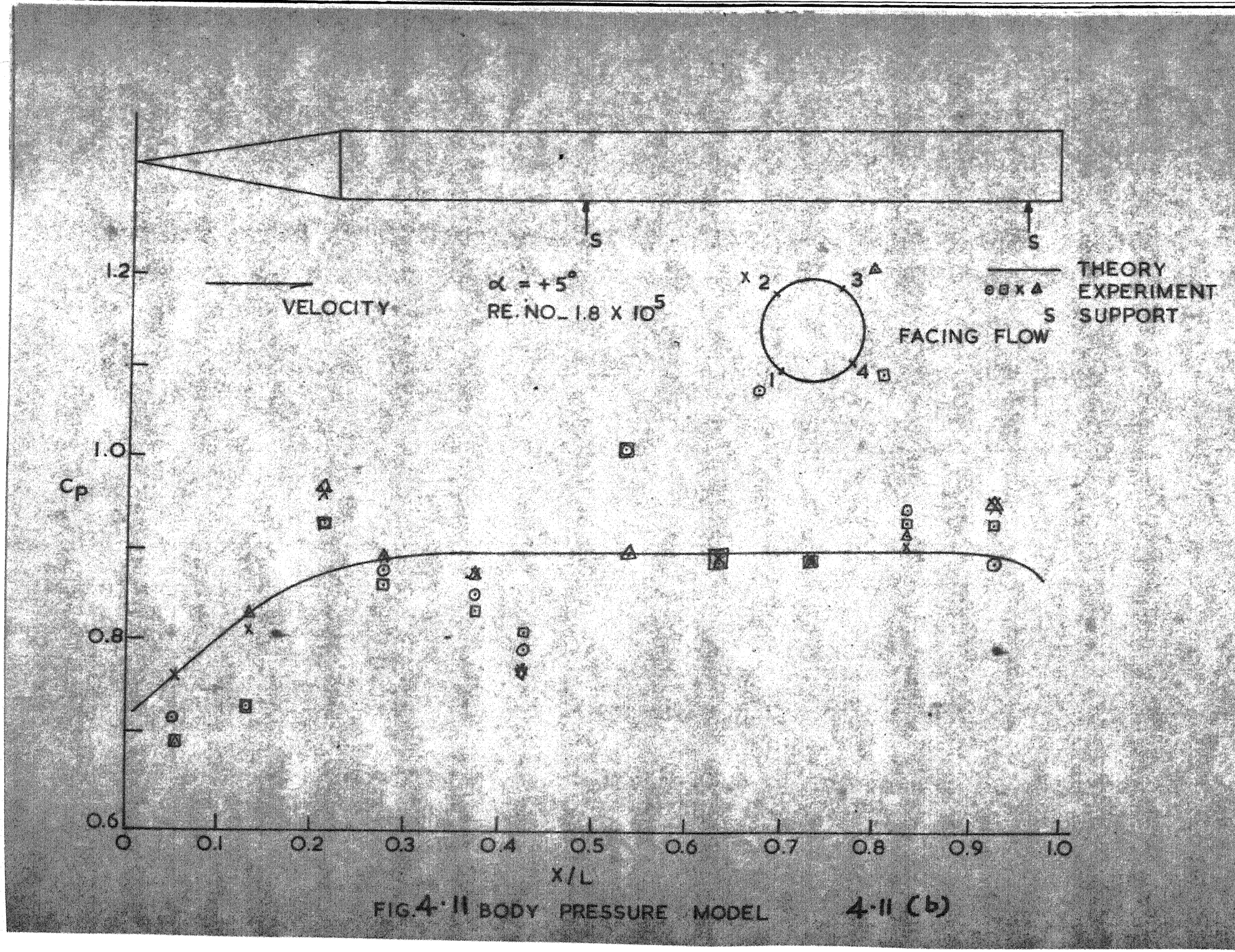

FIG. 4·11 BODY PRESSURE MODEL 4·11 (b)

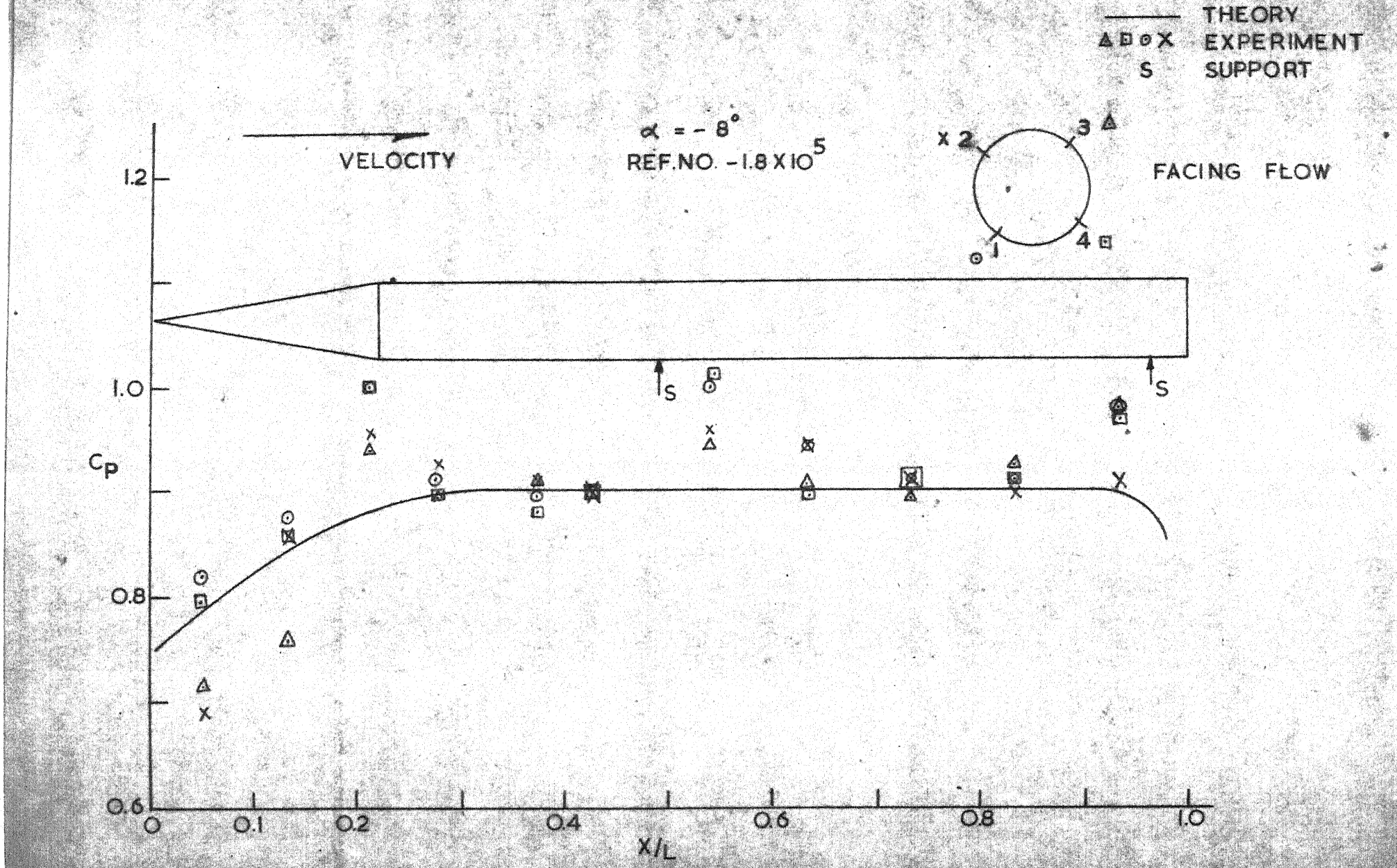

FIG 4·11 BODY PRESSURE MODEL 4·11 (C)

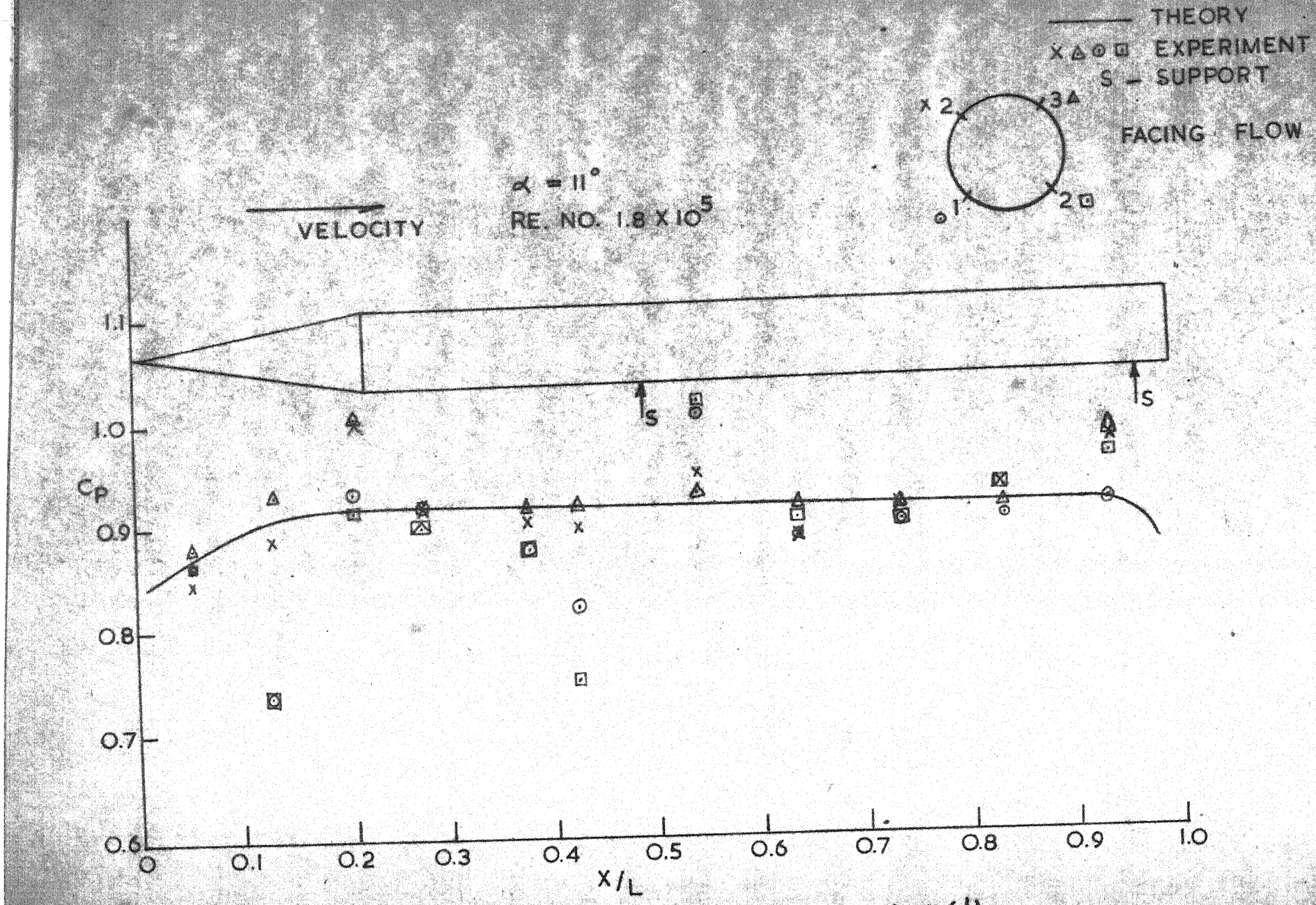

FIG 4·11 BODY PRESSURE MODEL 4·11(d)

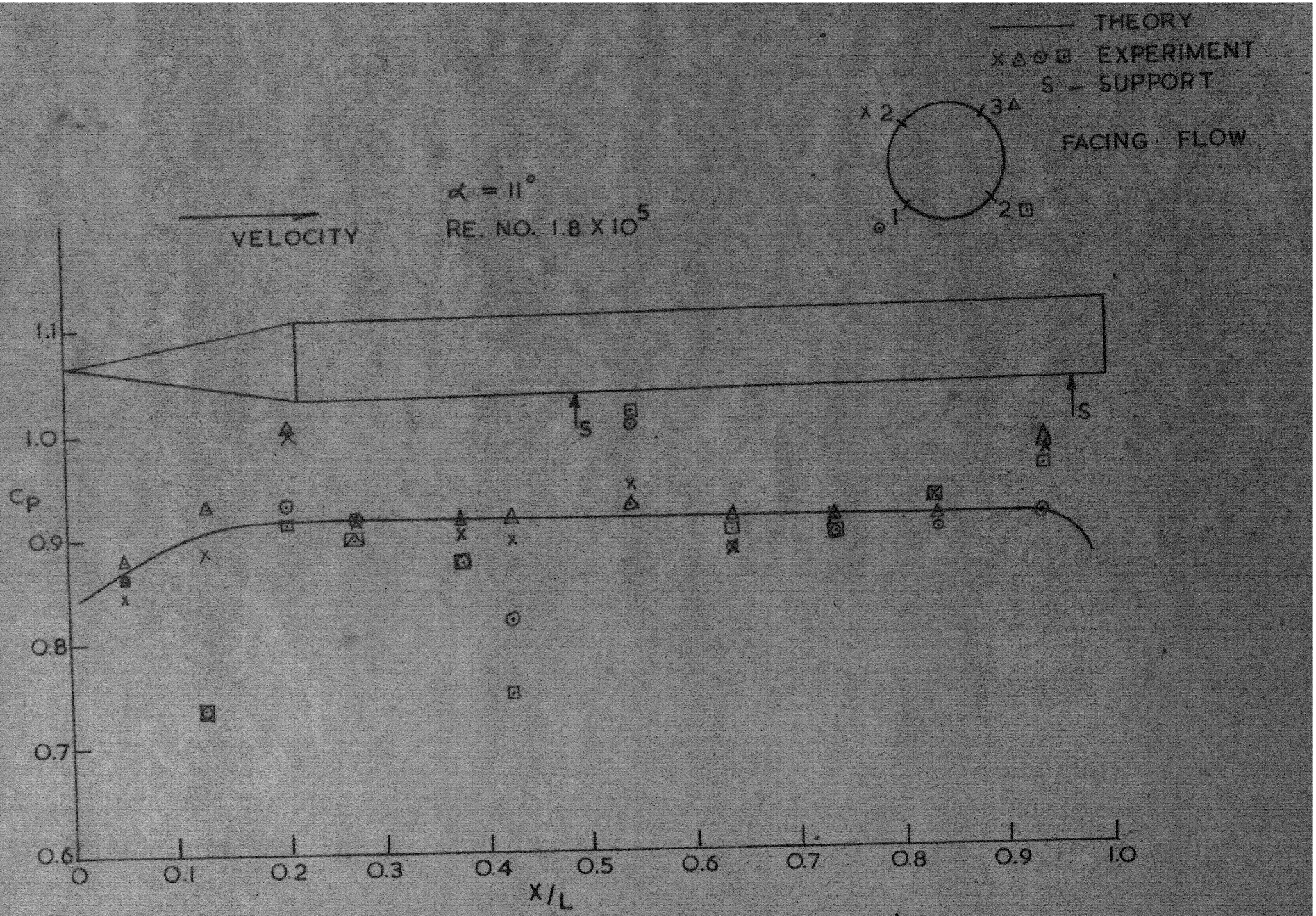

FIG 4·11 BODY PRESSURE MODEL 4·11(d)

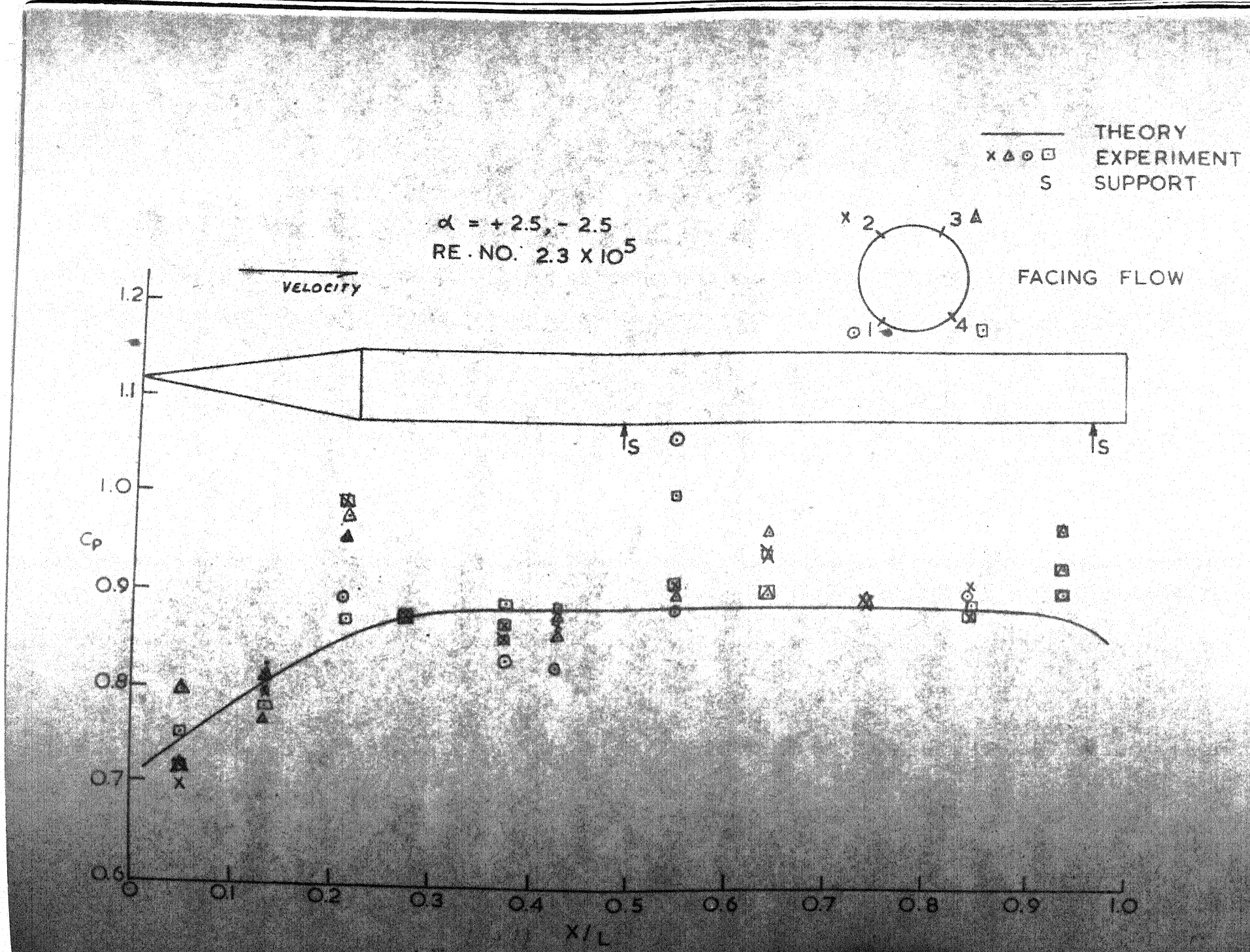

FIG. 4· 11 BODY PRESSURE

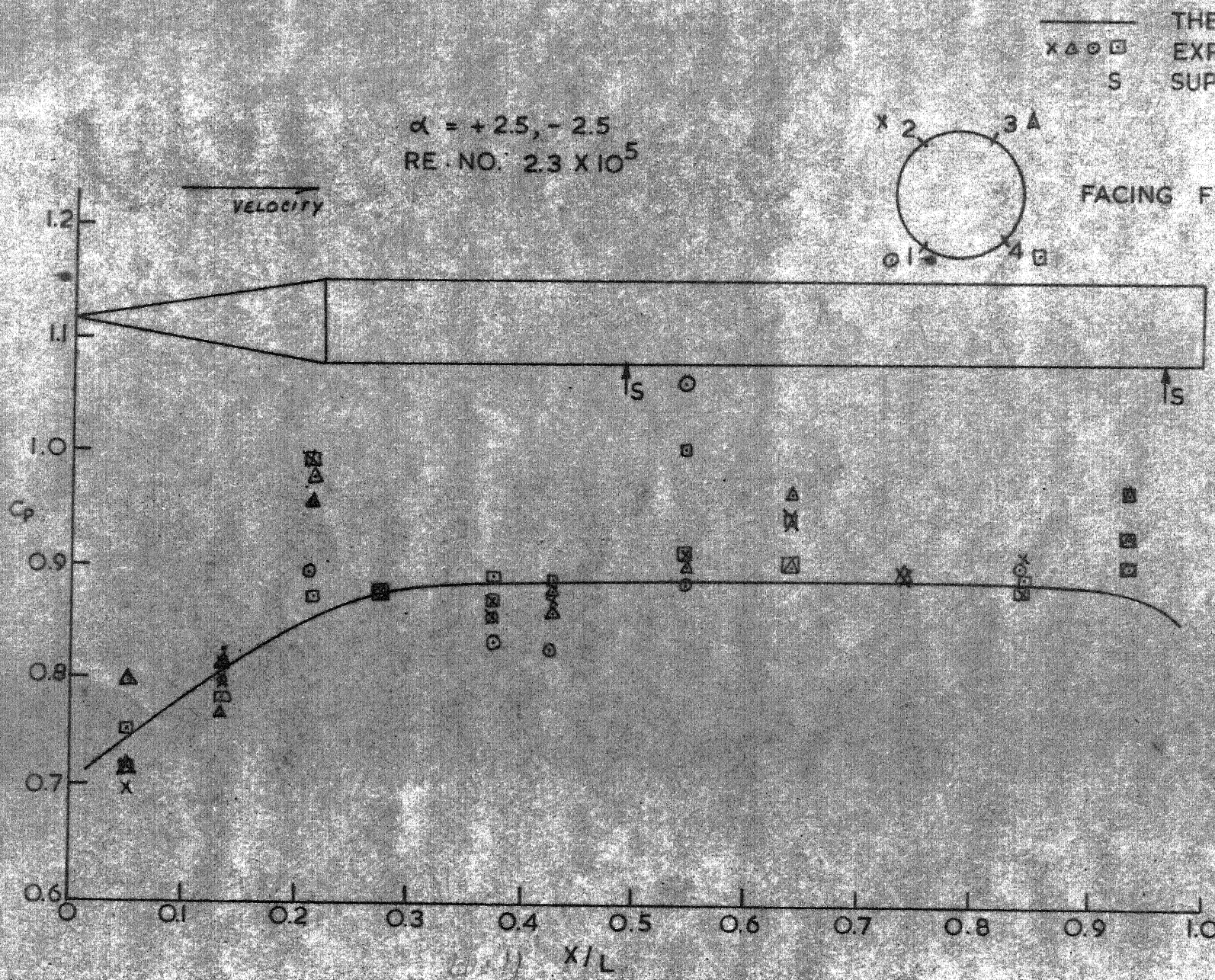

FIG. 4·11 BODY PRESSURE MODEL 4·11 (f)

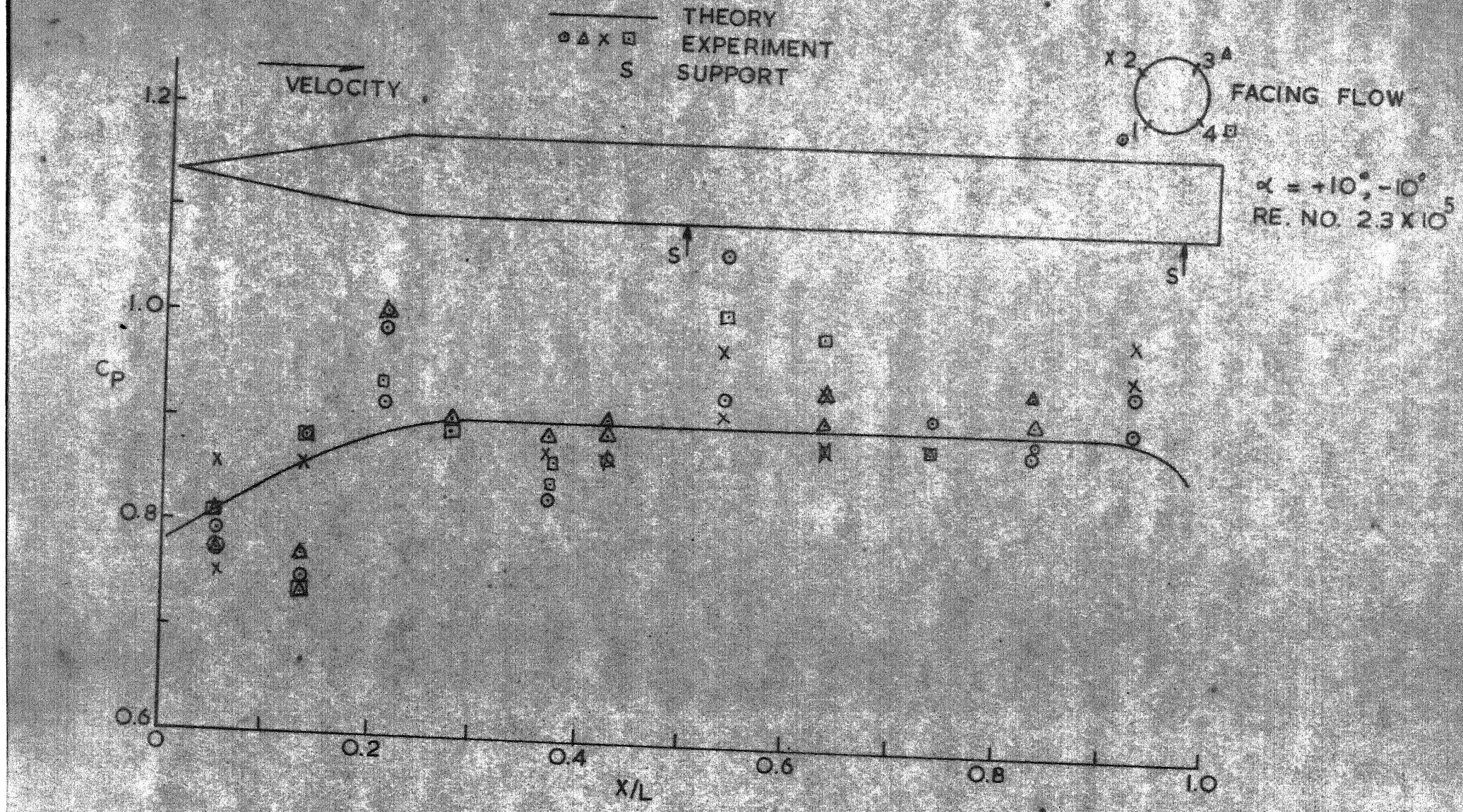

FIG 4·11 BODY PRESSURE MODEL 4·11 (9)

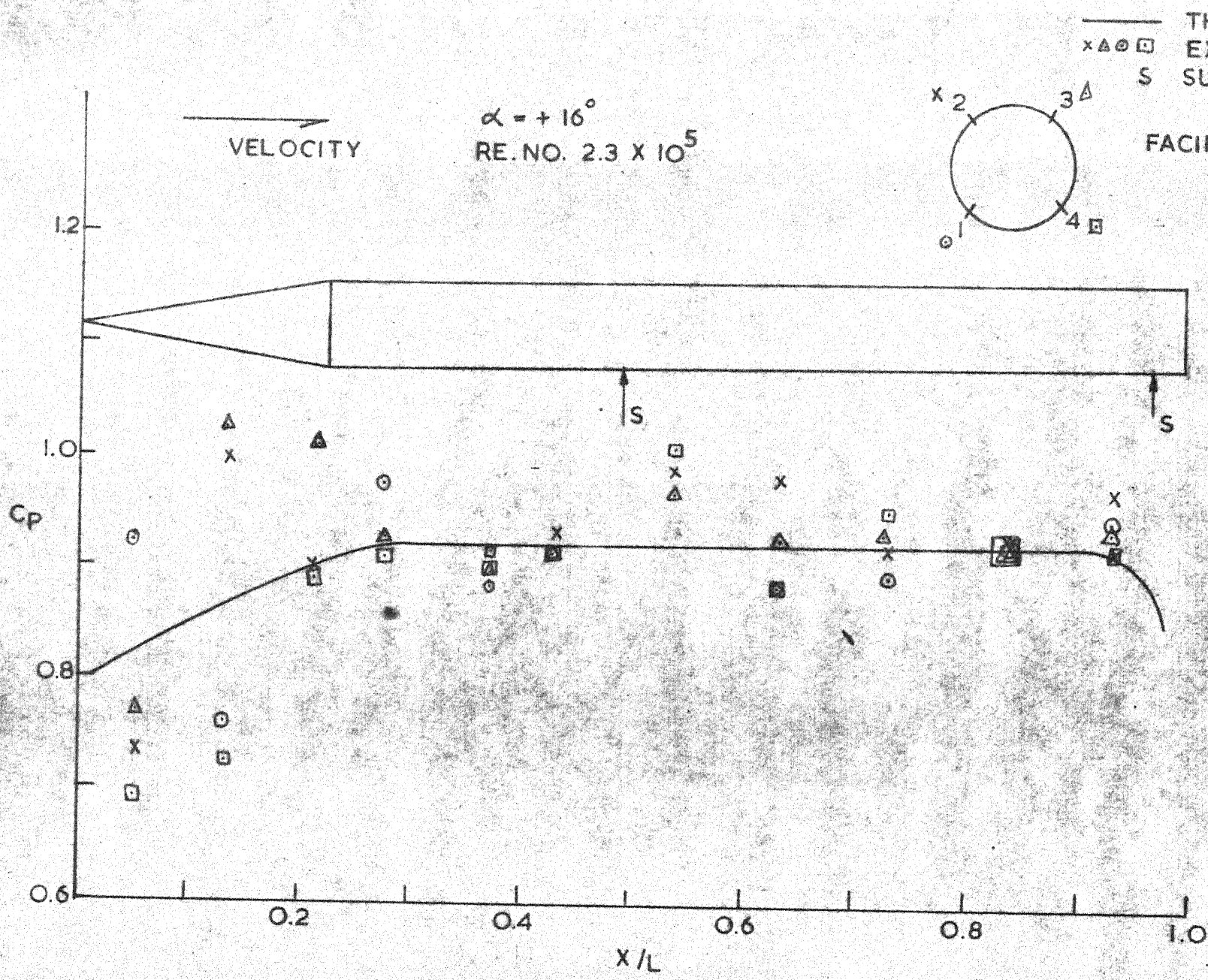

FIG 4·11 BODY PRESSURE MODEL 4·11 (b)

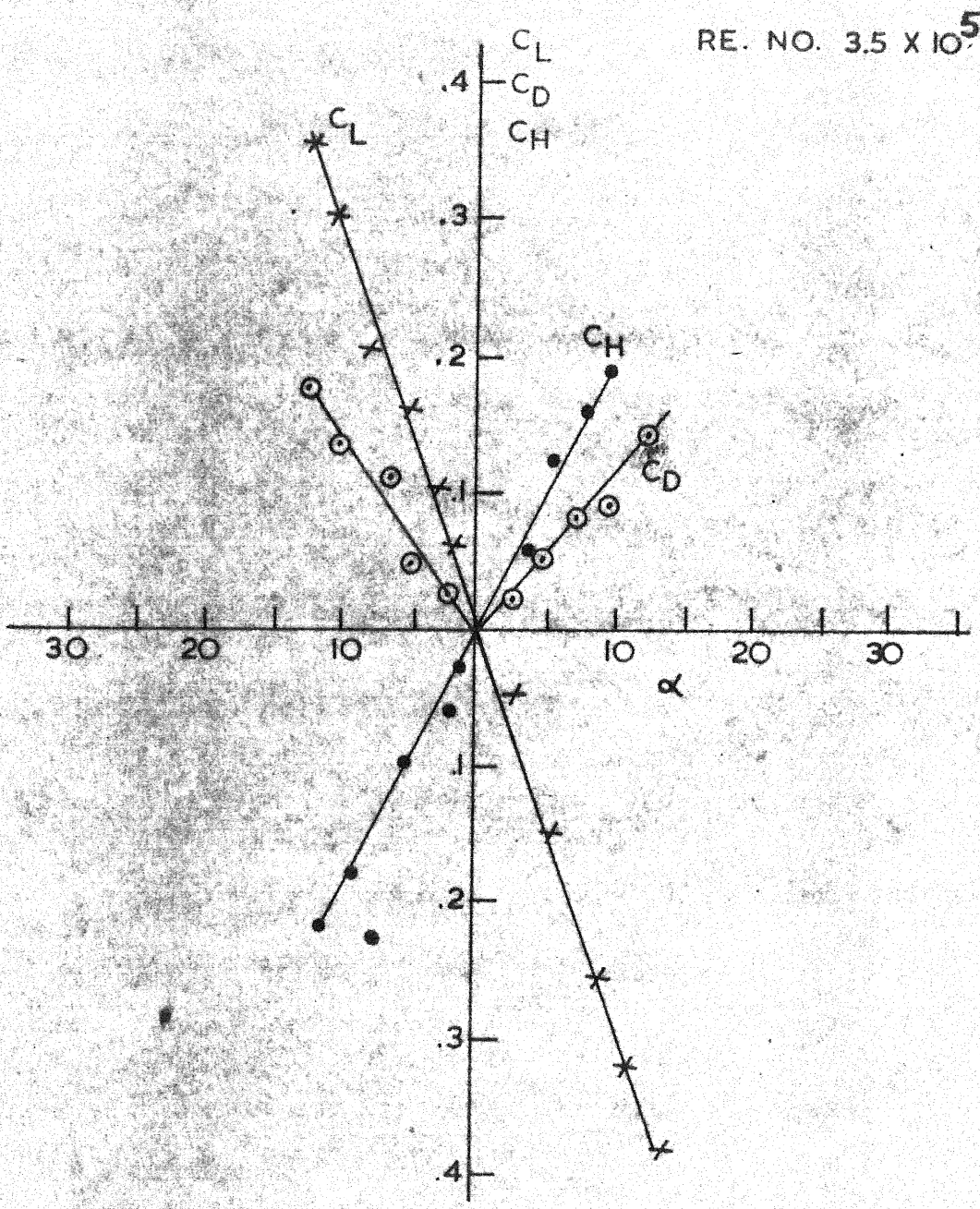

FIG. 4.12 BODY PRESSURE MODEL
BALANCE OUT PUT

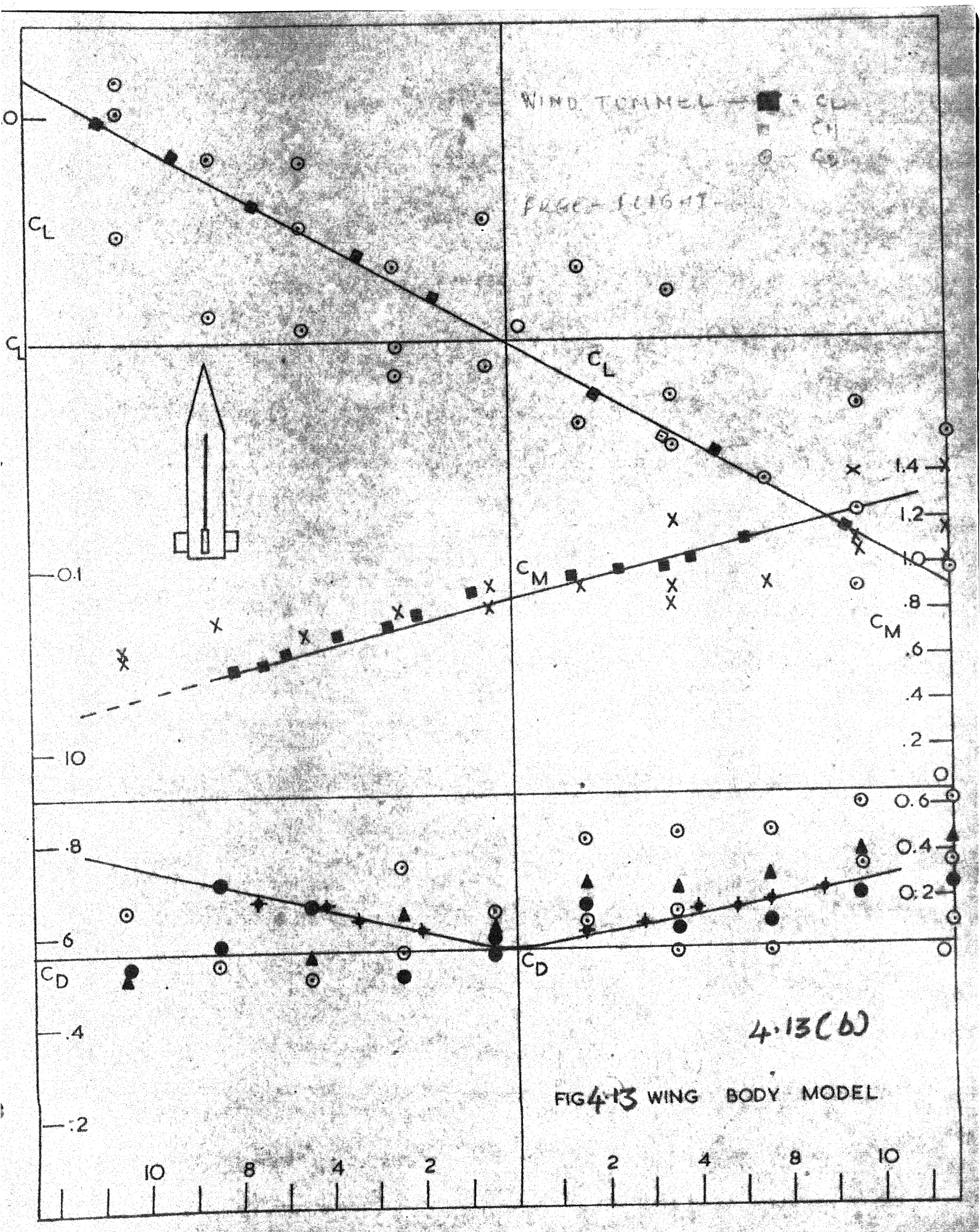

4.13(b)

FIG 4.13 WING BODY MODEL

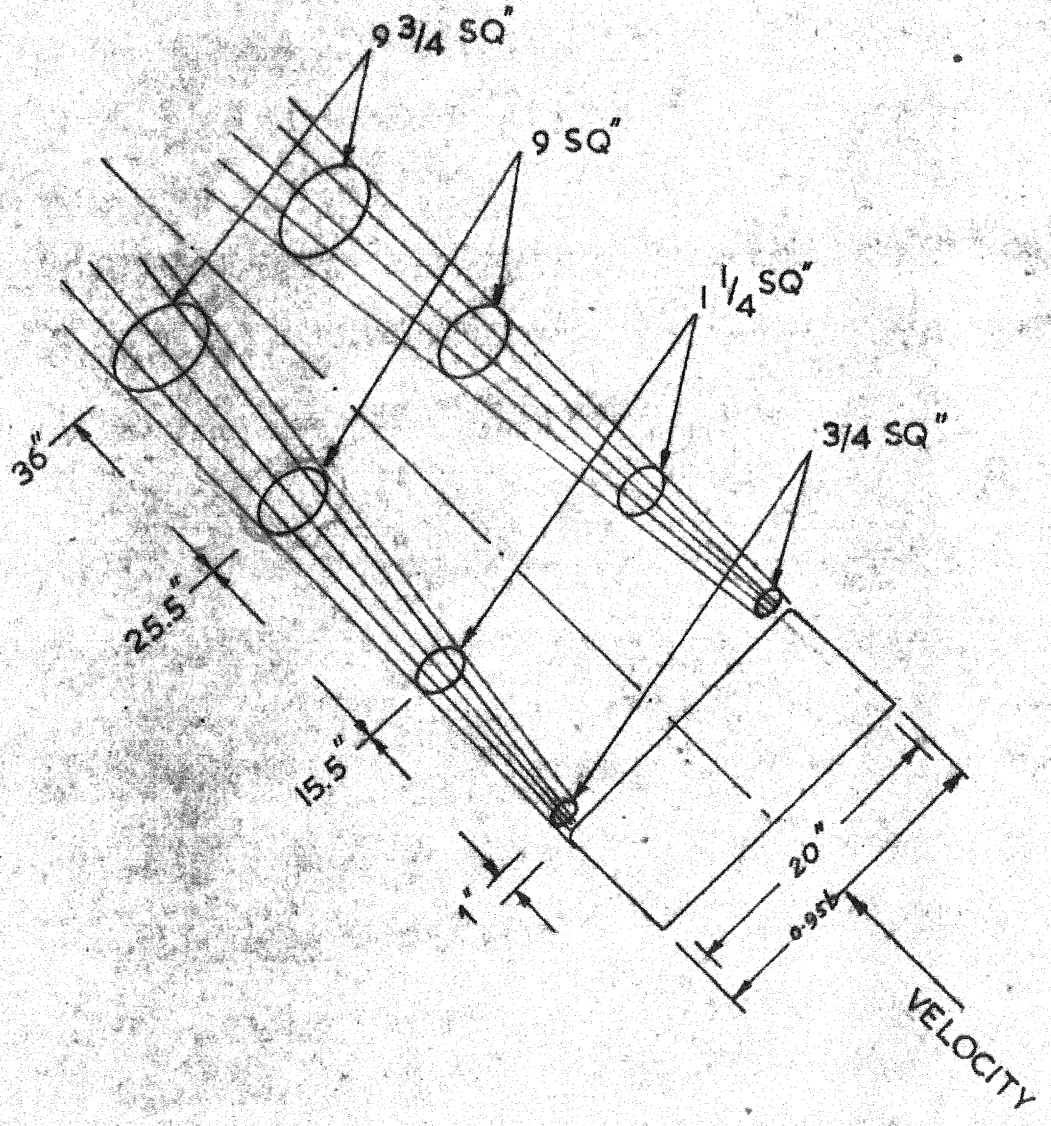

FIG. 4.14 _ TRAILING VORTEX SYSTEM

RESULTS FOR TABLE A(1)

SI NO	C_1	K_1	C_2	K_2
1	11.55	662.5	-1.662	8.245
2	1.03	256.2	18.52	1.34
3	10.20	3722	-5.15	-920
4	10.20	3722	-4.265	-2.220

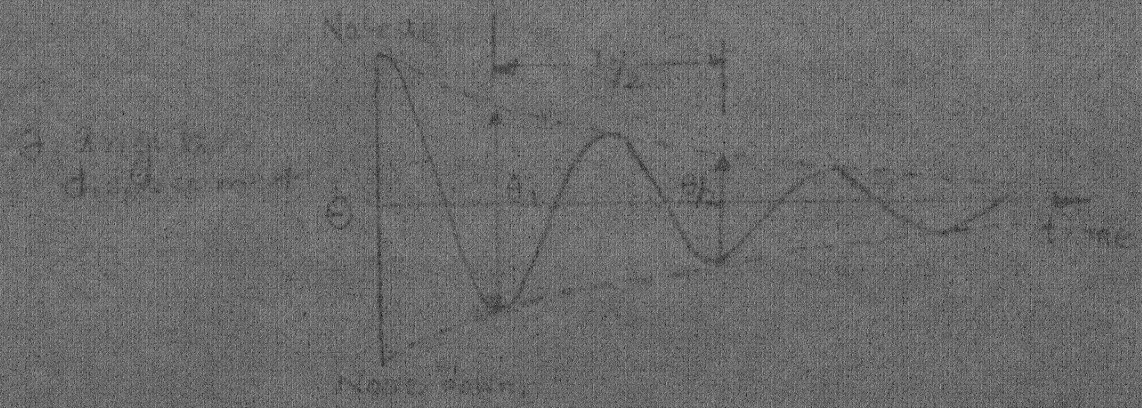

1.6 A1

TYPICAL USE: [illegible]
HISTORY: FOR A [illegible]
OF FREEDOM [illegible]
WIND TUNNEL

$$[\theta] = [A][F]$$

NORMAL FORCE. $\theta_1 =$ [illegible]

CHORD FORCE. $\theta_2 =$ [illegible]

PITCHING MOMENT $\theta_3 =$ [illegible]

YAWING MOMENT $\theta_4 =$ [illegible]

SIDE FORCE. $\theta_5 =$ [illegible]

THE RESULT CAN BE EXPRESSED AS FOLLOWS

NORMAL FORCE $Z = (0.334)\theta_1$

AXIAL FORCE $X = (0.200)\theta_2$

PITCHING MOMENT $m = (0.334)\theta_3$

YAWING MOMENT $n = (0.578)\theta_4$

SIDE FORCE $Y = (0.00)\theta_5$.

FIG. A-2 MATRIX EQUATION FOR 5-COMPONENT BALANCE CALIBRATION

$$[\theta] = [A][F]$$

NORMAL FORCE: $\theta_1 = .57 + 0.06x + .00y + \ldots$

CHORD FORCE $\theta_2 = 0.002 + .5x + \ldots$

PITCHING MOMENT $\theta_3 = 0.012 + 0.01x + 0.00y + \ldots$

YAWING MOMENT $\theta_4 = 0.002 + 0.00x + 0.00y + 0.00\eta + \ldots$

SIDE FORCE $\theta_5 = 0.002 + 0.0x + 0.0y + \ldots$

THE RESULT CAN BE EXPRESSED AS FOLLOWS

NORMAL FORCE $Z = (0.334)\theta_1$

AXIAL FORCE $X = (0.200)\theta_2$

PITCHING MOMENT $m = (0.334)\theta_3$

YAWING MOMENT $n = (0.5715)\theta_4$

SIDE FORCE $Y = (0.00)\theta_5$.

FIG. A-2 MATRIX EQUATION FOR S-COMPONENT BALANCE CALIBRATION

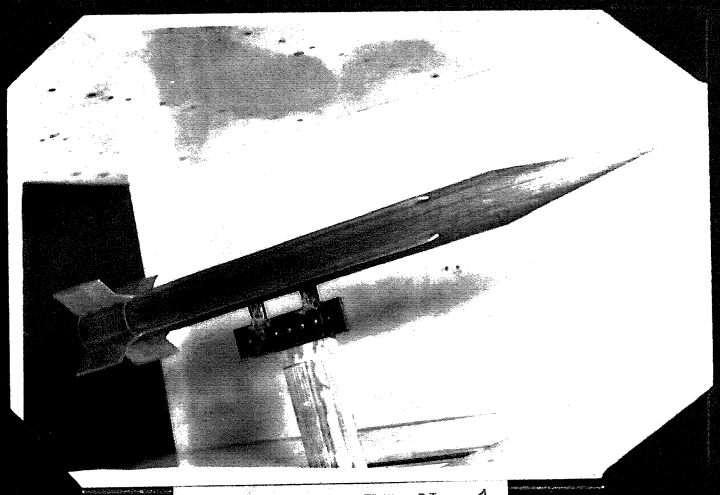

PHOTOGRAPH No.1

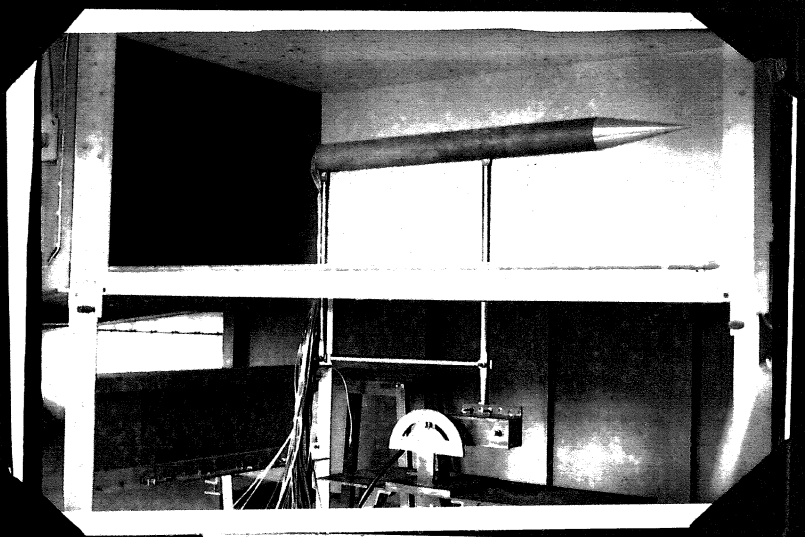

PHOTOGRAPH No.2

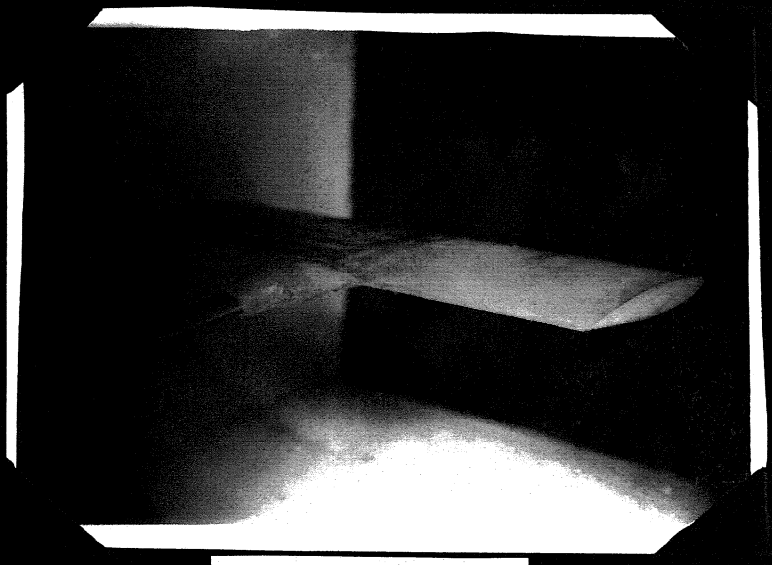

PHOTOGRAPH No.3

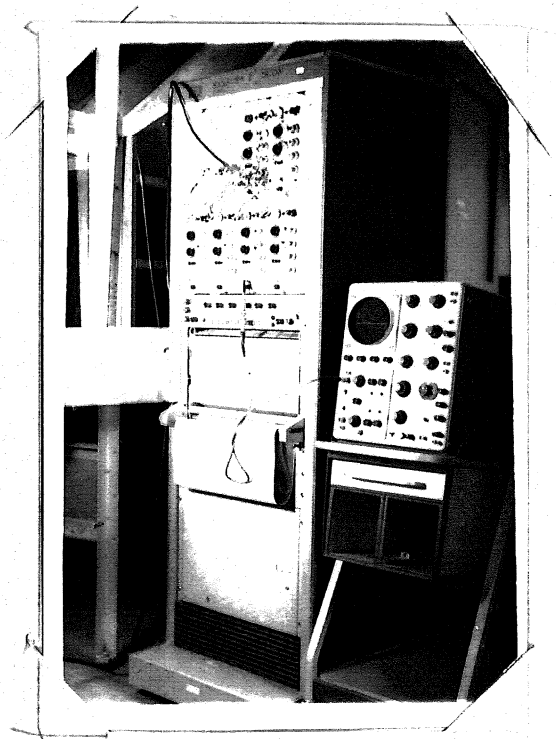

PHOTOGRAPH No.4

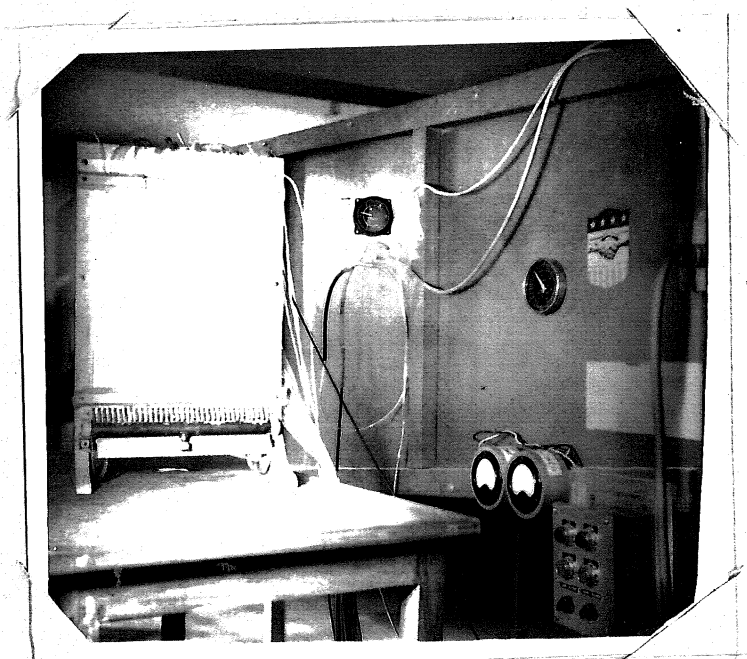

PHOTOGRAPH No.5

PHOTOGRAPH No.6

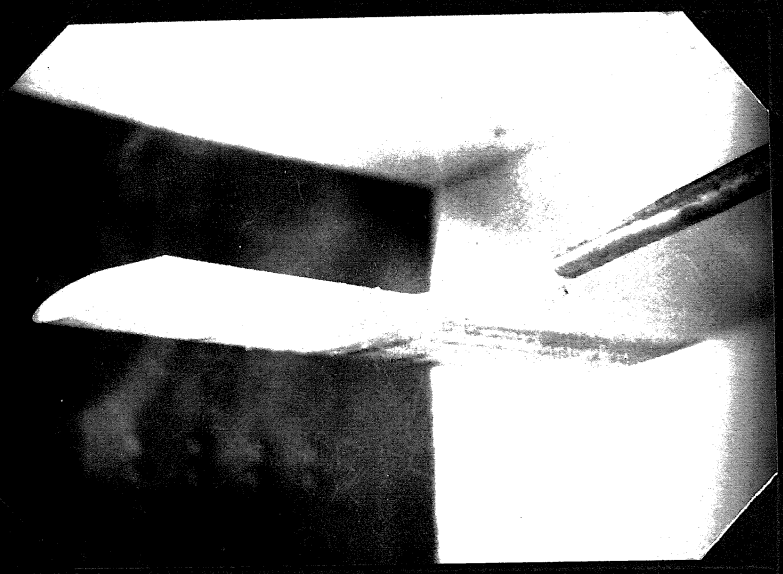

PHOTOGRAPH No.7

PHOTOGRAPH No.8

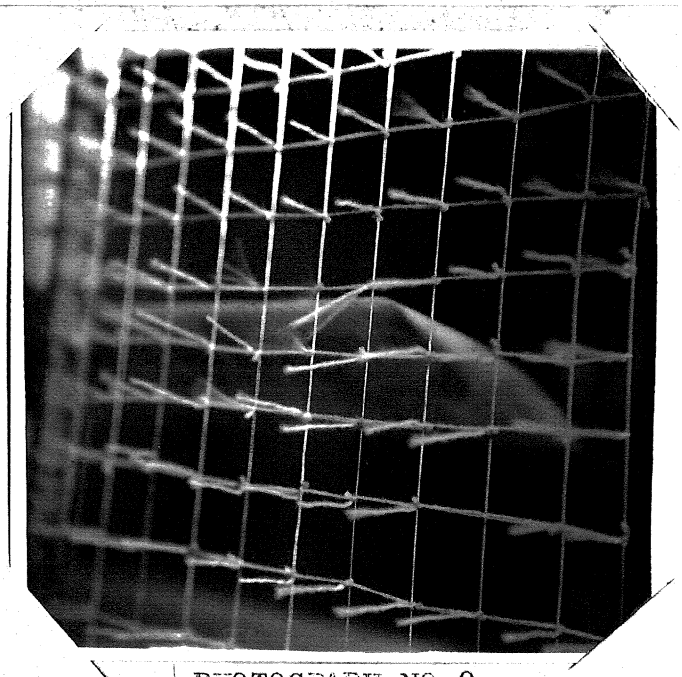

PHOTOGRAPH NO.9

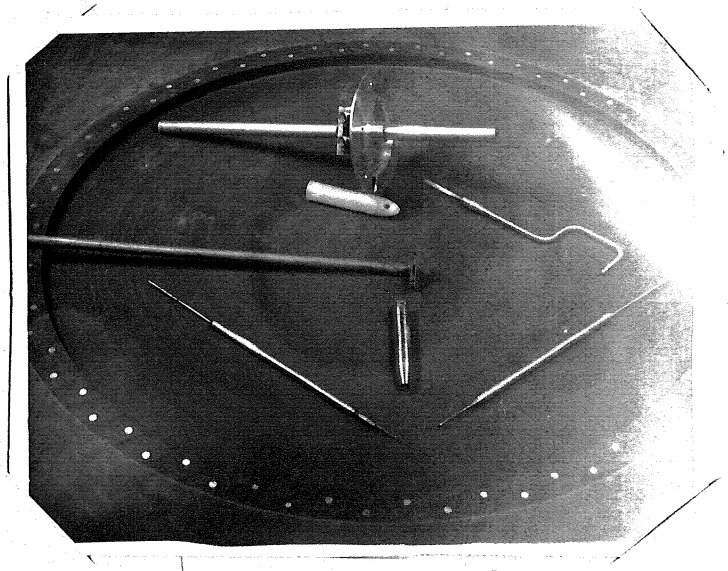

PHOTOGRAPH No.10

PHOTOGRAPH No.11

PHOTOGRAPH No.12

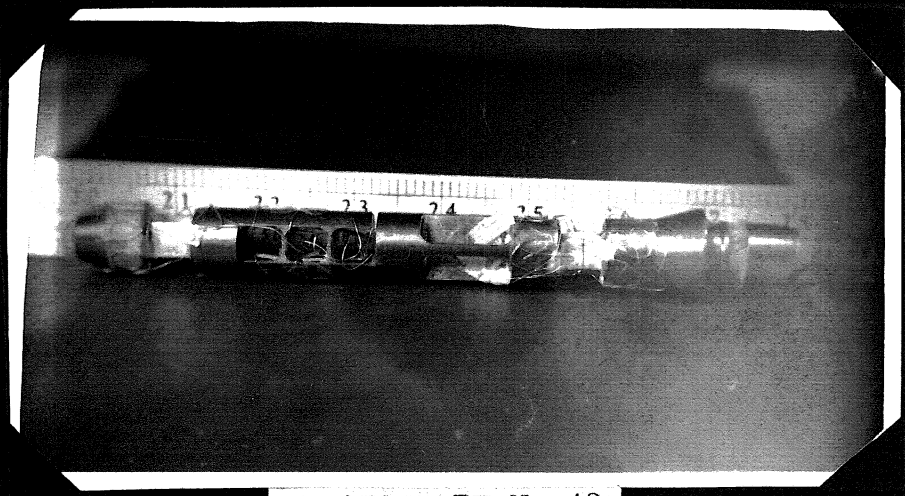

PHOTOGRAPH No.13

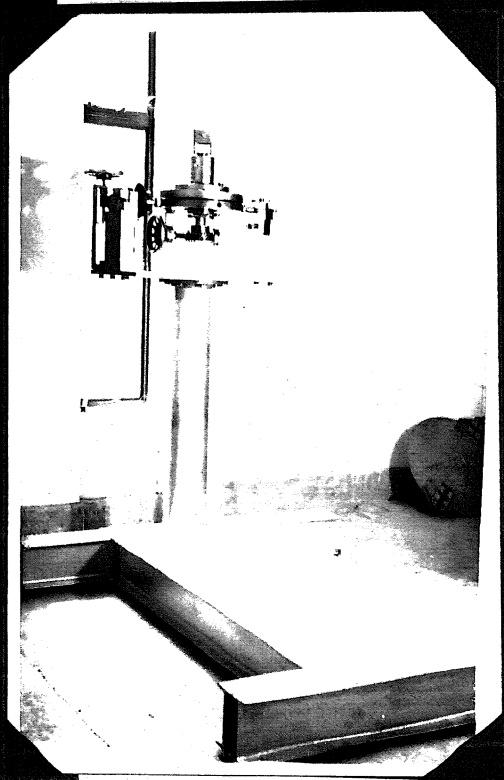

PHOTOGRAPH No.14

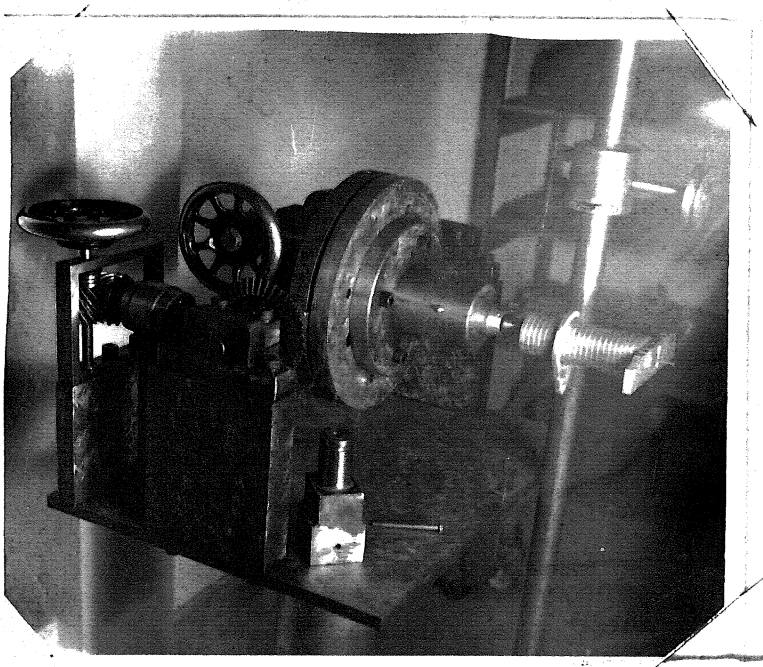

PHOTOGRAPH No.15

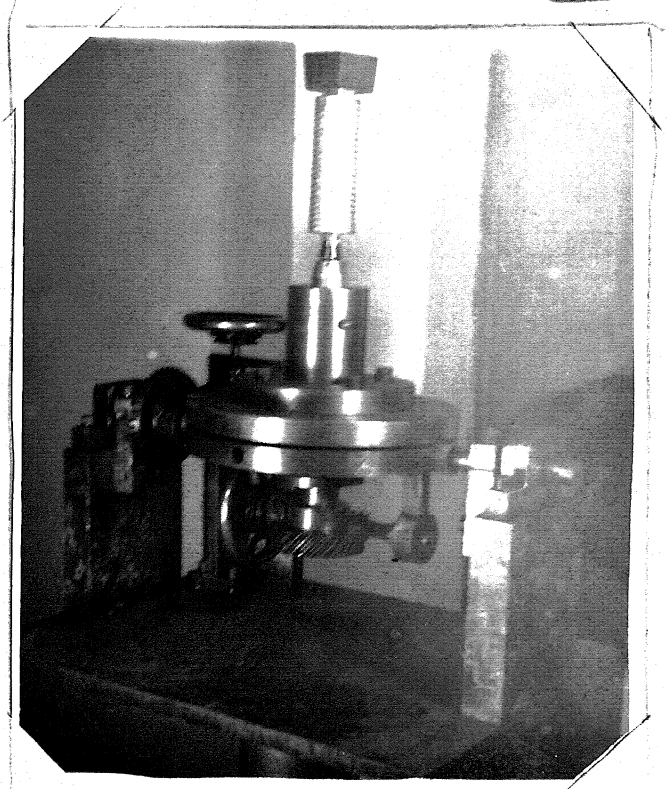

PHOTOGRAPH No.16

PHOTOGRAPH NO.17

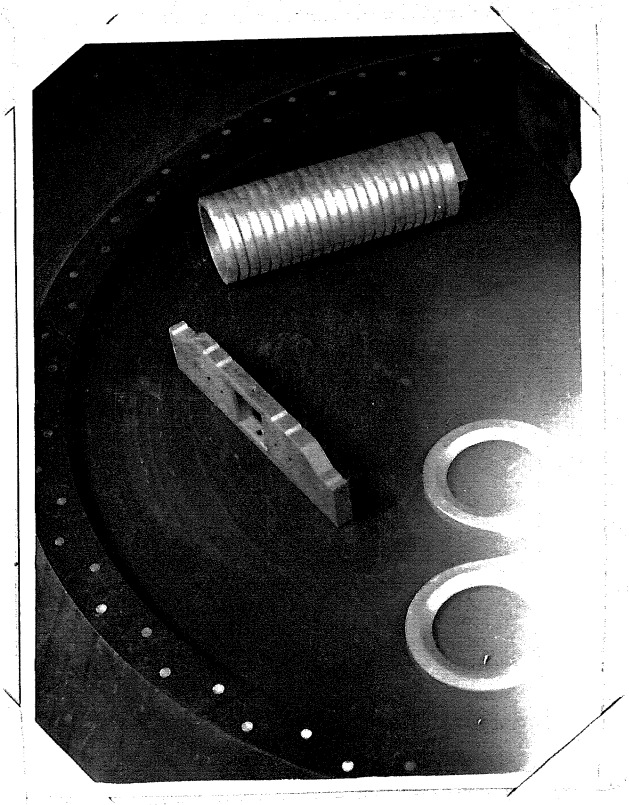

PHOTOGRAPH No.18

PHOTOGRAPH No.19